RP TU Rheinland-Pfälzische Technische Universität Kaiserslautern Landau

MitoTraP: Compromised mitochondria trap mitoribosomal precursor proteins in the intermembrane space

vom Fachbereich Biologie

der Rheinland-Pfälzischen Technischen Universität Kaiserslautern-Landau

zur Verleihung des akademischen Grades Dr. rer. nat. genehmigte

Dissertation

von

Tamara Flohr, M.Sc., geb. in Heidelberg

Mündliche Prüfung: 13.11.2024

Dekan:	Prof. Dr. Stefan Kins
Promotionskommissionsvorsitzender:	Prof. Dr. Michael Schroda
Berichterstattende:	Prof. Dr. Johannes M. Herrmann
	Prof. Dr. Tanja Maritzen

D 386

TABLE OF CONTENTS

Eidesstattliche Erklärung

Hiermit erkläre ich, dass die vorliegende Arbeit ohne unzulässige Hilfe Dritter und ohne Benutzung anderer als der angegebenen Hilfsmittel von mir persönlich angefertigt wurde. Die aus anderen Quellen übernommenen Daten und Konzepte sind unter Angabe der Quelle gekennzeichnet.

Ich habe nicht die entgeltliche Hilfe von Vermittlungs- beziehungsweise Beratungsdiensten in Anspruch genommen. Niemand hat von mir unmittelbar oder mittelbar geldwerte Leistungen für Arbeiten erhalten, die im Zusammenhang mit dem Inhalt der vorgelegten Dissertation stehen.

Die Arbeit wurde bisher weder im In- noch im Ausland in gleicher oder ähnlicher Form einer anderen Prüfungsbehörde vorgelegt.

Die Bestimmungen der Promotionsordnung des Fachbereichs Biologie der Universität Kaiserslautern sind mir bekannt. Insbesondere weiß ich, dass ich vor Vollzug der Promotion zur Führung des Doktortitels nicht berechtigt bin.

Tamara Flohr

Kaiserslautern, den 29.08.2024

Darlegung des Eigenanteils

Die Messung aller massenspektrometrischen Daten (Abb. 24, 27, 29) wurden von Markus Räschle, Center for MS Analytics, RPTU Kaiserslautern, durchgeführt. Die Level 2 Plasmide für den Split-GFP Reporter cHHYTK257, 258, 260, 261 (Abb. 22b, 26c) wurden von Lukas Nutz im Rahmen seiner Bachelorarbeit kloniert.

Die vorliegende Einschätzung über die erbrachte Leistung von Dritten wurden mit den genannten Personen einvernehmlich abgestimmt.

Tamara Flohr Prof. Dr. Johannes M. Herrmann

Kaiserslautern, den 29.08.2024

Darlegung aller benutzten Hilfsmittel und Hilfestellungen

Zur Erstellung dieser Arbeit wurde das Microsoft Office 365 Softwarepaket (Word und Excel) genutzt. Das Literaturverzeichnis und Literaturverweise wurden mittels Citavi erstellt. Alle statistischen Analysen erfolgten mittels Microsoft Excel oder R Studio. Alle gezeigten Abbildungen wurden mit Hilfe der Corel Technical Suite 2020 erstellt. Strukturdarstellungen wurden mittels ChimeraX visualisiert. Mikroskopische Aufnahmen wurden mit dem Softwarepaketen Fiji und Leica LasX analysiert. Zur Quantifizierung aller Western Blot Experimente wurde die Software ImageLab und Fiji genutzt. Zur Überprüfung des Textes wurde die Software Grammarly und DeepL Write verwendet. ChatGPT wurde zur Optimierung von Formulierungen genutzt.

Tamara Flohr

Kaiserslautern, den 29.08.2024

CURRICULUM VITAE

Tamara Flohr

Master of Science

Place of birth: Heidelberg, Germany

Education

Since 07/2020	**PhD student** Cell Biology University of Kaiserslautern
10/2018 - 05/2020	**Master of Science (M. Sc.)** Molecular Cell Biology University of Kaiserslautern Thesis: „*Mrp17 – Ein mitoribosomales Protein mit ungewöhnlichem Importweg in Mitochondrien“*
10/2015 - 09/2018	**Bachelor of Science (B. Sc.)** Biosciences University of Kaiserslautern Thesis: „*Herstellung eines genetischen Testsystems zur Untersuchung des Imports ribosomaler Proteine in Hefemitochondrien“*
09/2012 - 07/2015	**Abitur** Marie-Baum-Schule Heidelberg
09/2006 – 07/2012	**Mittlere Reife** Realschule Neckargemünd

Fellowships and Awards

2018 - 2020	Scholarship – Deutschlandstipendium
2019	Minerva Short Term Research Grant for a research internship in Israel
2023	Best Poster Prize – The 47th FEBS Congress

LIST OF PUBLICATIONS

2024 **Flohr T.**, Räschle M., Herrmann J.M., Dysfunctional mitochondria trap proteins in the intermembrane space, submitted

2023 Bertgen L., **Flohr T.**, Herrmann J.M., Methods to Study the Biogenesis of Mitoribosomal Proteins in Yeast, Methods Mol Biol. Book series (MIMB, volume 2661: 143-161), DOI: 10.1007/978-1-0716-3171-3_10

2022 Bykov Y.S.*, **Flohr T.***, Boos F., Zung N., Herrmann J.M., Schuldiner M., Widespread use of unconventional targeting signals in mitochondrial ribosome proteins, The EMBO Journal, DOI: 10.15252/embj.2021109519

2022 Güngör B., **Flohr T.**, Garg S.G., Herrmann J.M., The ER membrane complex (EMC) can functionally replace the Oxa1 insertase in mitochondria, PLOS Biology, DOI: 10.1371/journal.pbio.3001380

2021 Duarte M., Ferreira C., Khandpur G.K., **Flohr T.**, Zimmermann J., Castro H., Herrmann J.M., Morgan B., Tomás A.M., Leishmania type II dehydrogenase is essential for parasite viability irrespective of the presence of an active complex I, Proceedings of the National Academy of Sciences, Proceedings of the National Academy of Sciences, DOI: 10.1073/pnas.2103803118

2021 Schlagowski A.M., Knöringer K., Morlot S., Sánchez Vicente A., **Flohr T.**, Krämer L., Boos F., Khalid N., Ahmed S., Schramm J., Murschall L.M., Haberkant P., Stein F., Riemer J., Westermann B., Braun R.J., Winklhofer K.F., Charvin G., Herrmann J.M., Increased levels of mitochondrial import factor Mia40 prevent the aggregation of polyQ proteins in the cytosol, The EMBO Journal, DOI: 10.15252/embj.2021107913

2021 Backes S., Bykov Y.S., **Flohr T.**, Räschle M., Zhou J., Lenhard S., Krämer L., Mühlhaus T., Bibi C., Jann C., Smith J.D., Steinmetz L.M., Rapaport D., Storchová Z., Schuldiner M., Boos F., Herrmann J.M., The

chaperone-binding activity of the mitochondrial surface receptor Tom70 protects the cytosol against mitoprotein-induced stress, Cell Reports, DOI: 10.1016/j.celrep.2021.108936

SUMMARY

Most mitochondrial proteins are synthesized in the cytosol and subsequently have to be imported into mitochondria. An N-terminal mitochondrial targeting signal (MTS) guides these mitochondrial precursor proteins into the matrix. However, 25% of all mitoribosomal proteins (MRPs) do not have a typical MTS but use an internal targeting information instead. In this study, the model protein Mrp17 (bS6m) was used to investigate the import pathway of such a protein without a typical MTS. Despite its internal targeting signal, Mrp17 still is efficiently imported via the typical presequence pathway into the mitochondrial matrix. Like other matrix proteins, the translocation of Mrp17 depends on the TOM and TIM23 complex. Surprisingly, Mrp17 has a different energy dependency for the translocation compared to other matrix proteins. On one side, Mrp17 is highly dependent on the membrane potential which is built at the inner membrane by the respiratory chain. On the other side, the import motor with its core component the ATP-dependent mtHsp70 is not needed for the translocation of Mrp17 across the OM and is only needed to pass the inner membrane. This differs from other matrix proteins, which accumulate in the cytosol if the import motor is defective. Thereby low ATP levels, depletion of the import motor, or inhibition of the ATP synthase traps Mrp17 but also other MRPs in the intermembrane space (IMS). This Mitochondrial Triage of Precursor proteins (MitoTraP) is not simply the result of a general translocation block at the level of the inner membrane. Rather, MitoTraP specifically directs a defined subgroup of matrix proteins into the IMS, most of which are constituents of the mitochondrial ribosome. Due to the lack of rRNA in the IMS trapped MRPs will likely be degraded. Since non-imported Mrp17 interacts with assembly factors of the 90S pre-ribosome in the nucleolus, MitoTrap presumably acts as a safeguard mechanism by separating MRPs from the cytosolic ribosomal assembly machinery.

ZUSAMMENFASSUNG

Die meisten mitochondrialen Proteine werden im Zytosol synthetisiert und müssen in Mitochondrien importiert werden. Ein N-terminales mitochondriales Zielsignal (MTS) leitet diese mitochondrialen Vorläuferproteine in die Matrix. Allerdings besitzen 25 % aller mitoribosomalen Proteine (MRPs) jedoch keine typische MTS, sondern eine interne Zielinformation. In dieser Studie wurde das Modellprotein Mrp17 (bS6m) verwendet, um den Importweg eines Proteins ohne typische MTS zu untersuchen. Trotz einer internen Zielsequenz wird Mrp17 effizient über den typischen Präsequenzweg in die mitochondriale Matrix importiert. Dabei ist die Translokation wie bei anderen Matrixproteinen vom TOM- und TIM23-Komplex abhängig. Allerdings unterscheidet sich bei Mrp17 die Energieabhängigkeit für die Translokation von anderen Matrixproteinen. Die Translokation von Mrp17 ist stark abhängig von dem Membranpotential, welches an der inneren Membran durch die Atmungskette aufgebaut wird. Hingegen ist der Importmotor mit seiner Kernkomponente, dem ATP-abhängigen mtHsp70, für die Translokation von Mrp17 über die äußere Membran nicht erforderlich und wird nur zum Passieren der inneren Membran benötigt. Dies unterscheidet sich von anderen Matrixproteinen, welche bei einem defekten Importmotor im Zytosol akkumulieren. Niedrige ATP-Spiegel, die Depletion des Importmotors oder die Hemmung der ATP-Synthase führen dazu, dass Mrp17, aber auch andere MRPs im Intermembranraum (IMS) fehllokalisiert werden. Diese „*Mitochondrial Triage of Precursor proteins*“ (*MitoTraP*) ist nicht einfach das Ergebnis einer allgemeinen Translokationsblockade an der inneren Membran, vielmehr wird eine spezifische Untergruppe von Matrixproteinen in den IMS fehllokalisiert, nämlich Einheiten des mitochondrialen Ribosoms. Aufgrund des Fehlens von rRNA im IMS sind fehllokalisierte MRPs höchstwahrscheinlich nicht funktionsfähig und werden dort abgebaut. Da nicht-importiertes zytosolisches Mrp17 mit Assemblierungsfaktoren des 90S-Präribosoms im Nukleolus interagiert, könnte *MitoTrap* ein Schutzmechanismus darstellen, welcher MRPs räumlich von der Assemblierungsmaschinerie des cytosolischen Ribosoms trennt.

1 INTRODUCTION

Eukaryotic cells are characterized by having different compartments, separated by membranes, called organelles. One such organelles are mitochondria. Due to their α-proteobacterial origin, they still have their own genome, although most of the genes have been transferred to the nucleus [1,2]. However, in turn, hundreds of mitochondrial proteins are initially synthesized in the cytosol as precursors and have to be transported into the organelle. The interplay of targeting sequences and proteins that enable translocation ensure specific targeting of these precursor proteins. This translocation process is crucial as import problems lead to mitochondrial malfunction and can even lead to cell death [3,4]. The mitochondrial biogenesis and translocation pathways are well studied in the model organism *Saccharomyces cerevisiae* or baker's yeast. Studies in human cell culture show high similarities and homologs in the translocation pathways as well as energy production, making yeast a reliable and easy-to-use organism for scientific research [5].

1.1 The architecture of the powerhouse of the cell

Due to its endosymbiotic origin, mitochondria are double-membraned organelles [1]. These two membranes are the outer membrane (OM) which separates the organelle from the cytosol and the inner membrane (IM) which encloses the matrix. The intermembrane space (IMS) describes the enclosure between these two membranes [6]. The OM has large pores allowing the diffusion of small molecules like metabolites, amino acids, or redox-active substances such as hydrogen peroxide [7]. Additionally, the OM displays proteins, involved in mitochondrial biogenesis as it harbors proteins of the translocation and insertion machinery. Furthermore, the OM maintains the connection to cellular processes, as it can interact with cytosolic proteins such as chaperones or build contact sites with other organelles such as the endoplasmic reticulum (ER) [8,9]. In contrast to the OM, the IM does not allow free diffusion and therefore requires specific transporters for the exchange between the IMS and the matrix [10]. The IM forms large invaginations called cristae, thereby enlarging the surface and providing space for the respiratory chain complexes and thus ATP production [11].

1.1.1 Intermembrane space

The intermembrane space (IMS) is one of the two aqueous subcompartments of mitochondria. It is a small subcompartment of just about 20 nanometers in diameter [6]. In yeast, the IMS comprises ~51 proteins which is 5% of the total mitochondrial proteome, in humans the IMS compromises ~127 proteins [12,13]. Most IMS proteins are small (<25 kDa) and have simple structures, such as helix-loop-helix structure. The IMS serves as a crucial buffer system between the cytosol and the mitochondrial matrix. This subcompartment facilitates the transport of proteins, metabolites, and lipids, thereby ensuring mitochondrial functionality and maintaining a regulated redox state. Proteins located within the IMS are essential to maintain the optimal function of the respiratory chain, as they play a role in the assembly of certain respiratory chain complexes. Furthermore, IMS proteins are involved in the initiation of apoptosis [14,15].

1.1.2 Mitochondrial matrix

The mitochondrial matrix in yeast consists of 193 soluble matrix proteins, which is around 20% of the total mitochondrial proteome [16]. In the mitochondrial matrix, several biochemical processes take place that are essential for cellular energy production and metabolism. Such as the oxidation of pyruvate and fatty acids, and the tricarboxylic acid (TCA) cycle [17]. In addition, the matrix contains specialized ribosomes (mitoribosomes) that translate mainly subunits of the respiratory chain, which are encoded on the mitochondrial DNA [18]. In yeast only 8 proteins are mitochondrially encoded, these are seven hydrophobic proteins of the respiratory chain complexes and Var1, a poly-N mitoribosomal protein [19,20]. All the other mitochondrial proteins are synthesized in the cytosol and are imported into mitochondria (Fig 1a).

1.2 Protein translocation into mitochondria

1.2.1 Targeting signals not as predictable as assumed

To facilitate this mitochondrial import of precursor proteins, around 60% of mitochondrial proteins have an N-terminal mitochondrial targeting signal (MTS) which guides the proteins into the matrix. The length of these sequences varies from a few to around 100 amino acids but typically ranges from 15 to 50 amino acids. Presequences characteristically have an amphipathic α-helix with one positively charged surface and one hydrophobic surface [21]. This sequence is recognized by receptors of the outer mitochondrial membrane and guides the protein through the membranes into the matrix. In most cases, MTSs are removed proteolytically, resulting in mature forms of mitochondrial matrix or inner membrane proteins [22]. Due to the specific properties of an MTS, it is possible to make *in silico* predictions about the subcellular localization of proteins [23]. However, many mitoribosomal proteins (MRPs) lack N-terminal MTSs and do not show any high prediction score for mitochondrial localization [24]. Instead many MRPs harbor unconventional, non-cleavable, targeting signals that can't be predicted but still use the same import pathway as regular MTS-containing proteins [25].

1.2.2 TOM complex

The translocase of the outer membrane (TOM) complex is essential for the translocation of proteins across the outer mitochondrial membrane (Fig. 1a). It functions as the main entry gate for nearly all mitochondrial proteins [26]. The core component of the TOM complex is the channel Tom40, a beta-barrel protein embedded in the outer mitochondrial membrane [27]. There are three receptors associated with the TOM complex. The initial receptor is Tom20, it primarily recognizes the hydrophobic surface of the presequence and thereby initiates their import [28]. The precursor protein is then forwarded to the central receptor Tom22 that interacts with the positive surface of the presequence and facilitates the transfer to the Tom40 channel. Tom20 and Tom22 have partially overlapping substrate specificities and thereby can substitute each other [29]. Tom70 is involved in the recognition and import of a subset of precursor proteins, particularly those with hydrophobic patches or internal targeting signals. This receptor interacts with cytosolic chaperones that deliver preproteins to the TOM complex [30]. Besides the receptors, there are the small Tom

proteins, Tom5, Tom6, and Tom7. These subunits play crucial roles in complex assembly, stability, and regulation. Tom5 is involved in the initial stages of protein translocation, while Tom6 and Tom7 contribute to the structural integrity and dynamic regulation of the complex [31,32]. The TOM complex has two different assembly forms. There is a dynamic exchange between the major trimer form (Fig. 1b) and the minor dimer form [33]. For efficient translocation, the translocase of the OM interacts with the translocase of the IM, forming a TOM-TIM23 supercomplex [34].

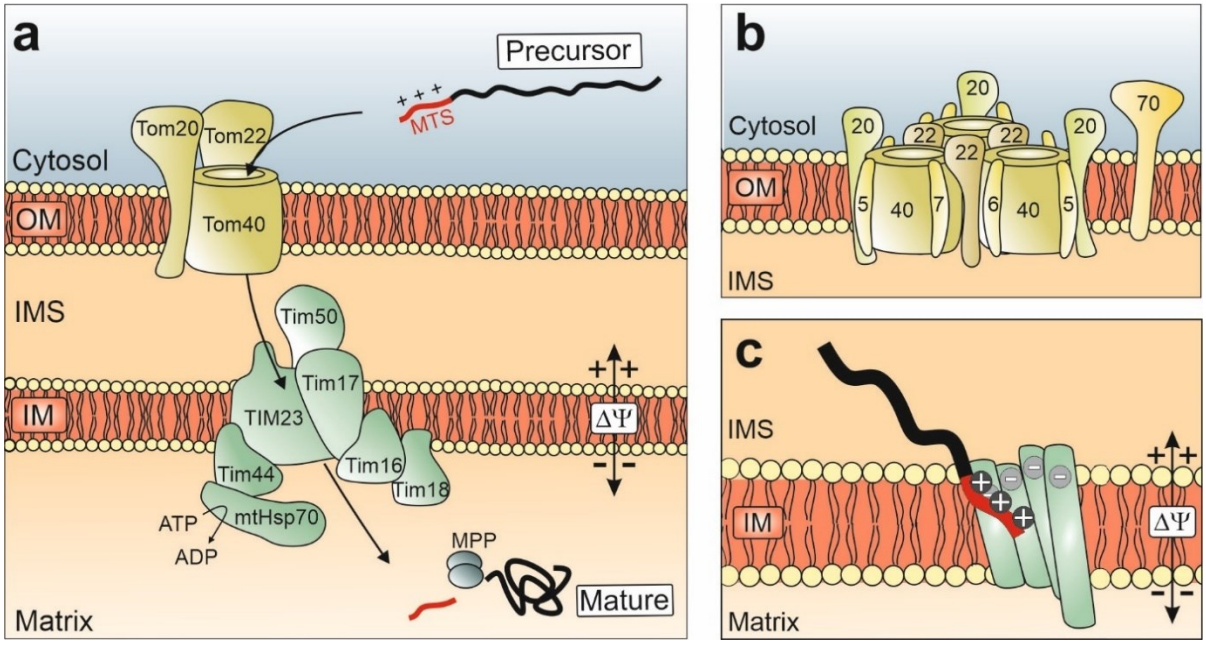

Fig. 1 | Translocation of proteins from the cytosol into the matrix. (a) Precursor proteins are synthesized in the cytosol and carry an N-terminal MTS. The MTS interacts with receptors of the TOM complex which guide the precursor protein through the Tom40 channel. Precursor proteins pass the IM via the TIM23 complex. Import is driven by the membrane potential ($\Delta\Psi$) and the import motor. In the matrix, MPP cleaves of the MTS, and the mature protein is folded. **(b)** The TOM complex comes in different assembly states. The Trimer is the major form in intact mitochondria. **(c)** Tim17 is the main player for protein translocation across the IM. The acidic patch of Tim17 interacts with the positively charged MTS and the hydrophobic part of the MTS interacts with the lipid bilayer. This environment allows the translocation of precursors through the IM without the presence of an IM channel.

1.2.3 TIM23 complex

The translocase of the inner membrane 23 (TIM23) complex is embedded in the mitochondrial inner membrane and is crucial for the import of precursor proteins into the mitochondrial matrix or insertion into the inner membrane. The complex is composed of several core components (Fig. 1a). Tim50 is the receptor and interacts with incoming precursors, guiding them to Tim23/Tim17. Tim23 was thought to be the central component of the complex, forming the channel through the inner membrane

and Tim17 was thought to have only a stabilizing function [35,36]. Current studies showed that Tim23 as well as Tim17 have channel-like structures, with Tim17 as the actual protein transferring precursors into the matrix. Tim17 and Tim23 form a back-to-back heterodimer that translocates precursors across the inner membrane at the Tim17 bilayer interface. The positively charged side of the MTS interacts with an acidic patch of Tim17 and the hydrophobic side interacts with the lipid bilayer (Fig. 1c) [37]. The translocation of the precursor is energized by two different factors, the membrane potential, and the PAM (presequence translocase-associated motor) complex. The membrane potential is generated by the respiratory chain, as protons are pumped into the IMS resulting in a positively charged IMS-, and a negatively charged matrix-side. The negatively charged matrix side exerts an electrophoretic effect on the positively charged MTS thereby guiding the precursor into the matrix [38]. The main driving force for matrix import is the PAM complex. The core component of this motor is the mitochondrial heat shock protein 70 (mtHsp70), an ATP-driven chaperone [39,40]. The exact mechanism of this motor is still discussed. In the Brownian ratchet model, mtHsp70 has a more passive function. It binds to the precursor protein to prevent backsliding. Brownian motion drives the translocation until the next mtHsp70 can bind. The pulling model describes a more active process. ATP hydrolysis leads to a conformational change in mtHsp70, creating an inward-directed force that pulls the protein into the matrix. This allows another mtHsp70 to bind the precursor protein [41]. Probably both mechanisms are needed to efficiently import precursors into the matrix. Next to the mtHsp70, the import motor consists of several other essential proteins. The matrix-side and membrane-bound protein Tim44 couples the mtHsp70 to the TIM23 complex, thereby supporting the transfer of the precursor to mtHsp70. Tim44 consists of two domains that undergo rearrangement during the precursor translocation, underlining its essential role in the import process. Additionally, two membrane-bound co-chaperones, the J-protein Tim14 (Pam18) and the J-like protein Tim16 (Pam16), regulate the ATP-hydrolyzing activity of mtHsp70 [42]. Mge1 promotes the release of ADP thus initiating a new round of ATP hydrolysis. In the matrix, the presequence is cleaved off by MPP (mitochondrial processing peptidase). Subsequently, the precursor protein is folded and assembled by soluble mtHsp70 and the matrix chaperonin Hsp60 [22,43].

1.2.4 Import into the IMS

All IMS proteins are synthesized in the cytosol and subsequently imported into the IMS. Two major import routes have been identified: the mitochondrial IMS import and assembly (MIA) pathway and the stop-transfer pathway [44,45]. The two main players in the MIA pathway are the oxidoreductase Mia40 and the FAD-dependent sulfhydryl oxidase Erv1. Mia40 is located in the IMS and is anchored via a N-terminal transmembrane domain in the IM. Substrates of this pathway contain conserved cysteine residues and contain a hydrophobic patch that acts as an IMS targeting signal. Mia40 acts as a receptor and binds to this signal after substrates passed the OM through the TOM complex. Mia40 introduces disulfide bonds in the substrate and thereby gets itself reduced and blocked for further import reactions. Erv1 constantly re-oxidizes Mia40 to maintain a functional MIA import pathway (Fig. 2a) [46]. IMS proteins that are imported via the stop-transfer pathway are proteins that are lateral released into the IM. A transmembrane segment that flanks the cleavable presequence differentiates the IMS signal from an MTS. These proteins are imported via the typical matrix pathway until translocation across the IM is stalled by the hydrophobic transmembrane signal. This leads to lateral release into the inner membrane (Fig. 2b) [47,48].

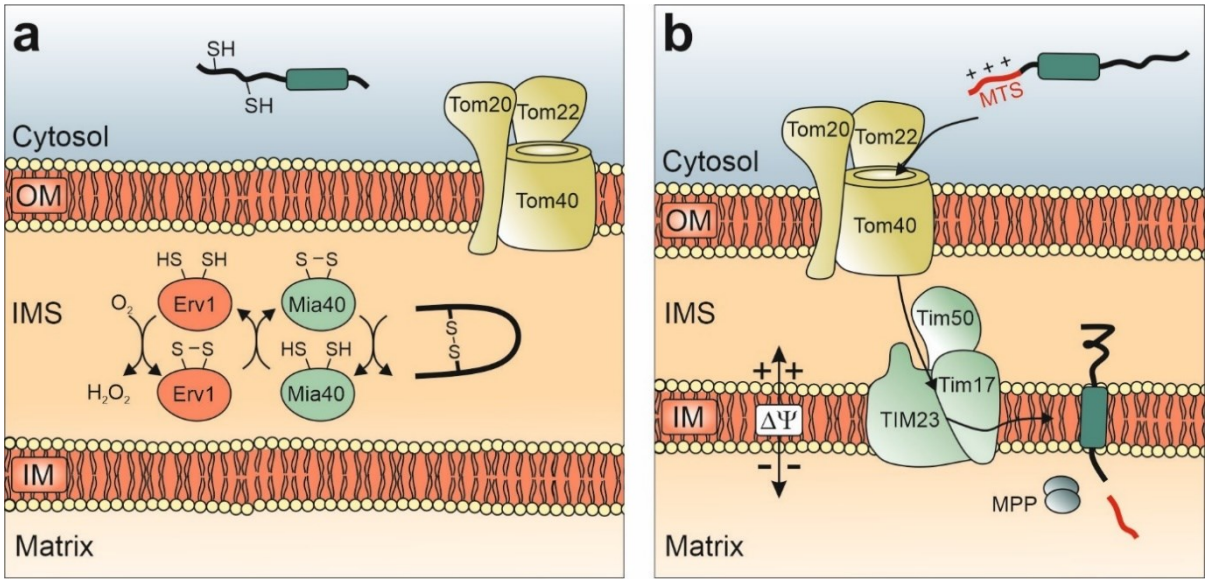

Fig. 2 | Import pathways into the IMS. (a) The MIA pathway has two main players, Mia40 and Erv1. Mia40 introduces a disulfide bond after the substrate passes the OM. This process reduces Mia40, Erv1 re-oxidizes Mia40 to keep Mia40 functional. **(b)** IMS proteins that are imported via the stop-transfer pathway have an MTS followed by a hydrophobic domain. This causes the lateral release from the TIM23 complex into the IM.

1.3 Two distinct ribosomes

1.3.1 Biogenesis of the cytosolic ribosome

Ribosomes are highly conserved ribonucleoprotein complexes essential for protein synthesis. These cellular machines consist of two subunits: the small, 40S subunit (SSU) and the large, 60S subunit (LSU). The small subunit in yeast contains one ribosomal RNA (rRNA) (18S, 1800 nucleotides) and 33 ribosomal proteins. The SSU binds the messenger RNA (mRNA) and serves as a decoding center to bring mRNA and aminoacylated transfer RNAs (tRNA) together. The large subunit consists of three rRNAs (5S, 121 nt; 5.8S, 158 nt; 25S, 3396 nt) and 46 ribosomal proteins. The LSU possesses peptidyl transferase activity, catalyzing the formation of peptide bonds between amino acids. Through the catalytic action of the large subunit, amino acids are polymerized into a polypeptide chain. This nascent polypeptide is subsequently released through the exit tunnel [49]. Ribosome biogenesis is a multistep process and occurs in three cellular compartments: the nucleolus which is a non-membrane-bound subcompartment of the nucleus, the nucleoplasm, and the cytosol (Fig. 3). First the 35S pre-rRNA is transcribed which includes all rRNA for the SSU and the LSU, except of the 5S rRNA that is transcribed separately. Processing, folding, and modifications of pre-rRNA and assembly with some ribosomal proteins happens mainly in the nucleolus [50]. Pre-rRNA modifications occur frequently and are carried out by small nucleolar ribonucleoproteins (snoRNPs) [51]. These modifications are important as otherwise ribosomes show reduced translation efficiency [52]. Assembly of ribosomes requires 76 different small nucleolar RNAs and more than 200 assembly factors. They associate with the pre-ribosome and get released during maturation and ensure efficient and correct assembly [53]. This process is more pronounced for the 40S particle. U3

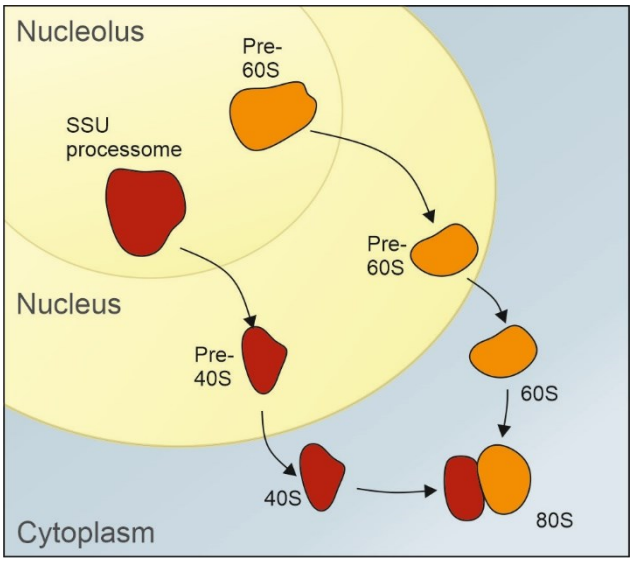

Fig. 3 | Assembly of the cytosolic ribosome. Assembly factors are involved in building the SSU processome and the Pre-60S in the nucleolus. In the nucleus further processing occurs until the two subunits are exported from the nucleus into the cytoplasm were the final assembly step of the 80S ribosome take place.

snoRNA and more than 75 proteins ensure correct folding and pre-rRNA processing and build together with ribosomal proteins the SSU processome, a dynamic macromolecule [54]. Efficient assembly is crucial, as over 2000 ribosomes are assembled each minute in a fast-growing yeast cell [55]. Complete loss-of-function mutations in many assembly factors and r-proteins is lethal in yeast and in higher organisms. Finally, the assembled ribosome has rRNAs located in its core that are surrounded by ribosomal proteins, sometimes protruding into the rRNA core [49].

1.3.2 The mitoribosome and Mrp17

Eukaryotic cells face the challenge of synthesizing next to the cytosolic ribosome a second ribosome within mitochondria, called the mitochondrial ribosome (mitoribosome). This specialized ribosome compromises in yeast a total of 78 proteins, with 44 proteins forming the large subunit and 34 constituting the small subunit. Notably, none of these proteins exhibit dual localization in the cytosolic ribosome [24]. Evolutionarily, mitoribosomes are derived from bacterial ribosomes, yet they exhibit distinct differences in composition, function, and structure. The yeast 74S mitoribosome (Fig. 4) has a molecular weight of 3.3 MDa and is larger than the 70S bacterial ribosome, which has a molecular weight of 2.3 MDa [56]. Although many mitoribosomal proteins have homologs in bacteria, numerous proteins are unique to the mitoribosome. These specific proteins are primarily localized on the ribosome surface. In addition to an increased number of ribosomal proteins, there is an observed increase in the length of these proteins. The specialization of the mitoribosome probably enhances the stability of the complex and contribute to the regulation of translation [24]. Functional specialization of the mitoribosome primarily facilitates the synthesis of mitochondrial membrane proteins. To prevent the aggregation of these proteins, they are co-translationally integrated into the inner mitochondrial membrane by the mitoribosome. This process necessitates two key factors: Oxa1, an integrase, and Mba1, which plays a crucial role in the binding of the mitoribosome to the membrane [57].

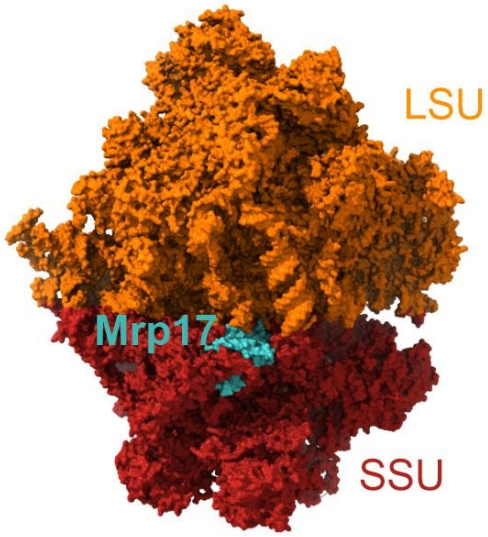

Fig. 4 | Structure of the yeast mitoribosome. Shown is the 74S mitoribosome of *S. cerevisiae* (PDB: 5MRC). The large subunit (LSU) is colored in orange, the small subunit (SSU) in red. Location of the small subunit protein Mrp17 is colored in cyan.

The mitoribosomal protein Mrp17 is part of the small 37S subunit (Fig. 4). It consists of 131 amino acids and has a molecular weight of 15 kDa. This categorizes Mrp17 as relatively small among mitoribosomal proteins, which typically range from 10 to 56 kDa. With the nomenclature proposed by Desai et al. (2017), Mrp17 is also referred to as bS6m. Notably, Mrp17 has a single homolog in bacteria, known as S6. Structurally, Mrp17 is located within a V-shaped canyon at the mRNA exit tunnel of the mitoribosome. It is suggested that this positioning improves translation initiation. Furthermore, Mrp17 interacts with Pet122, a translational activator specific for a subunit of cytochrome c oxidase, suggesting a role in the regulation of mitochondrial protein synthesis [18].

1.4 Respiratory chain

The mitochondrial respiratory chain, also known as the electron transport chain (ETC), is a series of protein complexes located in the inner mitochondrial membrane that play a critical role in cellular respiration. Through oxidative phosphorylation, the main energy source for the cell, ATP is generated (Fig. 5). Carbohydrates and lipids are converted in various metabolic pathways to Acetyl-CoA which is the fundamental substrate for the tricarboxylic acid cycle (TCA) in mitochondria [17]. Electrons that originate from NADH and $FADH_2$ produced in the TCA cycle are passed over to the complexes of the respiratory chain. NADH transfers two electrons to complex I, which is in mammals a complex consisting of several proteins [58]. The electrons are transferred from NADH to quinone (Q), a lipid in the IM that can be reversibly reduced and oxidized. During this process, protons are transported by an antiporter from the matrix into the IMS [58,59]. In yeast, there is not a complex perse but several NADH dehydrogenases (Nde1, Nde2, Ndi1) that use NADH without proton translocation [60]. In parallel electrons from succinate can be transferred to quinone via the succinate dehydrogenase (complex II), also in this step no protons are transported across the

IM. Reduced quinone further transfers both electrons to cytochrome c (Cyt c) via the cytochrome bc1 reductase (complex III). In this reaction, protons are translocated from the matrix into the IMS [61,62]. Cyt c functions as a mobile electron carrier and transfers electrons from Complex III to Complex IV. The Cyt c oxidase (complex IV) reduces molecular oxygen to water, thereby pumping protons into the IMS [63]. The translocation of protons at complex III and IV generates an electrochemical gradient across the IM. This membrane potential is used by the ATP synthase (complex V) that phosphorylates ADP to ATP, whereby protons flow back into the matrix via a rotary mechanism of the ATP synthase [62].

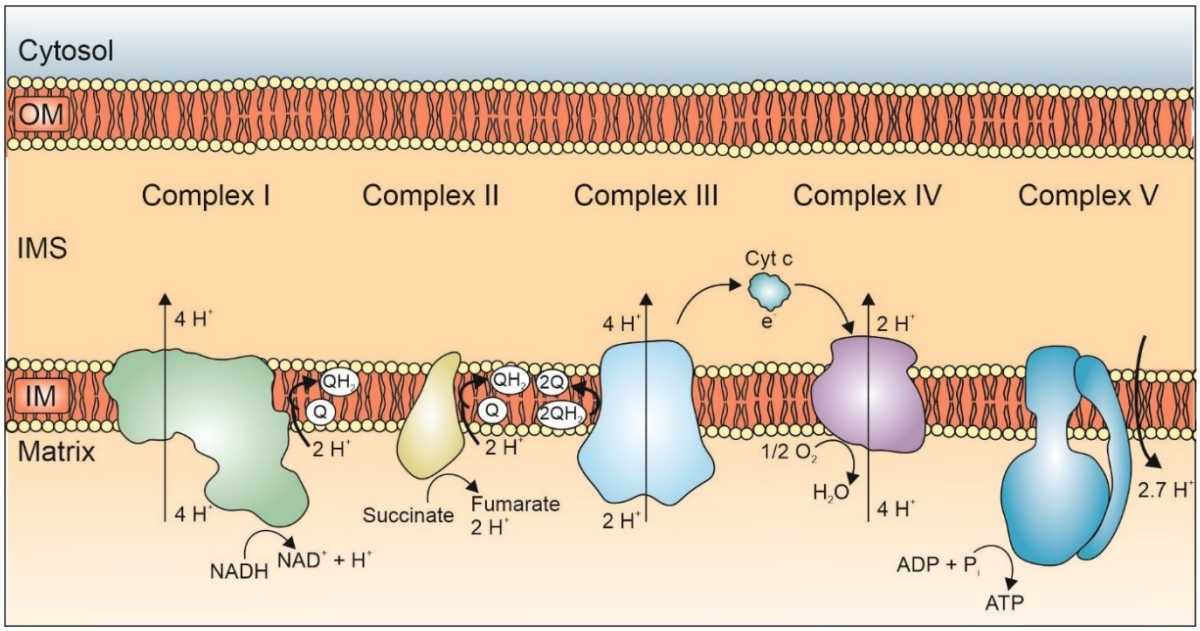

Fig. 5 | The respiratory chain. The complexes of the respiratory chain are located in the IM of mitochondria. Protons originating from the TCA cycle are transported via several complexes into the IMS, thereby generating a membrane potential. This potential can be used by the ATPase (Complex V) to generate ATP. In yeast, there is no complex I, instead several NADH dehydrogenases use NADH without transferring protons into the IMS.

1.4.1 The ATP synthase

The ATP synthase consists of two main parts, the F_0 and the F_1 subunit (Fig. 6a). The globular shaped hydrophilic F_1 part reaches into the mitochondrial matrix. The hydrophobic F_0 part is embedded into the IM [64,65]. The F_0 part is sensitive to Oligomycin and treatment leads to inhibition of the ATPase [66]. In yeast the F_0 sector consists of eight subunits, three of which are mitochondrially encoded (Atp6, Atp8, Atp9). An oligomer of Atp9 forms a ring-like structure that rotates in the IM. Together with Atp6, which is also embedded into the membrane, they facilitate proton transfer

across the IM. Six other components build the stator arm to connect F1 and F_0, among them Atp4, Atp8, and the oligomycin sensitivity-conferring protein (OSCP). The F_1 consists of the rotating central stalk that is build out of 3 subunits (γ, δ, ε) and the static hexamer that consists of 3 α- and β-subunits each [65,67–69]. Efficient assembly of the nuclear and mitochondrially encoded subunits is ensured by several proteins such as Hsp60 and Hsp70 but also substrate specific proteins [70,71]. The maturation and assembly of Atp6 is well studied (Fig. 6b). Atp6 is mitochondrially encoded and newly synthesized Atp6 initially interacts with Atp10, an IM protein facing its domain into the matrix. Atp10 assists in the binding of Atp6 to an oligomer of Atp9 at the late stages of F_0 assembly [65]. Though Atp6 interacts with another assembly factor as it carries an N-terminal extension of ten amino acids that is cleaved off. Atp23 was identified as the peptidase that cleaves off this N-terminal extension and thereby maturate Atp6. The metallopeptidase Atp23 is located in the IMS and is able to cleave Atp6 as the N-terminus is translocated into the IMS upon insertion of Atp6 into the IM. The maturation of Atp6 is not required for the formation of a functional ATP synthase, however the presence of Atp23 is. Additionally to its function as peptidase, Atp23 has a dual activity that is essential for respiration but not dependent on the proteolytic activity. It has been shown that Atp23 chaperones the assembly of Atp6 into the F_0 part and is essential for the assembly of the F_0 into the F1F0-ATP synthase [65,72].

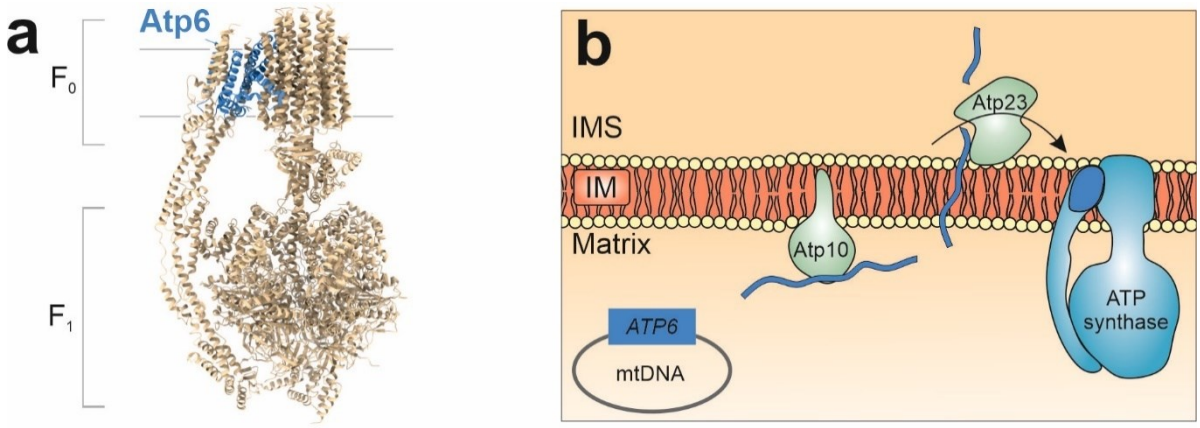

Fig. 6 | ATP synthase and the subunit Atp6. (a) Structure of the ATP synthase (PDB: 6CP6). The F_0 is embedded in the IM of mitochondria and the F_1 globular head reaches into the matrix. Indicated in blue is the protein Atp6 which is part of the F_0 subunit. **(b)** ATP6 is encoded on the mitochondrial genome. After translation in the matrix, Atp6 interacts with Atp10 and gets proteolytically cleaved by Atp23. Additionally to the processing activity, Atp23 is also needed for ATP synthase maturation and assembly.

1.5 Quality control mechanisms of mitochondria

1.5.1 Quality control mechanism at the OM

Mitochondrial quality control mechanisms are essential to deal with the high load of incoming precursor proteins and to monitor their folding [73]. However, different situations could negatively impair mitochondrial import. First, precursor proteins have to be kept in a soluble form as only unfolded proteins can be translocated through the Tom40 channel [74]. Prematurely folded proteins can block the import pore and especially precursors of the inner membrane can form strong clogger proteins and thereby have severe effects on the cellular viability [75]. Second, mitochondrial dysfunction and hence a disrupted membrane potential across the IM can lead to impaired import [76]. Both scenarios can lead to the accumulation of non-imported precursor proteins in the cytosol causing cellular stress. Consequently, the cell upregulates protein folding and proteolytic systems in the cytosol and downregulates cytosolic translation of mitochondrial metabolic enzymes, probably to minimize the workload at the mitochondrial import systems [75]. This unfolded protein response activated by mistargeting of proteins (UPRam) includes higher expression of proteasomal subunits and modulation to increase its activity (Fig. 7 left) [4,77]. Ubiquitylated proteins are not able to pass the Tom40 channel and are degraded by the 26S proteasome [78]. There are different mechanisms to remove arrested proteins from the translocase. The mitochondrial compromised protein import response (mitoCPR) is activated upon import failure and extracts arrested precursor proteins. Accumulation of precursor proteins lead to upregulation of the cytosolic protein Cis1 which recruits Msp1 to the Tom70 receptor. Msp1 is an OM-bound AAA-ATPase that facilitates the extraction of arrested proteins from the TOM channel which is followed by proteasomal degradation (Fig. 7 right) [3,79]. Another mechanism to extract precursor proteins is the mitochondrial protein translocation associated degradation (mitoTAD). This mechanism continuously monitors the TOM complex under non-stress conditions. A pool of Ubx2 binds to the TOM complex and thereby recruits the AAA ATPase Cdc48. Cdc48 can remove arrested precursor proteins from the TOM channel and hand it over to the proteasome for degradation (Fig. 7 middle) [80,81].

Beside the cytosolic response precursor proteins can be transported to compartments where their compartment-specific mechanisms can take effect. Hence, accumulated precursors can be translocated to the nucleus which has a high concentration of

proteasomes and therefore allow efficient degradation [82–84]. Membrane proteins can be translocated to the ER [85].

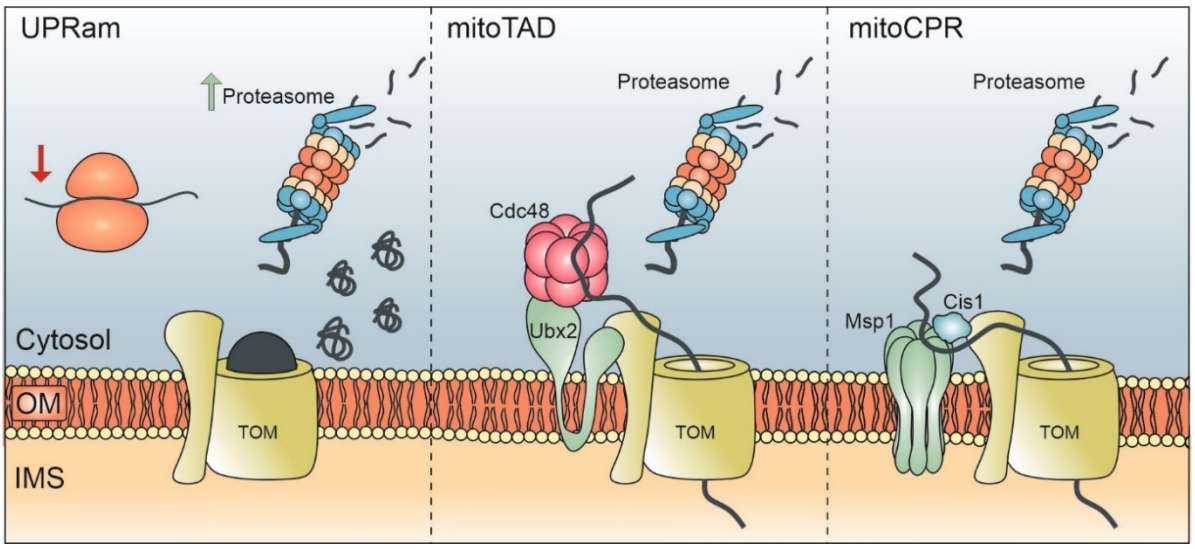

Fig. 7 | Quality control mechanisms at the OM. Precursor accumulation in the cytosol upon import blockage leads to the upregulation of the proteasome system and general downregulation of the cytosolic translation (UPRam). Mitochondria have different mechanisms to clear clogged import routes. In mitoTAD Ubx2 recruits Cdc48 to the import pore, removes the stuck precursor protein and hands it over for proteasomal degradation. In mitoCPR, Cis1 recruits Msp1 which clears the import pore. The extracted protein is degraded by the proteasome system.

1.5.2 Quality control mechanisms in the IMS

Several mechanisms ensure the regulation and maintenance of the proteome within the IMS, preventing the detrimental effects of protein misfolding and aggregation. Whereas the cytosol relies on ATP-driven chaperones, e.g., Hsp70 or Hsp90 the IMS employs a set of specialized, small Tim proteins. These proteins, including Tim8, Tim9, Tim10, Tim12, and Tim13, play crucial roles in the maintenance and sorting of mitochondrial proteins (Fig. 8 left) [86]. The small Tim proteins operate independently of ATP, relying instead on their inherent structural properties to perform their chaperone functions [87].

Yme1 is an ATP-dependent AAA-protease that degrades proteins within the IMS to maintain mitochondrial protein homeostasis (Fig. 8 middle). The protease is anchored in the inner mitochondrial membrane facing the IMS [88,89]. Studies show that Yme1 is involved in protein quality control of the IMS but also the OM and IM. Misfolded MIA substrates, such as the small Tim proteins are degraded by Yme1 [90,91]. Furthermore, Yme1 is implicated in regulating the number of functional respiratory chain complexes [92,93]. In addition to its proteolytic activity, Yme1 has a chaperone-

like function since it can bind unfolded proteins, initiate their refolding, and overtake the function of missing assembly factors [94,95]. Also in the import into the IMS Yme1 is involved since it helps in translocation across the OM and directs precursors to the TIM23 translocase and facilitates release into the IMS [96].

Another process is the retro-translocation of proteins into the cytosol followed by the degradation via the ubiquitin-proteasome system (UPS) (Fig. 8 right). This mechanism has been identified for MIA substrates that get stalled. Retro-translocation enables the escape from the IMS of unfolded proteins through the TOM complex [97,98]. This process is mainly limited by the topology and size of the proteins, as large proteins are probably not capable of being retro-translocated [99].

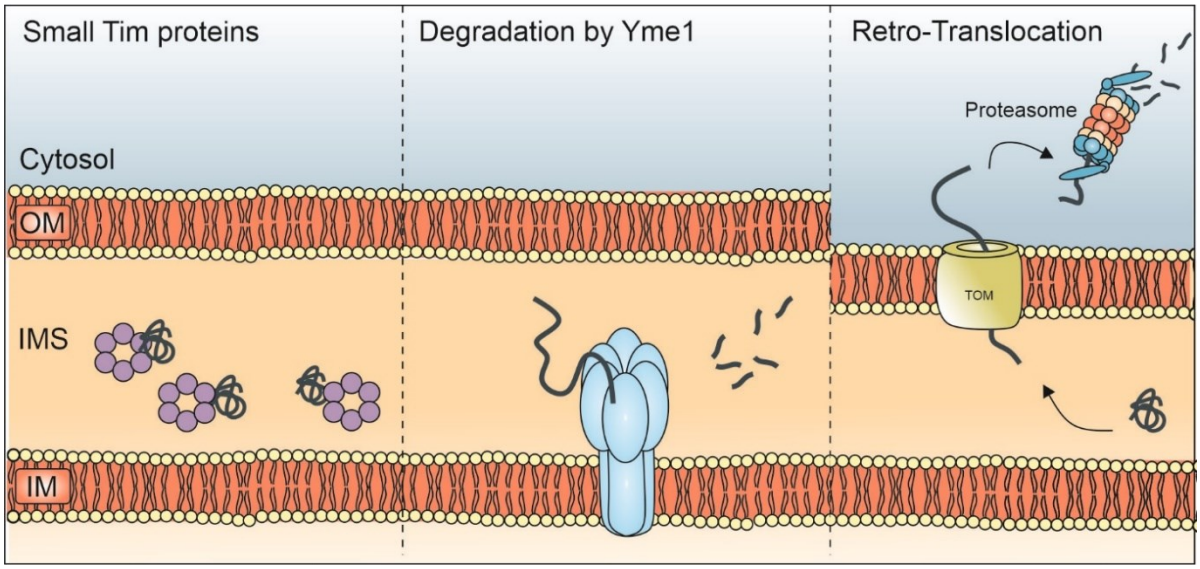

Fig. 8 | Quality control in the IMS. The small Tim proteins are ATP-independent chaperones that are involved in the maintenance and sorting of mitochondrial proteins. Yme1 is an ATP-dependent protease that degrades proteins in the IMS and thus is involved in the quality control in the IMS. However, instead of degrading proteins in the IMS, proteins can be retro-translocated into the cytosol where they are degraded by the proteasome system.

1.5.3 Proteostasis network in the mitochondrial matrix

In contrast to the IMS, the matrix has a proteostasis network akin to the one in the cytosol. However, there are only three out of five chaperone families present in the matrix: Hsp60, Hsp70, and Hsp100. The most essential one is the Hsp70 family. Within this family, Ssc1 is the most abundant and essential component. Apart from its function in the PAM complex, Ssc1 facilitates the folding and assembly of nuclear encoded proteins and proteins encoded on the mitochondrial genome [22,39]. Ssc1 chaperones the assembly of the ATP synthase as it interacts with the Atp9 oligomer and Atp6 [71].

Ssc1 ATPase activity can be stimulated by the co-chaperone Mdj1 which belongs to the Hsp40 family [40,100]. The matrix also has its own chaperonin complex. Hsp60 forms a folding chamber in which proteins up to 50 kDa can be folded. The co-chaperone Hsp10 acts as a lid and encloses the chamber [101]. Hsp60 is not only involved in protein folding but also in protein translocation, acting subsequently to Hsp70 [43]. Besides Hsp60 there is the protein Tcm62 which has a similar sequence to Hsp60 and is involved in complex biogenesis [102].

If folding and refolding are not successful, the mitochondrial matrix has a backup system that acts downstream of the chaperone system: the AAA proteases. The matrix facing AAA proteases Yta10 and Yta12, which form a heterohexamer facilitate the degradation of non-assembled IM proteins. Additionally, the complex is involved in assembly of the ATP synthase [103]. The matrix equivalent to the cytosolic proteasome is the master protease Pim1. This ATP-dependent serine protease is highly conserved to its bacterial homolog Lon1 [104]. The Pim1 AAA+ domain unfolds substrates, and the protease domain degrades them. Pim1 controls the selective turnover of proteins in the matrix and degrades misfolded proteins. These proteases are necessary to clear the matrix from misfolded or even aggregated proteins. HSP78 encodes a yeast mitochondrial heat shock protein in the Hsp100 family of ATP-dependent proteases [105]. Besides its function as a disaggregase, it plays a role in protein folding of newly imported proteins [106].

2 AIM

Since 25% of all mitoribosomal proteins do not have a typical presequence, I wanted to investigate MRP targeting signals using the model protein Mrp17 [25]. Already in my master thesis I was able to identify an internal targeting information between amino acid 30-60 and discovered that positive charges distributed over the whole protein are essential to import Mrp17 into the mitochondrial matrix. I could also show that the interaction of Mrp17 with the Tom20 receptor is crucial for translocation [107]. To this point, it seemed like despite the unconventional targeting signal Mrp17 just takes the typical matrix import pathway. Surprisingly, initial *in vitro* import analysis showed that Mrp17 can be imported into mitochondria even without ATP, the main energy source needed for a functional import motor.

The aim of this work is to investigate the import pathway of Mrp17 in more detail, in particular how the protein passes the IM. I want to focus on the importance of the energetic factors that drive mitochondrial import, the membrane potential, and the import motor. Therefore, I want to establish a system to deplete essential constituents of the PAM complex. Furthermore, I want to generate a reporter system to investigate the exact localization of proteins within mitochondria. With the reporter system, it should be possible to conclude whether a protein is located in the IMS or in the matrix. Additionally, I want to use proximity labeling followed by proteomics to have a global view on the submitochondrial proteome under low energy conditions. The matrix and the IMS of mitochondria contain distinct sets of proteins to carry out their compartment-specific functions. Whether mitochondrial dysfunction upon ATP depletion affects the intramitochondrial distribution of proteins is not known. Using the mitoribosomal protein Mrp17 as a model, I want to answer whether the possibly distinct import pathway of Mrp17 is a common feature of MRPs to be able to be imported into mitochondria under low ATP level conditions. Furthermore, it would be interesting to check if the 25% of MRPs that do not have a conventional MTS are the ones being imported under these conditions.

3 RESULTS

3.1 Mrp17 uses the translocation route through the TOM and TIM complex

Most matrix proteins contain N-terminal mitochondrial presequences that guide the precursor proteins into the mitochondrial matrix. However, about 25% of all mitoribosomal proteins (MRPs) in yeast lack such conventional MTS and use internal targeting sequences instead. Why mitoribosomal proteins use such unconventional targeting signals is unknown. One of these proteins is the mitoribosomal protein Mrp17 (bS6m). In my previous studies, I characterized the targeting signal of Mrp17 and was able to determine an internal targeting sequence that could not be predicted *in silico*. I wanted to figure out if Mrp17, despite the unconventional targeting sequence, still takes the typical precursor pathway into the matrix. To investigate this, I performed *in vitro* imports with deletion and temperature-sensitive (*ts*) mutants of different components of the translocation machinery. Isolated mitochondria were energized by ATP and NADH and incubated with radiolabeled protein. After the indicated time points, the import reaction was stopped, and external Proteinase K (PK) was added to degrade non-imported proteins. Samples were separated in an SDS-PAGE and signals were detected by autoradiography.

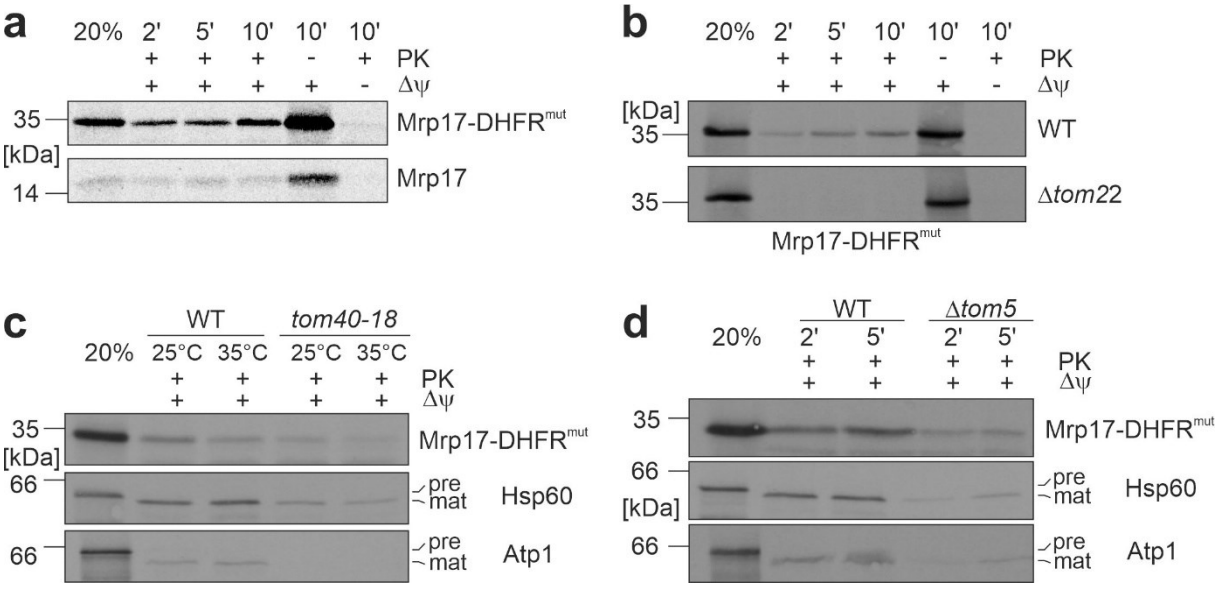

Fig. 9 | Mrp17 passes the OM via the TOM complex. (a-d) Radiolabeled Mrp17-DHFR^{mut}, Mrp17, Hsp60, and Atp1 was incubated with isolated mitochondria from wild type (WT) cells and the indicated mutants. In the case of the temperature-sensitive (ts) and the corresponding wild type mitochondria (c), samples were pretreated for 10 min at 35°C before the experiment. Non-imported protein was removed by treatment with Proteinase K (PK). To dissipate the membrane potential, a control sample was treated

with a mix of valinomycin, oligomycin, and antimycin A (VAO). The 20% sample shows one fifth of the radiolabeled protein that was used per time point of the import reaction. Shown is the autoradiography.

Due to the low number of methionine residues in Mrp17, fewer ^{35}S is incorporated and therefore the signal appeared weak in the autoradiogram (Fig. 9a). To add more methionine residues and thereby get a more intense signal, a variant of the cytosolic protein Dihydrofolate reductase $DHFR^{mut}$ which is unable to fold was fused to Mrp17. This fusion protein gave a strong signal in the autoradiogram and showed a similar import kinetic compared to Mrp17 (Fig. 9a). Therefore Mrp17-$DHFR^{mut}$ was used for the following *in vitro* import assays. To test whether the TOM complex is critical for the import of Mrp17, radiolabeled Mrp17-$DHFR^{mut}$ precursor was incubated with isolated mitochondria of *Δtom22* or *Δtom5* or with mitochondria of temperature-sensitive Tom40 (*tom40-ts*). Depletion of the receptor Tom22 resulted in no import of Mrp17 (Fig. 9b). Likewise, the depletion of Tom5 showed a highly reduced import rate (Fig. 9d). In mitochondria of the *tom40-ts* strain import of Mrp17 is already reduced under permissive temperatures which is exacerbated under higher temperatures (Fig. 9c). The control proteins Hsp60 and Atp1 that are known to use the TOM complex, show reduced import in both mutant strains. This suggests that Mrp17, just like typical MTS-containing proteins, interacts with the Tom20/Tom22 receptors and crosses the outer membrane through the TOM complex.

Next, I wanted to investigate how Mrp17 passes the inner membrane. To test if Mrp17 depends on the TIM23 complex, radiolabeled Mrp17-$DHFR^{mut}$ precursor was incubated with isolated mitochondria of *tim17-ts*.

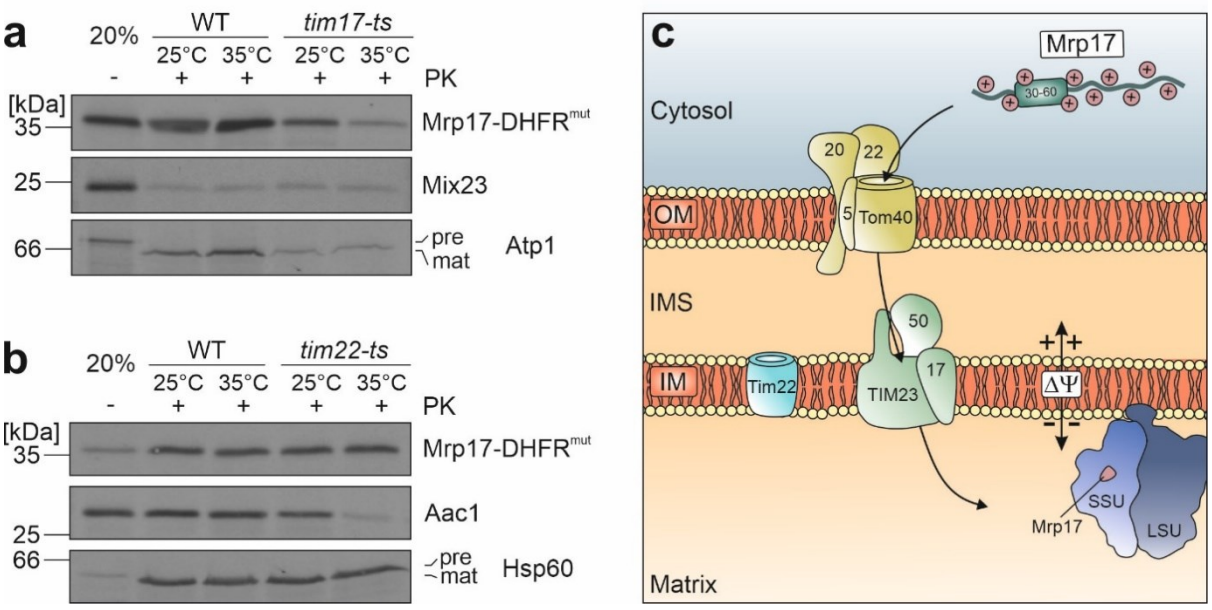

Fig. 10 | Mrp17 is translocated into the matrix through the TIM23 complex. (a-b) Radiolabeled Mrp17-DHFR^{mut}, Hsp60, Atp1, Mix23, and Aac1 was incubated with isolated mitochondria from wild type (WT) cells and the indicated mutants. Temperature-sensitive (ts) and the corresponding wild type mitochondria samples were pretreated for 10 min at 35°C before the experiment. Non-imported protein was removed by treatment with Proteinase K (PK). The 20% sample shows one fifth of the radiolabeled protein that was used per time point of the import reaction. **(c)** Schematic model of the import pathway of Mrp17. The internal targeting signal of Mrp17 is recognized by the receptors of the TOM complex and guided through the Tom40 channel. The TIM23 complex is needed for translocation across the inner membrane. In the matrix, Mrp17 is not processed by a peptidase before it is assembled into the mitoribosome.

Mrp17 import efficiency decreases in the *ts* mutant and is even more impaired under higher temperatures. Radiolabeled Atp1, a control that is known to be dependent on the TIM23 complex, shows also a decreased import rate. In contrast, radiolabeled Mix23 which is independent of TIM23 doesn't show reduced import efficiency compared to the WT (Fig. 10a). Another translocase of the inner membrane is Tim22. Aac1, a carrier protein that is laterally released into the inner membrane by Tim22 showed hardly any import into *tim22-ts* mitochondria. In contrast, the matrix protein Hsp60 can be imported into mitochondria at the same rate as in WT mitochondria. Likewise, Mrp17 can be efficiently imported into isolated *tim22-ts* mitochondria (Fig. 10b). These results show that Mrp17 despite its unconventional targeting signal is imported like other typical MTS-containing proteins. It interacts with the receptors of the TOM complex Tom22 and Tom20 and is translocated through the Tom40 channel. Translocation into the matrix is mediated by Tim17 or in more general via the TIM23 complex (Fig. 10c). In the matrix, Mrp17 is not cleaved by MPP as no processing can be detected in the *in vitro* imports (Fig. 9 a-d, Fig. 10 a, b).

3.2 The membrane potential is the main driver of Mrp17 translocation

Further, I wondered how the translocation process is energized. The two main energetic factors that drive the import reaction are the membrane potential at the inner membrane and the import motor with its core component mtHsp70 which is associated with the TIM23 complex. To test if the import of Mrp17 relies on the membrane potential radiolabeled precursor was incubated with isolated WT mitochondria that were treated with different concentrations of the ionophore CCCP that uncouples the membrane potential.

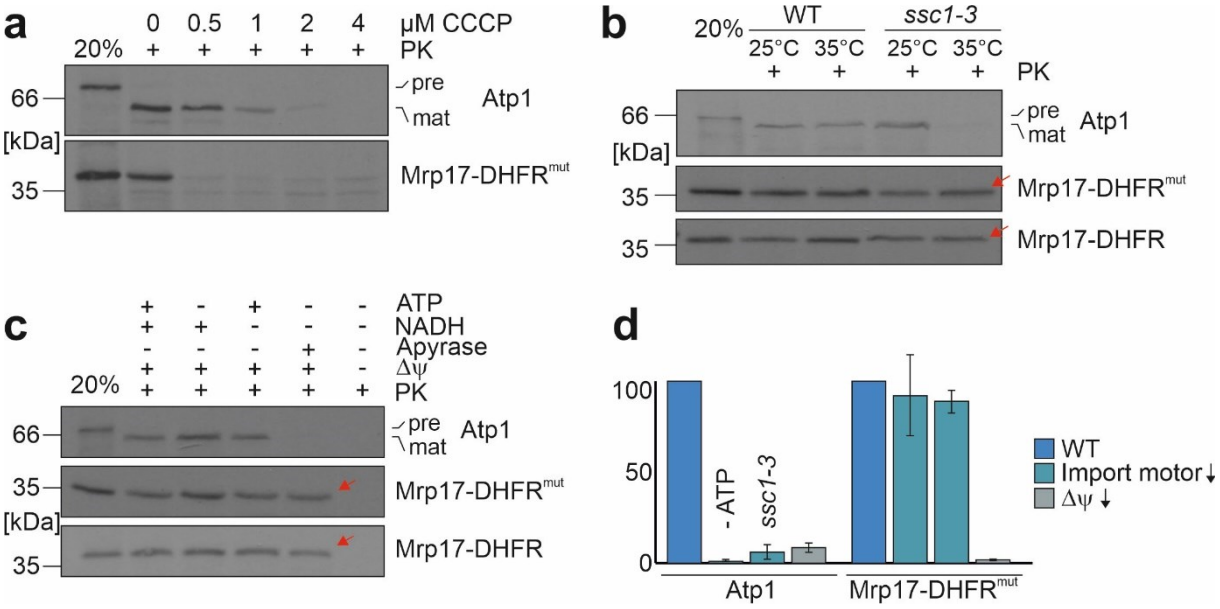

Fig. 11 | Mrp17 translocation is highly dependent on the membrane potential. (a-c) Radiolabeled Mrp17-DHFR^{mut}, Mrp17-DHFR, and Atp1 was incubated with isolated mitochondria from wild type (WT) cells and the indicated mutants. **(a)** To uncouple the membrane potential indicated concentrations of CCCP were added to the import reaction. **(b)** Temperature-sensitive *ssc1-3* and the corresponding wild type mitochondria samples were pretreated for 10 min at 35°C before the experiment. **(c)** To hydrolyze ATP Apyrase was added into the import reaction. To dissipate the membrane potential, a control sample was treated with a mix of valinomycin, oligomycin, and antimycin A (VAO). Non-imported protein was removed by treatment with Proteinase K (PK). The 20% sample shows one fifth of the radiolabeled protein that was used per time point of the import reaction. **(d)** Quantification of *in vitro* imports, n=3. Error bars indicate the standard deviation.

The control protein Atp1 is efficiently imported into WT mitochondria, however, the import abates with increasing concentration of CCCP. The effect of CCCP is even stronger for Mrp17-DHFR^{mut}. Already low amounts of CCCP prevented Mrp17 translocation into mitochondria. This shows that the import of Mrp17 is highly dependent on the membrane potential and even small changes in the membrane potential have a huge impact on the translocation capability of Mrp17 (Fig. 11a). Then I wanted to investigate the importance of the import motor for the translocation of

Mrp17. Therefore, the radiolabeled precursor was incubated with isolated mitochondria of temperature-sensitive *ssc1-3* and the corresponding WT. Ssc1 belongs to the Hsp70 family and is a constituent of the mitochondrial import motor. Under permissive temperature, Atp1 is efficiently imported into *ssc1-3* mitochondria however high temperature led to a total stop of Atp1 translocation into mitochondria. Surprisingly, the *ssc1-3* mutant showed no effect on the import ability of Mrp17-DHFR^{mut}. Even Mrp17 which is fused to tightly folded DHFR can be translocated into mitochondria (Fig. 11b). This suggests that Mrp17 does not depend on the import motor to get into mitochondria. To confirm this result, isolated WT mitochondria were treated with apyrase which hydrolyzes all ATP needed for a functional import motor. Similarly, Atp1 showed no import whereas the import of Mrp17-DHFR^{mut} as well as Mrp17-DHFR was unaffected by the treatment (Fig. 11c). These results suggest that typical MTS-containing proteins like Atp1 need the membrane potential as well as the import motor to get into mitochondria. However, Mrp17 does not need the import motor but is highly dependent on the membrane potential (Fig. 11d).

3.3 CRISPR interference (CRISPRi) efficiently depletes *TIM44*

Ssc1 is not only associated with the TIM23 complex but also functions as soluble foldase in the mitochondrial matrix. Therefore, the temperature-sensitive mutant as well as the depletion of ATP can have secondary effects on the import process. To specifically inhibit the import motor, I generated a knockdown strain of different subunits of the import motor (Tim14, Tim16) and Tim44. Tim44 tethers the import motor to the TIM23 complex, therefore depleting Tim44 should result in less complex bound mtHsp70. To knock down these proteins I used an inducible CRISPR interference (CRISPRi) approach that should quickly deplete these proteins from cells and thereby enable to study direct effects of losing the import motor. Another big advantage of CRISPRi is that essential proteins such as Tim44, where a knockout is lethal, can be investigated. CRISPRi is an established system that constitutively expresses catalytically dead Cas9 (dCas9) fused to the transcriptional repressor Mxi1. The gene-specific guide RNA (gRNA) is expressed from an inducible promotor in the presence of tetracycline (Fig. 12a). To get a knockdown strain I cloned different gRNAs into the CRISPRi plasmid and transformed these into yeast cells. The cells were grown in glucose media and induced with anhydrotetracycline (ATc). After 2 hours I harvested

the cells, isolated RNA, and tested the guide efficiency by quantitative real-time PCR (RT qPCR).

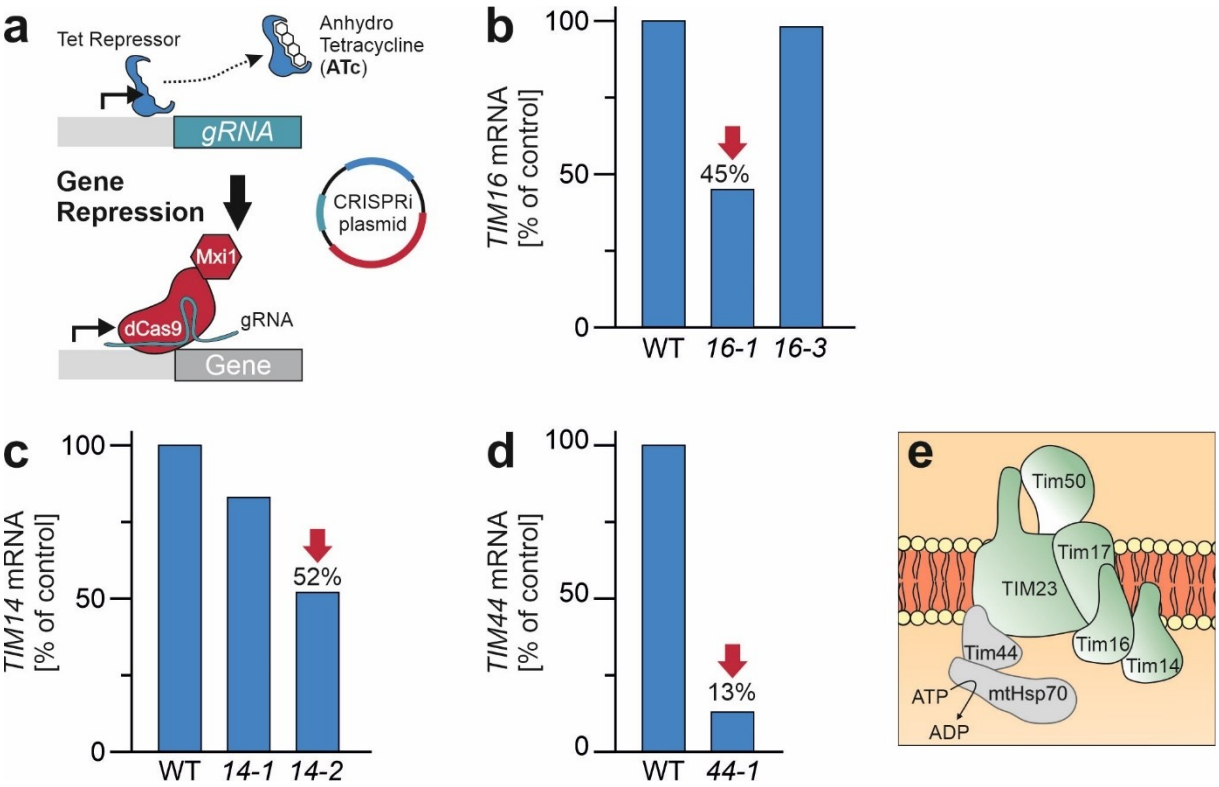

Fig. 12 | Addition of Tetracycline induces knockdown of TIM16, TIM14 and TIM44. (a) Schematic representation of the CRISPRi approach. The Tet Repressor is inhibited by ATc, which leads to the expression of a specific gRNA. The gRNA guides the dCas9-Mxi1 fusion to the promotor and thereby blocks transcription of the respective gene. **(b-d)** CRISPRi plasmid or empty vector was transformed into wild type cells. Cells were grown to early log phase and induced with 960 ng/ml ATc. RNA was isolated after 2h of induction and the mRNA levels were quantified by qPCR. **(e)** Tim44 tethers the core component of the import motor mtHsp70 to the TIM23 complex. Knockdown of TIM44 results in less complex bound mtHsp70.

To knock down Tim16 and Tim14, I tested two different gRNAs. After 2 hours of induction, the mRNA of TIM16 was depleted to 45% by using guide 1, though guide 3 reduced the mRNA levels only by 2% (Fig. 12b). The mRNA of TIM14 was depleted to 83% with guide 1 and depleted to 52% with guide 2 (Fig. 12c). The mRNA of TIM44 was efficiently depleted to 13% (Fig. 12d). For further experiments, I decided to focus on the TIM44 knockdown strain. On one hand, the knockdowns of Tim14 and Tim16 were not as efficient as the knockdown of TIM44 and on the other hand, Tim44 might have a more direct effect on the functionality of the import motor, as it tethers MtHsp70 to the TIM23 complex (Fig. 12e).

To further validate the knockdown of TIM44, I wanted to check how fast the protein level of Tim44 is depleted. Therefore, I grew the cells in liquid glucose media and

induced the knockdown by the addition of ATc. Samples for whole cell lysates were taken before (0 h) and after 4 and 8 hours of induction, before they were analyzed via western blotting.

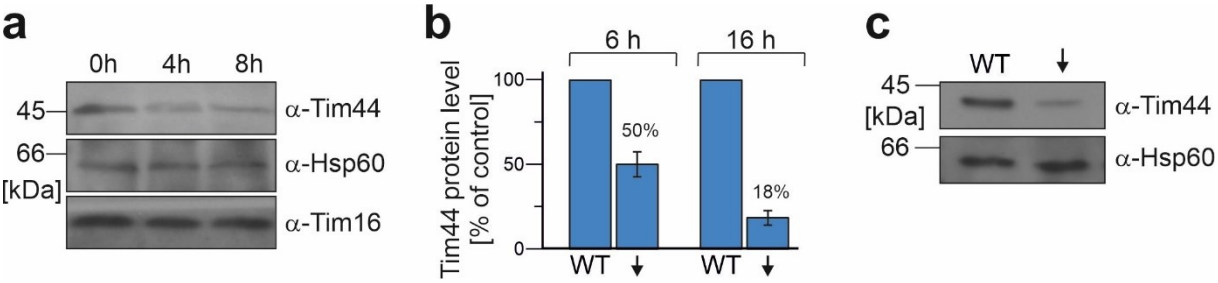

Fig. 13 | Tim44 protein levels are efficiently depleted. (a) Western blot analysis of whole cell lysates. WT cells with CRISPRi-TIM44 plasmid were induced with 960 ng/ml ATc. Cells were harvested after indicated time points, lysed, and separated by SDS-PAGE. Protein levels of Tim44, Hsp60, and Tim16 were analyzed. **(b)** Quantification of Western blot analysis. Cells were grown in liquid galactose media and induced with ATc. Mitochondria were isolated after indicated time points. Protein levels of Tim44 were analyzed in WT cells and quantified. n=4 **(c)** Western blot of isolated mitochondria. Cells were grown in liquid galactose media and mitochondria were isolated after 18h of ATc induction.

The protein level of Tim44 decreases to ~40% already after 4 hours of induction and to ~35% after 8 hours. For quantification, 3 replicates were used (data not shown) and one replicate is shown in Fig. 13a. This proves that also on protein level CRISPRi knockdown rapidly depletes Tim44. Tim16 which is another component of the TIM23 complex doesn't show changes in protein level, indicating that TIM44 knockdown does not affect protein stability of other components of the complex. To optimize the western blot analysis and get clearer bands I isolated mitochondria of WT cells with an empty vector or CRISPRi plasmid. Cells were grown in liquid galactose medium, induced with ATc for indicated time points. For the Quantification of the western blot, four biological replicates were used. After 6 hours of induction, 50% of Tim44 was left. After 16 hours of induction, the protein level further decreased to 18% (Fig. 13b). A western blot of isolated mitochondria clearly shows the reduced protein level of Tim44, demonstrating again an efficient and reproducible depletion of Tim44 (Fig. 13c).

As the deletion of Tim44 is lethal, I wondered if depleting Tim44 also has a strong impact on the fitness of the cell and on mitochondrial function. Therefore, I performed growth assays in liquid media. WT cells harboring an empty vector or the CRISPRi-TIM44 plasmid were grown in galactose-containing media. Cells were diluted into media containing fermentable or non-fermentable carbon sources in a 96-well plate

format. The OD_{600} was measured in a 96-well plate reader every 10 minutes for 72 hours while shaking.

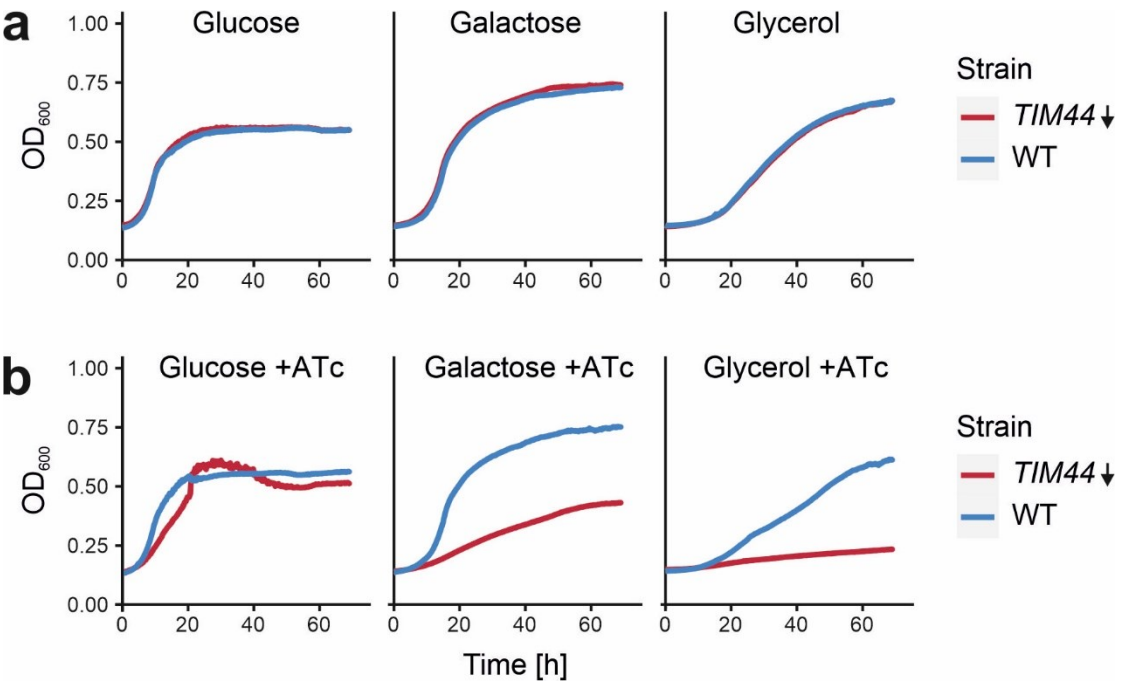

Fig. 14 | Growth on respiratory media is highly impaired in the CRISPRi-TIM44 strain. (a,b) WT cells with an empty vector (WT) or CRISPRi-TIM44 plasmid were grown on galactose medium. Cells were diluted in 96 well plates into media containing indicated carbon sources and grown at 30°C. The graphs show the mean values of three technical replicates. **(b)** Cells were preincubated with ATc 6h before starting the measurements. Fresh ATc was added into the wells.

The growth curves show that without addition of ATc, the CRISPRi strain grows like the WT strain on all of the three different media (Fig. 14a). However, upon induction with ATc, the CRISPRi strain has a strong growth defect on the respiratory medium glycerol and on the fermentable media galactose. Only on the fermentable glucose medium, the CRISPRi strain grows like the WT (Fig. 14b). This result indicates that the depletion of Tim44 has a strong effect on the function of mitochondria.

3.4 Tim44 deficient mitochondria can translocate Mrp17

Since Tim44 can be efficiently depleted, this strain is well-suited to study the import ability of mitochondria in which the PAM complex is specifically inhibited. I wanted to validate my previous findings that Mrp17 can be translocated into mitochondria even without a functional import motor. Therefore, I induced the knockdown of TIM44 via the addition of ATc. As control, ATc was added to wild type cells containing an empty vector. After 18 hours of induction, mitochondria were isolated and incubated with radiolabeled precursor protein for indicated time points.

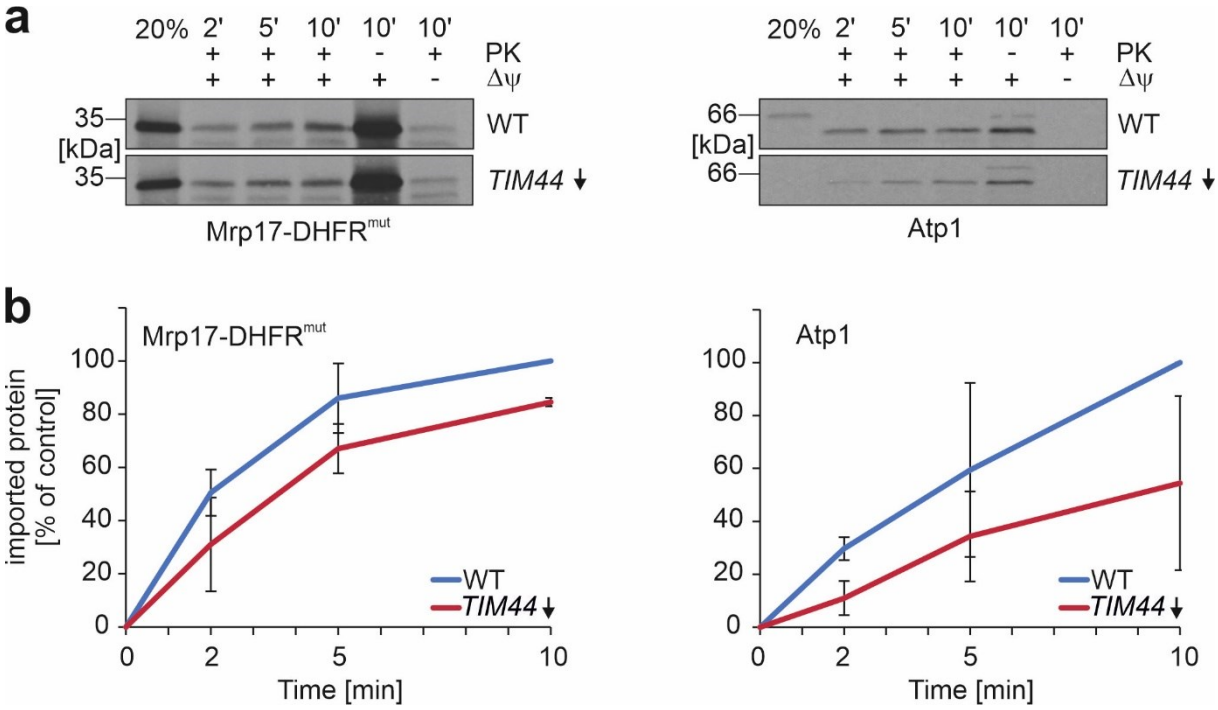

Fig. 15 | Mrp17 is translocated into Tim44 depleted mitochondria. (a) Radiolabeled Mrp17-DHFR^{mut} and Atp1 was incubated with isolated mitochondria from wild type (WT) and CRISPRi-*TIM44* cells. Samples were incubated at 30°C for indicated time points. Non-imported protein was removed by treatment with Proteinase K (PK). A control sample was treated with a mix of valinomycin, oligomycin and antimycin A (VAO) to dissipate the membrane potential ($\Delta\Psi$). The 20% sample shows one fifth of the radiolabeled protein used per time point of the import reaction. **(b)** Quantification of *in vitro* import assay as shown in (a). Error bars indicate the standard deviation. n=3

Atp1 that depends on the import motor can be efficiently imported into wild type mitochondria. However, knockdown of TIM44 leads to a decreased import rate. In contrast, Mrp17-DHFR^{mut} is efficiently imported into wild type and Tim44 depleted mitochondria (Fig. 15a). Quantification of three replicates show that depletion of Tim44 has a more severe effect on Atp1 compared to Mrp17-DHFR^{mut} (Fig. 15b). In line with the previous results, this suggests that, unlike other matrix proteins, Mrp17 does not need the import motor to be translocated into mitochondria.

3.5 Sublocalized viral proteases used as a reporter system for tracking mitochondrial import into subcompartments

The previous results show that Mrp17 can be imported into mitochondria without the import motor. However, it is impossible to determine where Mrp17 is exactly located within mitochondria. Mrp17 is protected from the PK digest and thus the outer membrane has been passed. Since there is no processing in the matrix, the final destination is not clear. Therefore, I wanted to establish an *in vitro* assay with which it

is possible to conclude the sublocalization within the organelle. The idea is, to express and guide a viral protease in one of the subcompartments of mitochondria and add radiolabeled precursor protein that is fused to multiple cleavage sites (cs) that are specifically recognized and cleaved by the respective viral protease. Hence, cleavage would mean that the protease and precursor have met and are in the same subcompartment, such as the mitochondrial matrix (Fig. 16a). Since enzymatic activity highly depends on the conditions and I don't know which would work within yeast mitochondria, I screened for several different viral proteases (Appendix Table 1). Each of them was fused to Su9, a commonly used mitochondrial targeting signal that guides the protease into the matrix. To guide the protease into the intermembrane space (IMS), the protease was fused to the first 70 amino acids of Mia40 which anchors the protease in the IM (Fig. 16b).

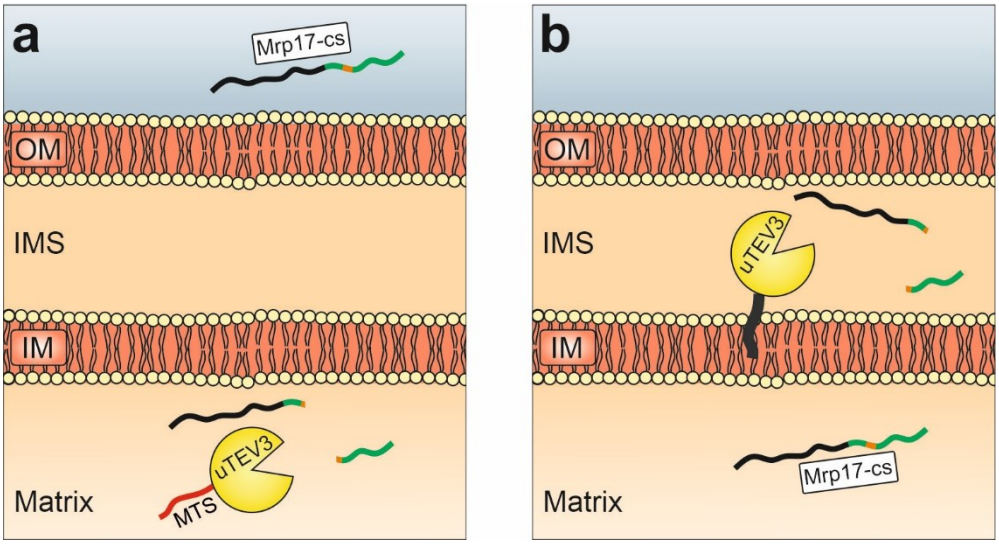

Fig. 16 | Protease reporter system to determine submitochondrial localization. (a) Scheme of the viral protease reporter system in the matrix. The MTS Su9 guides the viral protease uTEV3 into the mitochondrial matrix. If the protein of interest reaches the mitochondrial matrix, the protease recognizes and cleaves the fused cleavage site. **(b)** Scheme of the viral protease reporter system in the IMS. The membrane anchor of Mia40 guides the viral protease uTEV3 into the IMS. If the cleavage site fusion protein is localized to the IMS it gets cleaved by the protease, if the fusion protein reaches the matrix it is protected from the protease and remains uncleaved.

These proteases were integrated into the genome and constitutively expressed. To ensure that the expressed viral proteases do not negatively affect the fitness of the cells, I performed drop dilution assays.

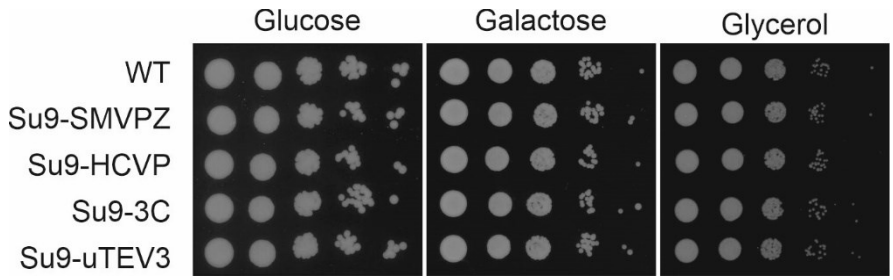

Fig. 17 | Viral proteases have no negative effect on cell growth. Cells of the indicated strains were grown to log phase in galactose medium before tenfold serial dilutions were dropped onto plates with the indicated carbon sources and incubated at 30°C.

All tested proteases grew exactly like the wild type strain on fermentable as well as respiratory medium (Fig. 17). This suggests that the expression of the proteases does not harm the cell or mitochondrial fitness.

The big advantage of these viral proteases is that they have a highly specific recognition and cleavage site which is not found in the yeast proteome. These sites were fused to the protein of interest from which the localization should be determined. The cleavage sequence consists of six different cleavage sites as I started with six different viral proteases (Fig. 18a). However, I was able to create expression plasmids of only four proteases. To test if the viral proteases can cleave and are functional in the mitochondrial matrix, I performed *in vitro* import assays. Radiolabeled precursor protein was incubated with isolated mitochondria containing the respective viral protease or wild type mitochondria. Proteinase K was added after the indicated time points to digest non-imported precursors.

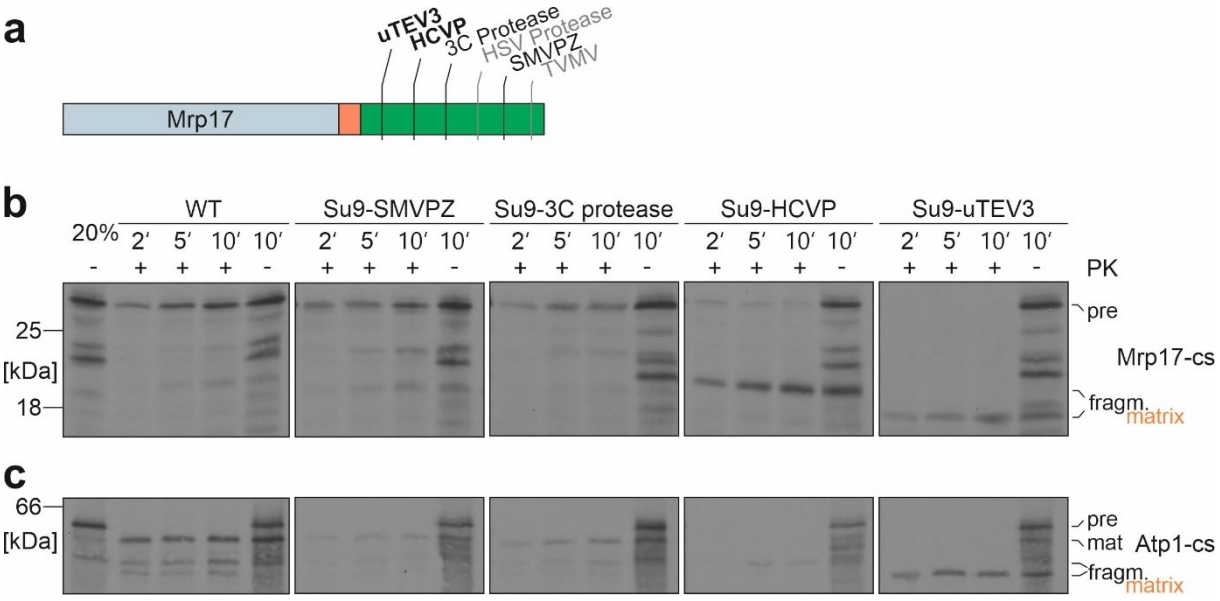

Fig. 18 | Viral Proteases cleave the cleavage sequence in the mitochondrial matrix. (a) Scheme of the fusion protein. The protein of interest e.g., Mrp17 is fused to a linker sequence (orange) and the cleavage sequence (green). This sequence contains the recognition and cleavage site of the six indicated proteases. **(b, c)** Radiolabeled Mrp17-cs and Atp1-cs was incubated with isolated mitochondria from wild type (WT) cells and cells expressing the indicated proteases. Samples were incubated at 30°C for indicated time points. Non-imported protein was removed by treatment with Proteinase K (PK). The 20% sample shows one fifth of the radiolabeled protein used per time point of the import reaction.

Mrp17-cs, as well as Atp1-cs, can be efficiently imported into wild type mitochondria. Hence, the fused cleavage sites do not impair the import capability. Cleavage of SMVPZ should result in a Mrp17 fragment around 23 kDa, but most imported Mrp17-cs remain uncleaved. A similar result can be seen for mitochondria with the 3C protease. Mrp17-cs can be imported but is not cleaved. Otherwise, mitochondria containing the HCV protease, import and efficiently cleave Mrp17-cs, resulting in a fragment around 19 kDa. The protease uTEV3 cleaves Mrp17-cs even more efficiently, as only the fragment around 17 kDa is detectable, and none of the precursor form (Fig. 18b). The same result can be seen for Atp1-cs, SMVPZ and 3C do not show any cleavage. HCVP, as well as uTEV3, cleave imported Atp1-cs (Fig. 18c). According to these results, I will use the strains expressing HCVP or uTEV3 for the following experiments.

The viral proteases are targeted into the matrix and have to be imported via the presequence pathway. Thereby the proteases must traverse the IMS and might have contact with proteins located in the IMS. To be sure that the proteases specifically cleave proteins in the matrix and not proteins located in the intermembrane space, I performed an *in vitro* import with b2-DHFR-cs which localizes to the IMS.

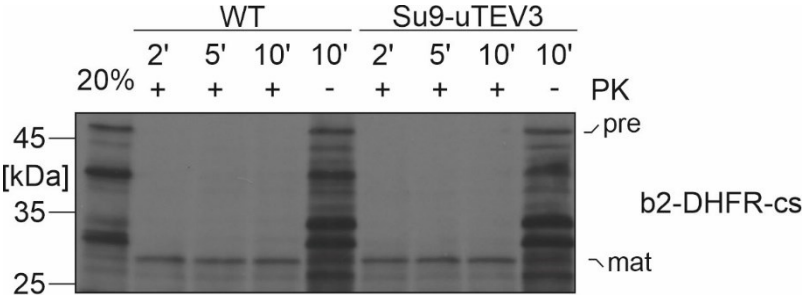

Fig. 19 | Matrix-targeted viral protease does not cleave the IMS protein. Radiolabeled b2-DHFR-cs was incubated with isolated mitochondria from wild type (WT) cells and cells expressing Su9-uTEV3. Samples were incubated at 30°C for indicated time points. Non-imported protein was removed by treatment with Proteinase K (PK). The 20% sample shows one fifth of the radiolabeled protein used per time point of the import reaction.

This fusion protein is imported into mitochondria as it is PK-resistant. However, it does not show cleavage by uTEV3, demonstrating the compartment-specific cleavage of the matrix-targeted protease (Fig. 19).

3.6 Mrp17 is efficiently imported into the IMS of ATP-depleted mitochondria

With the newly established reporter system, it is possible to determine the submitochondrial localization of proteins *in vitro*. The question I want to answer now is whether Mrp17 can reach the mitochondrial matrix without the import motor. Therefore, isolated mitochondria with or without the matrix HCV protease were incubated with radiolabeled precursor protein (Fig. 20a). Before adding precursor protein to the reaction, samples were treated with Apyrase to hydrolyze ATP, thereby inactivating the import motor.

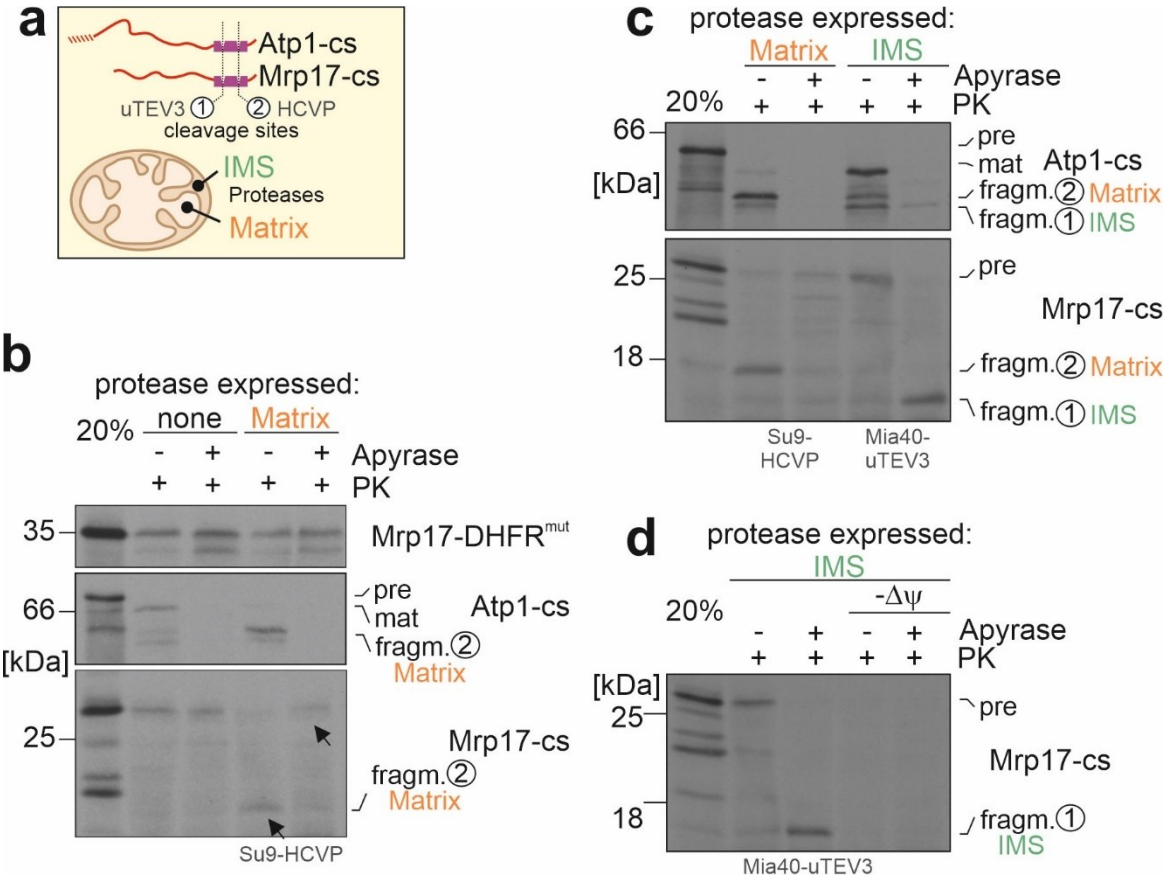

Fig. 20 | ATP depletion leads to mislocalization of Mrp17 into the IMS. (a) Proteases are localized either into the IMS or matrix. Atp1 or Mrp17 are fused to multiple recognition sites that can be cleaved by the respective protease. **(b-d)** Radiolabeled Mrp17-DHFR^{mut}, Atp1-cs, and Mrp17-cs was incubated with isolated mitochondria from wild type (WT) cells and cells expressing Su9-HCVP or IMS-uTEV3. Apyrase was added to indicated samples and were incubated at 30°C for 5 minutes. Non-imported protein was removed by treatment with Proteinase K (PK). To dissipate the membrane potential, a control sample was treated with a mix of valinomycin, oligomycin, and antimycin A (VAO).

The 20% sample shows one fifth of the radiolabeled protein that was used per time point of the import reaction.

As seen in previous experiments Mrp17-DHFR^{mut} is resistant to PK digest even in apyrase-treated samples, meaning that Mrp17-DHFR^{mut} passed at least the outer membrane (Fig. 20b). Atp1-cs is imported and cleaved by HCVP in the untreated sample which is not the case if Apyrase is added into the reaction. As expected Atp1-cs cannot be imported if apyrase was added to the reaction. In contrast, Mrp17-cs is imported in both cases, as shown previously, however not cleaved in the Apyrase sample. This implies that Mrp17 crosses the OM but gets stuck in the IMS upon depletion of ATP (Fig. 20b). To validate that Mrp17 is localized to the IMS under this condition, I isolated mitochondria from cells that express IMS-uTEV3 and repeated the experiment. Under normal conditions, Mrp17-cs is imported into mitochondria but low levels of ATP lead to cleavage of Mrp17-cs by uTEV3, meaning that Mrp17 is localized to the IMS (Fig. 20c). Only depleting the membrane potential by adding a mixture of valinomycin, antimycin A, and oligomycin (VAO) lead to no import of Mrp17-cs (Fig. 20d).

Depleting ATP by the external addition of apyrase is an artificial way to mimic low energy levels within mitochondria. To investigate a more physiological condition I wanted to perform *in vitro* import assays with isolated mitochondria which lack Atp23. Atp23 is a protease that processes Atp6, a subunit of the F_0 sector of mitochondrial ATP-synthase. Deletion of Atp23 leads to less functional ATP-synthase and therefore to low ATP levels in mitochondria [108].

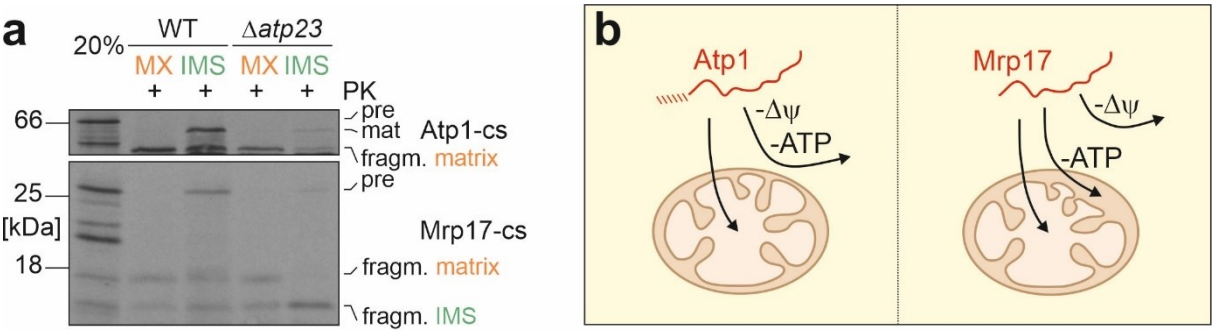

Fig. 21 | Depletion of the ATP-synthase leads to the localization of Mrp17 into the IMS. (a) Radiolabeled Atp1-cs and Mrp17-cs was incubated with isolated mitochondria from wild type (WT) and *Δatp23* cells expressing Su9-HCVP or IMS-uTEV3. Samples were incubated at 30°C for 5 minutes. Non-imported protein was removed by treatment with Proteinase K (PK). The 20% sample shows one fifth of the radiolabeled protein that was used per time point of the import reaction. **(b)** Schematic model of translocation of Atp1 and Mrp17 under different energetic conditions. Atp1 needs the membrane potential as well as the import motor to be translocated into mitochondria. Mrp17 also

needs both factors to reach the matrix. If ATP levels are low but the membrane potential is intact, Mrp17 can be localized into the IMS.

Atp1-cs can be imported in *⊿atp23* mitochondria though in lower amounts compared to the wild type. The import rate of Mrp17-cs into *⊿atp23* mitochondria is not reduced compared to the wild type. Matching to previous results, Mrp17-cs is cleaved by the IMS protease in the mutant (Fig. 21a). Translocation seems even more efficient. By inhibiting the ATP-synthase, the membrane potential tends to be higher, which could explain the slightly increased import rate. However, inhibition of the ATP-synthase and thus low ATP levels lead to the mislocalization of Mrp17 into the intermembrane space, again supporting the previous findings (Fig. 21b).

3.7 APEX-based mapping of the submitochondrial proteome

Previous experiments show that Mrp17 is routed into the IMS under low ATP levels. In contrast, other matrix proteins like Atp1 cannot be translocated into mitochondria. This raises the question of whether other proteins behave similarly to Mrp17. To address this point in a more global fashion I utilized APEX labeling and mass spectrometry to analyze the proteome of the mitochondrial intermembrane space. Previous studies showed that APEX2, an engineered and improved version of ascorbate peroxidase, is well suited for proteomic mapping as it biotinylates proteins with spatial and temporal control in subcellular compartments as well as mitochondrial subcompartments [13,109,110]. I generated strains in which APEX2 was targeted selectively to the IMS or the matrix by fusion of subcompartment-specific targeting sequences (Fig. 22 a, b). However, since the budding yeast *Saccharomyces cerevisiae* has an impermeable cell wall for biotin-phenol, the labeling has to be performed on isolated mitochondria. After isolation, mitochondria were incubated with biotin-phenol, and hydrogen peroxide was added to start the labeling reaction (Fig. 22a).

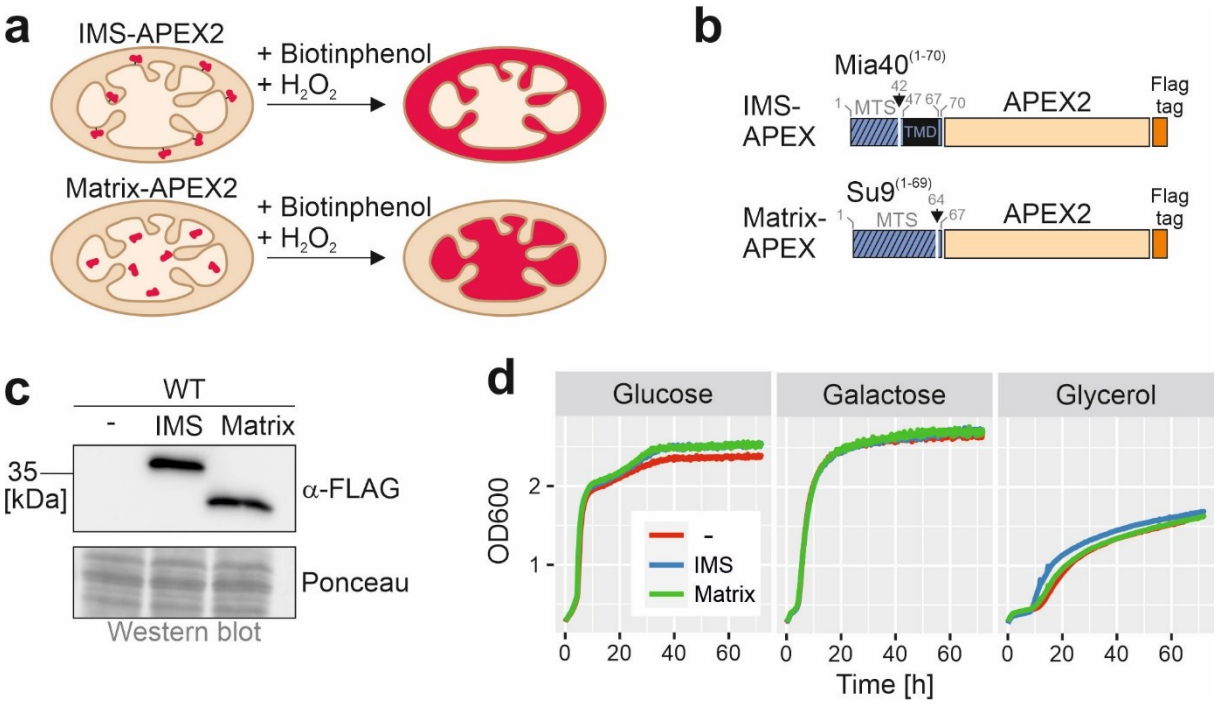

Fig. 22 | APEX2 expression does not compromise mitochondrial fitness. (a) Scheme of Compartment-specific proximity labeling. APEX2 is targeted to either the IMS or the matrix. Isolated yeast mitochondria are treated with biotin-phenol and hydrogen peroxide to label subcompartments of mitochondria. **(b)** Scheme of APEX2 fusion protein. The targeting sequence of Mia40 is fused to APEX2 and a FLAG-tag. The transmembrane domain (TMD) anchors the APEX2 into the inner membrane. Su9 presequence is used to target APEX2 into the matrix. **(c)** Whole cell lysates of wild type cells expressing no APEX (-), IMS-APEX or matrix-APEX are analyzed via western blot. Ponceau was used as loading control. FLAG-antibody was used to detect fusion proteins. **(d)** WT cells with or without APEX2 were grown in galactose medium. Cells were diluted in 96 well plates into media containing indicated carbon sources and were grown at 30°C. The graphs show mean values of three technical replicates.

Western blot analysis of whole cell lysates show that both APEX2 fusions are detectable with a FLAG-antibody (Fig. 22c). To ensure that APEX2 fusions do not have a negative effect on the cellular and mitochondrial fitness, I performed growth curves. Strains with or without APEX fusions were grown in galactose-containing liquid media. Cells were diluted into media containing fermentable or non-fermentable carbon sources in a 96-well plate format. The growth curves reveal that expression of APEX2 in the different subcompartments does not impair cell growth as the strains expressing APEX2 grow like the WT strain. Also, mitochondrial fitness is not affected as the growth rate is not compromised on respiratory glycerol media (Fig. 22d).

The accurate localization into the IMS and the matrix was confirmed by protease protection assays (Fig. 23a) and split-GFP reporters (Fig. 23b). For the protease protection assay isolated mitochondria were incubated with Proteinase K (PK) for 30 min on ice. Samples were analyzed via western blot.

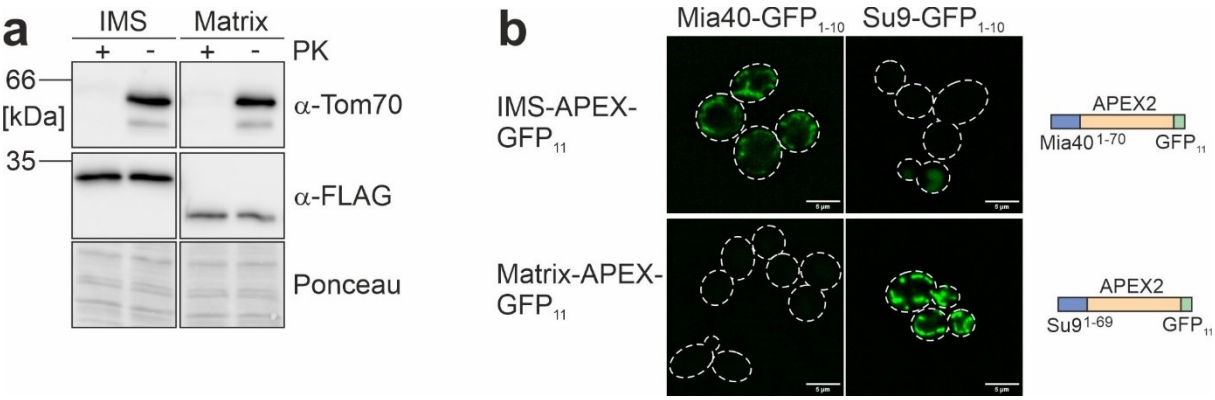

Fig. 23 | Submitochondrial localization of APEX2. (a) Mitochondria isolated from the indicated strains were treated with Proteinase K (PK) to show that the APEX2 enzymes are protease-inaccessible and thus within the mitochondria; the outer membrane protein Tom70 served as surface-accessible control. **(b)** Split-GFP reporters validate the location of the APEX2 enzymes in the IMS and matrix, respectively.

The outer membrane receptor Tom70 is degraded when PK is added. In contrast, Matrix-APEX as well as IMS-APEX are protected from PK digest indicating that both fusions are fully imported into mitochondria (Fig. 23a). PK digest can be used to determine whether the fusions are in the mitochondria or not. However, it does not tell whether the fusions are in the correct subcompartment. To answer this, I used a split-GFP reporter system. GFP_{1-10} was targeted selectively to the IMS or the matrix by fusion to subcompartment-specific targeting sequences. GFP_{11} was fused to IMS-APEX or Matrix-APEX. Both GFP_{1-10} and GFP_{11} fusions were constitutively expressed. Microscopic analysis showed that IMS-APEX-GFP_{11} interacts only with GFP in the IMS and not with GFP in the matrix. Matrix-APEX-GFP_{11} only gives signals with GFP in the matrix (Fig. 23b). These results indicate that both fusions are located within mitochondria and in the correct subcompartment.

As APEX2 is targeted to the correct subcompartment, biotin-phenol and hydrogen peroxide must be added so that APEX2 covalently labels surrounding proteins with the biotin-phenoxyl radicals (Fig. 24a). Since APEX labeling has been mainly used in human cells, I had to find the optimal conditions for yeast. Isolated mitochondria were incubated with biotin-phenol for 30 minutes. Hydrogen peroxide was then added to start the labeling reaction. After the indicated time points, the reaction was stopped with a quencher solution. The samples were analyzed by SDS-PAGE and western blot. Streptavidin was used to detect biotinylated proteins.

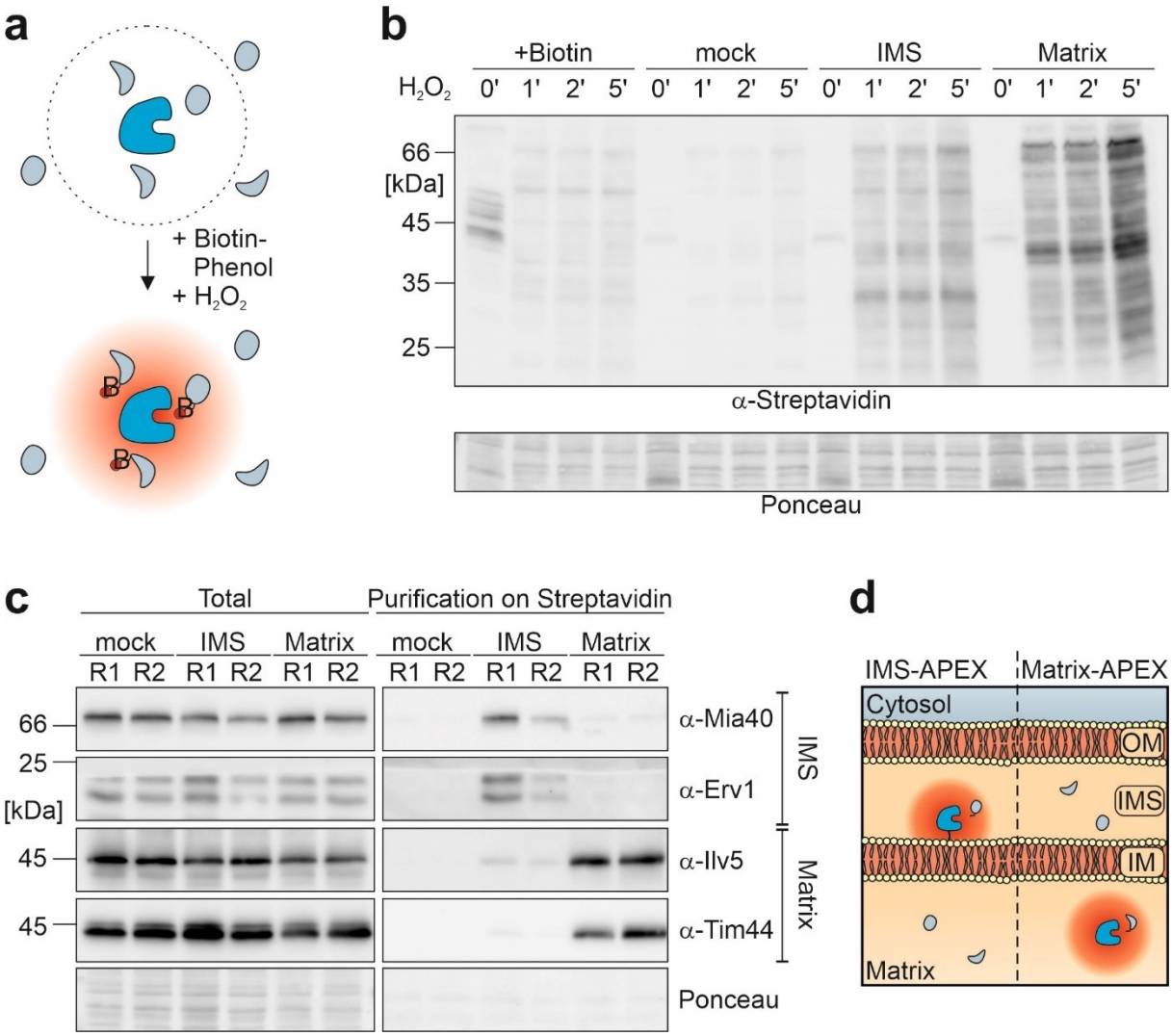

Fig. 24 | APEX2 functions in both subcompartments of mitochondria (a) Scheme of proximity-based APEX Labeling. The labeling reaction is started by adding biotin-phenol and hydrogen peroxide. **(b)** Mitochondria of the indicated strains were H_2O_2-treated for the times indicated before biotinylated proteins were visualized with luminol staining using peroxidase-coupled streptavidin. **(c)** Mitochondria of the indicated strains were H_2O_2-treated for 2 min and lysed. Biotinylated proteins were isolated with streptavidin-beads and subjected to Western blotting. Mitochondria of two biological replicates were used (R1, R2). **(d)** Scheme of APEX labeling within mitochondria. APEX targeted to the IMS specifically labels IMS proteins. APEX targeted to the matrix specifically labels matrix proteins.

Mitochondria from cells grown in full galactose medium (+Biotin) showed little background. This background could be further minimized by first growing the cells in full galactose medium and diluting them in medium without biotin 16 hours before mitochondrial isolation (mock). The addition of H_2O_2 to mitochondria with APEX in the IMS as well as in the matrix resulted in a rapid (within 1 min) accumulation of streptavidin-bound proteins. The amount of biotinylated protein could be minimally increased by a longer labeling time for IMS-APEX. With Matrix-APEX, the amount hardly changes from one to two minutes. However, more proteins accumulate after 5

minutes. The biotinylated proteins reveal subcompartment-specific patterns (Fig. 24b). To further verify that only proteins from the respective subcompartments were labeled, I performed APEX labeling followed by affinity purification on streptavidin beads and western blotting. Mia40 and Erv1 were selected as controls for the IMS and are enriched in the IMS-APEX sample. The matrix proteins Ilv5 and Tim44 are highly enriched in the matrix-APEX sample (Fig. 24c). This confirms the subcompartment-specific nature of the IMS-APEX- and matrix-APEX-based proximity labeling approach (Fig. 24d).

Next, I wanted to determine the subproteomes using mass spectrometry, therefore I isolated mitochondria of wild type cells expressing IMS-APEX, matrix-APEX, or no APEX enzyme (mock) in four replicates. Cells were grown in full galactose media. 16 hours before the isolation of mitochondria, the culture was diluted into galactose medium without biotin to reduce the background signal. After incubation of isolated mitochondria with biotin-phenol for 30 minutes and H_2O_2 for 5 minutes, biotinylated proteins were purified with magnetic streptavidin beads and analyzed by mass spectrometry (Fig. 25a).

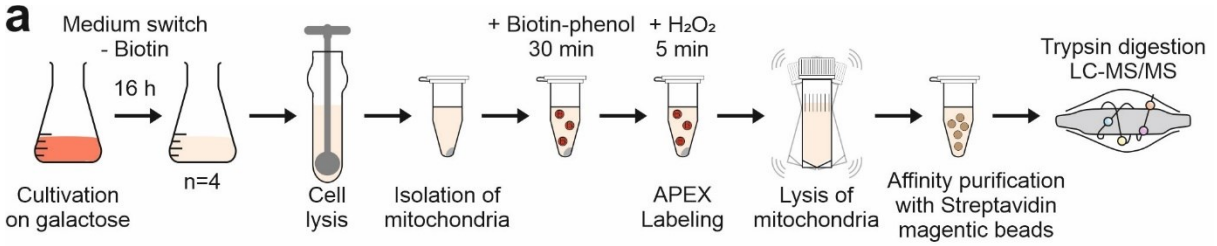

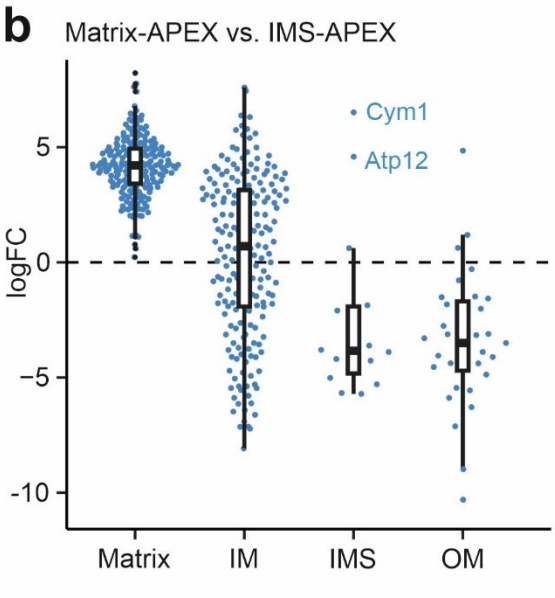

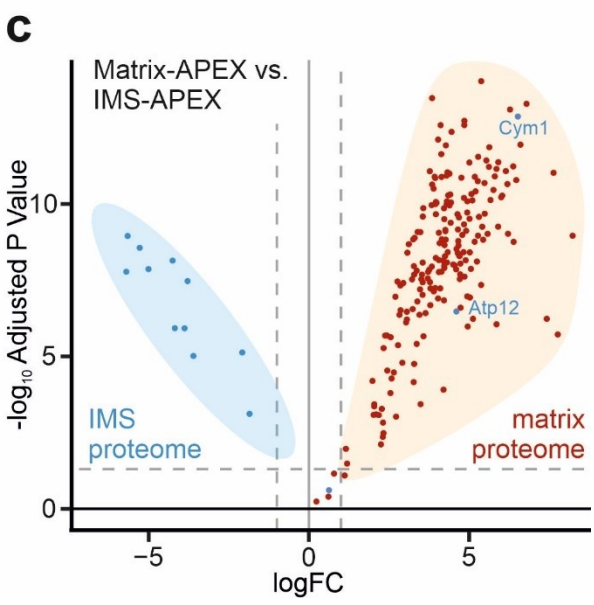

Fig. 25 | Proximity-based mapping of the submitochondrial proteome. (a) Schematic workflow of the proteomic analysis. Biotinylation patterns from n=4 experiments allowed to distinguish the proteins of the two mitochondrial subcompartments. **(b, c)** Relative enrichment (log2-fold change, logFC) for the samples indicated were plotted for proteins residing in the matrix, the inner membrane (IM), the intermembrane space (IMS) and the outer membrane (OM), respectively. Boxes of the violin plots represent the data range from the first (Q1) to the third quartile (Q3), with the line in the middle representing the median. The minimum/maximum whisker values were calculated as Q1/Q3 ± 1.5 * interquartile range (IQR). The volcano plot shows the comparison of the IMS (blue) and the matrix proteome (red).

Both APEX reporters were highly specific: matrix proteins were predominantly biotinylated by the matrix-APEX enzyme and IMS and outer membrane proteins by the IMS-APEX enzyme (Fig. 25 b, c). Inner membrane proteins showed a mixed behavior, reflecting their individual topology in the inner membrane (Fig. 25b). The proteins Cym1 and Atp12 which are listed as IMS proteins in the SGD database, behaved like matrix proteins (Fig. 25b) [111]. And indeed for both proteins experimental studies had documented the misdiagnosed IMS annotation and had proved their steady-state occurrence in the mitochondrial matrix [112,113]. Thus, using the APEX enzymes allows the reliable and comprehensive mapping of the submitochondrial localization of proteins on a proteome-wide scale.

3.8 Mitoribosomal proteins accumulate in the IMS of compromised mitochondria

Mitochondrial dysfunction impairs protein import efficiency and results in proteotoxic stress [3,4]. However, whether mitochondrial dysfunction also affects the intramitochondrial localization of proteins is unknown (Fig. 26a). Mitochondrial defects can arise from mutations of the mitochondrial genome, a common phenomenon in aging human cells [114]. Therefore, I used a mutant in which the *ATP6* gene of the mitochondrial genome was replaced by *ARG8* which had been modified to adhere to the mitochondrial genetic code (Fig. 26b) [115]. Thus, selection on arginine-deficient media prevents the loss of the mitochondrial genome (Fig. 26c). To prove that the mitochondrial genome is still present in the mutant strain, I performed an *in organello* translation where mitochondrial translation products are radiolabeled.

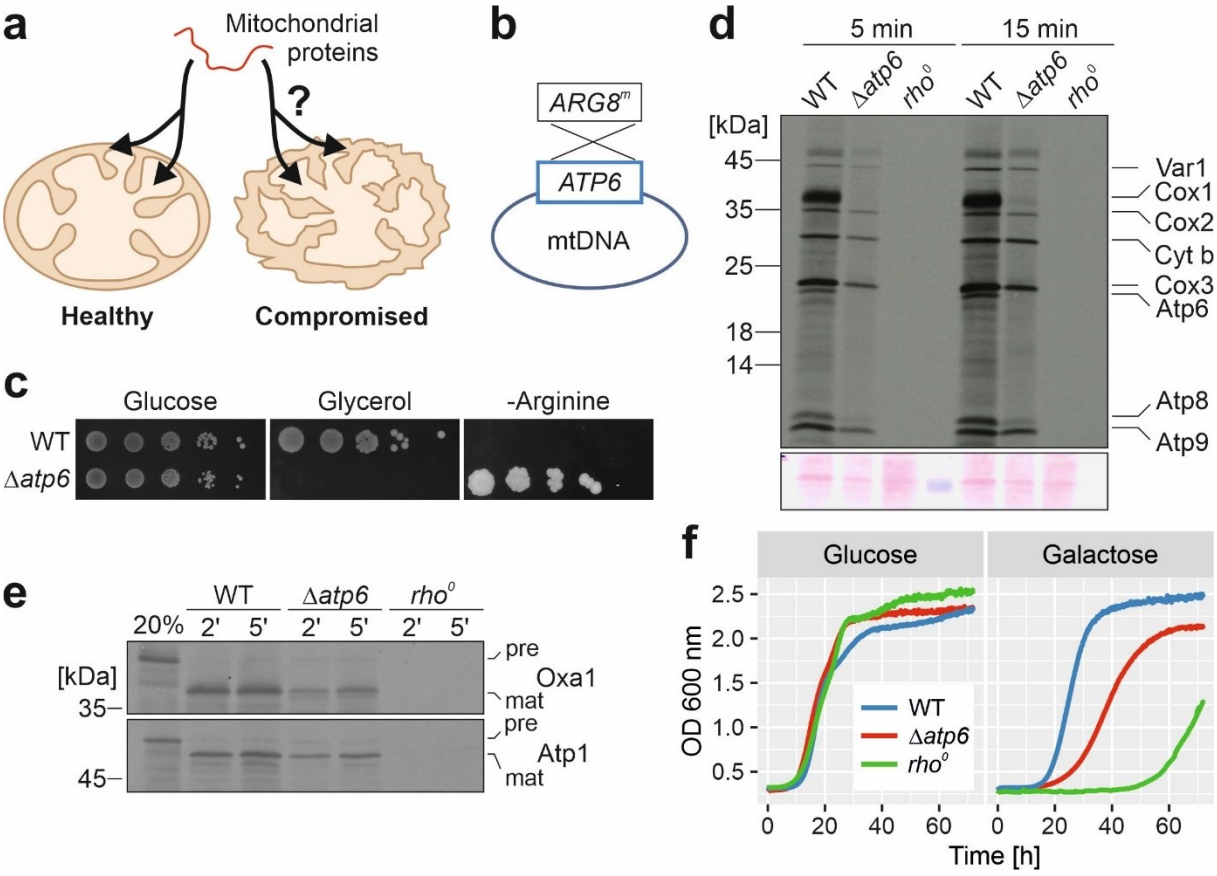

Fig. 26 | *Δatp6* mitochondria are compromised but can fulfill mitochondrial functions. (a) How mitochondrial dysfunction affects intramitochondrial localization is unknown. **(b)** *ATP6* gene is deleted by *ARG8* on the mitochondrial genome. **(c)** Mitochondrial translation products were radiolabeled in isolated mitochondria of the indicated strains for 10 min at 30°C. Radiolabeled proteins were separated by SDS-PAGE and visualized by autoradiography. Atp6 is only visible in the WT, confirming the deletion. **(d)** Radiolabeled Oxa1 and Atp1 was incubated with isolated mitochondria from wild type (WT), *Δatp6* and *rho*^{0} cells. Samples were incubated at 30°C for indicated time points. Non-imported protein was removed by treatment with Proteinase K (PK). The 20% sample shows one fifth of the radiolabeled protein that was used per time point of the import reaction. **(e)** Cells of the indicated strains were grown to log phase in galactose medium before tenfold serial dilutions were dropped onto plates with the indicated carbon sources and incubated at 30°C. **(f)** WT, *Δatp6,* and *rho*^{0} cells were grown in galactose medium. Cells were diluted in 96 well plates into media containing indicated carbon sources and were grown at 30°C. The graphs show mean values of three technical replicates.

The autoradiogram shows that, except for Atp6, all translation products can be translated. However, the translation rate is decreased in the mutant strain compared to the wild type, especially Cox1 and Atp8 show a lower translation rate (Fig. 26d). As control *rho*^{0} mitochondria were used. There is no translation in these mitochondria since they lost the mitochondrial DNA. To test if the mitochondria are competent to import proteins, I performed an *in vitro* import. Wild type, *Δatp6,* and *rho*^{0} mitochondria were incubated with radiolabeled precursors of Oxa1 and Atp1. The autoradiogram shows that Δ*atp6* mitochondria are competent to import proteins efficiently albeit at reduced rates compared to the WT (Fig 26e). Growth assays such as growth curves and drop dilutions reveal that the mutant strain can grow on fermentable media like the

wild type but is unable to grow on respiratory media (Fig. 26c). Growth on galactose media is impaired in the mutant strain but again shows that the strain has intermediate fitness between WT and the *rho*^{0} strain (Fig. 26f).

Since the *Δatp6* mutant strain has impaired ATPase activity but still can import proteins, albeit at reduced rates, I chose this mutant strain to express IMS- and matrix-APEX (Fig. 27a). As the *Δatp6* strain is not as fit as the wild type I wanted to check if the expression of the APEX fusions has a negative effect. Therefore, I performed growth curves in liquid media. *Δatp6* cells expressing no APEX, IMS-APEX, or matrix-APEX were grown in galactose-containing media. Cells were diluted into media with the indicated carbon source in a 96-well plate format. The OD600 was measured every 10 minutes for 72 hours while shaking.

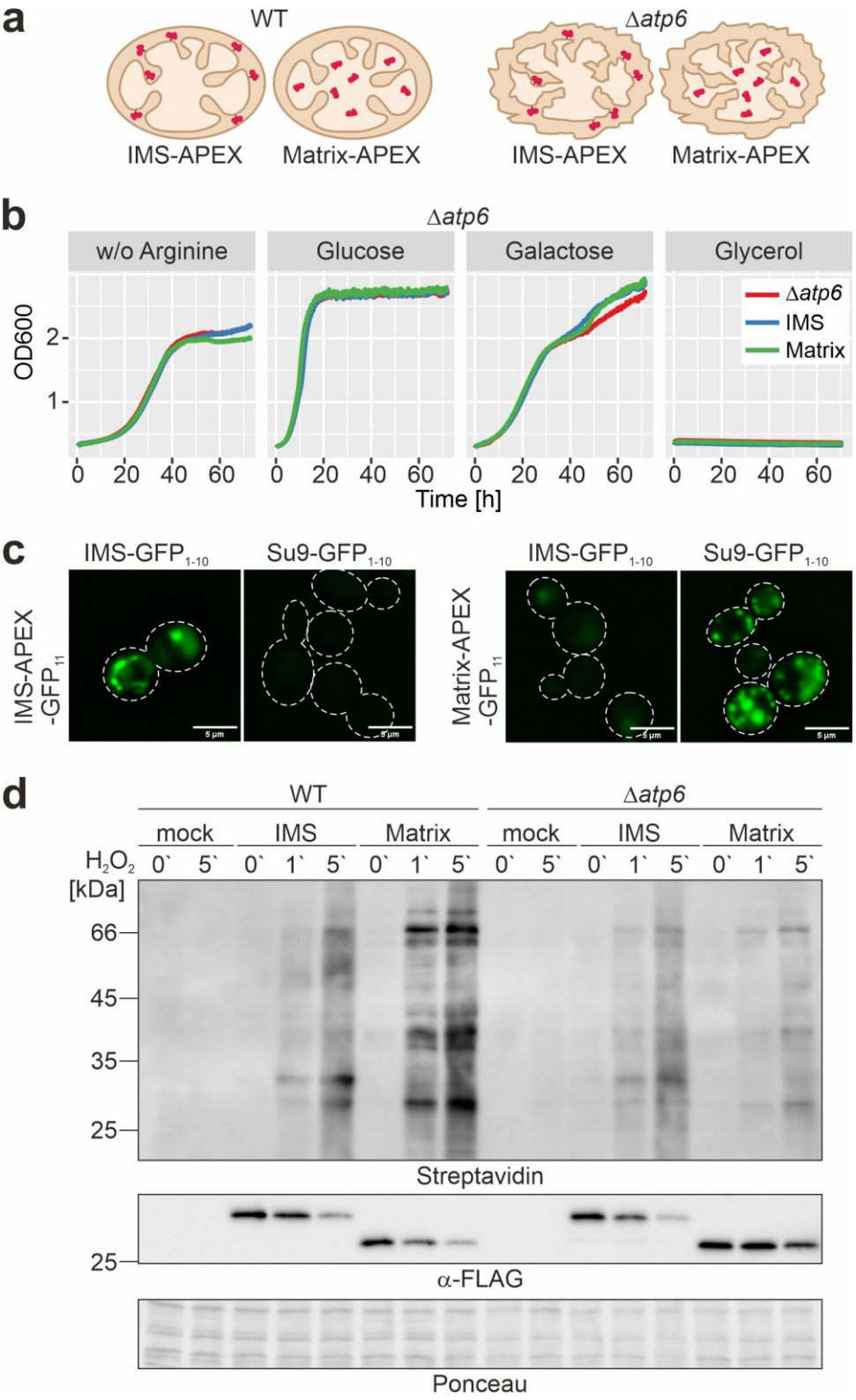

Fig. 27 | Expression of APEX fusions in *Δatp6* yield in a subcompartment-specific biotinylation pattern. (a) Targeting of APEX fusions into the IMS and the matrix in WT and *Δatp6*. **(b)** *Δatp6* cells expressing IMS-APEX, matrix-APEX, or no APEX enzyme were grown in galactose medium. Cells were diluted in 96 well plates into media containing indicated carbon sources and were grown at 30°C. Media without Arginine had the carbon source galactose. The graphs show mean values of three technical replicates. **(c)** Split-GFP reporters validate the location of the APEX2 enzymes in the IMS and matrix, respectively. **(d)** Mitochondria of the indicated strains were H_2O_2-treated for the times indicated before biotinylated proteins were visualized with luminol staining using peroxidase-coupled streptavidin. APEX fusions were visualized with a FLAG-antibody.

The growth curves show that the APEX fusions did not compromise cell growth. All strains contained their mitochondrial DNA as the strains can grow on arginine selective media (Fig 27b). Further, I checked with the split-GFP reporter if the APEX fusions are correctly localized. IMS-APEX-GFP_{11} only gives a signal with the GFP_{1-10} targeted to the IMS and Matrix-APEX-GFP_{11} only gives a signal with GFP_{1-10} directed to the matrix. Hence, the sensitive split-GFP assay confirmed the reliable targeting to the IMS and matrix in the *Δatp6* strain (Fig. 27c). However, there is no mitochondrial network, but rather a fragmented pattern, again underlining that the deletion of *ATP6* has severe effects on mitochondrial fitness. Furthermore, I wanted to test APEX labeling in the mutant strain. Isolated mitochondria of wild type and *Δatp6* were incubated with biotin-phenol, the addition of H_2O_2 resulted in a rapid (within 1 min) accumulation of biotinylated proteins in both strains. Despite equal amounts of APEX enzyme, the amount of biotinylated protein is lower in the mutant. However, labeling in the mutant strain yielded the same subcompartment-specific biotinylation pattern as in the wild type (Fig. 27d).

To analyze the proteomes of the mitochondrial subcompartments in the mutant strain, I grew wild type and *Δatp6* cells to mid-exponential phase on the fermentable carbon source galactose, isolated mitochondria, labeled the respective subcompartment with the APEX-based biotinylation assay and subjected them to mass spectrometry (Fig. 25a).

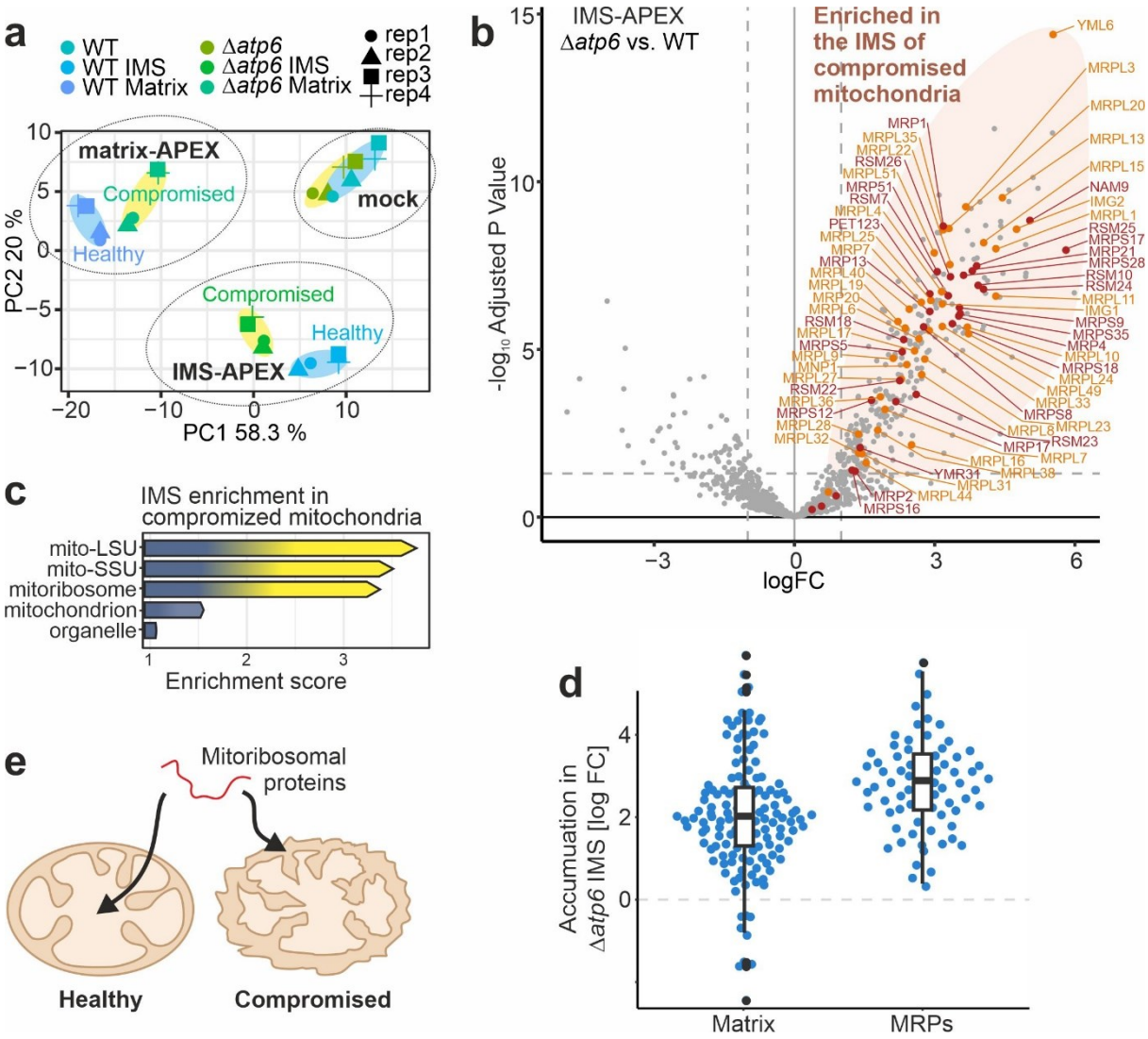

Fig. 28 | Mitoribosomal proteins accumulate in the IMS of compromised mitochondria. (a) Principal component analysis of the proximity-based mapping data of the proteomes of wild type and *Δatp6* mutants showed that compromised mitochondria have an altered protein composition. **(b-d)** In the *Δatp6* mitochondria, many matrix proteins, in particular MRPs, were found to be biotinylated by the IMS reporter; the log2 fold change (logFC) values were calculated from n=4 samples. Proteins of the small subunit of the mitoribosome are colored in red and of the large subunit in orange. **(c)** The proteins that were specifically enriched (logFC>1, p-value<0.05) in the IMS of *Δatp6* mitochondria were further analyzed by gene ontology (GO) enrichment, using the GOrilla tool (http://cbl-gorilla.cs.technion.ac.il/). **(d)** Relative enrichment scores (logFC) for the samples indicated were plotted for matrix proteins and MRPs, respectively. Boxes of the violin plots represent the data range from the first (Q1) to the third quartile (Q3), with the line in the middle representing the median. The minimum/maximum whisker values were calculated as Q1/Q3 ± 1.5 * interquartile range (IQR). (e) Mitoribosomal proteins are localized into IMS in compromised mitochondria.

Principal Component Analysis (PCA) revealed that the general proteome pattern of the two subcompartments and the background samples (mock) make APEX-construct specific clusters. All samples in the mock, independent of the strain background are almost identical. However, within the APEX clusters, two different subgroups are found highlighting the changes between the WT and the mutant strain (Fig. 28a). Further

analysis of the IMS proteome showed drastic differences in protein compositions in healthy and compromised mitochondria. Particular one protein group showed big accumulation in the *Δatp6* mitochondria, namely mitoribosomal proteins (Fig. 28b). GO enrichment analysis verifies that mostly mitoribosomal proteins are enriched in the IMS of compromised mitochondria (Fig. 28c). Comparing MRPs to all other matrix proteins enriched in the IMS, MRPs show a clear difference (Fig. 28d). Thus, the functional state of the mitochondria determines the submitochondrial proteome. Defects in the mitochondrial ATPase results in the mislocalization of matrix proteins to the IMS. This Mitochondrial Triage of Precursor proteins (MitoTrap) was not simply the result of an import block of matrix proteins as the mislocalization affected only a specific subgroup of proteins, most of which were proteins of the small and large subunits of the mitochondrial ribosome (Fig. 28 c, d).

3.9 MitoTrap prevents the accumulation of MRPs in the nucleus

Why do cells trap non-imported MRPs in the IMS rather than accumulating them in the cytosol to allow their degradation by the ubiquitin-proteasome system? To assess the physiological consequences of the accumulation of MRPs in the cytosol, I expressed Mrp17 with an N-terminal green fluorescent protein (GFP) thereby blocking its translocation through the TOM complex (Fig. 29a). To see the direct effects of non-imported Mrp17, I expressed GFP-Mrp17 from a galactose-inducible promoter. As a control, I used a C-terminal fusion which still is imported.

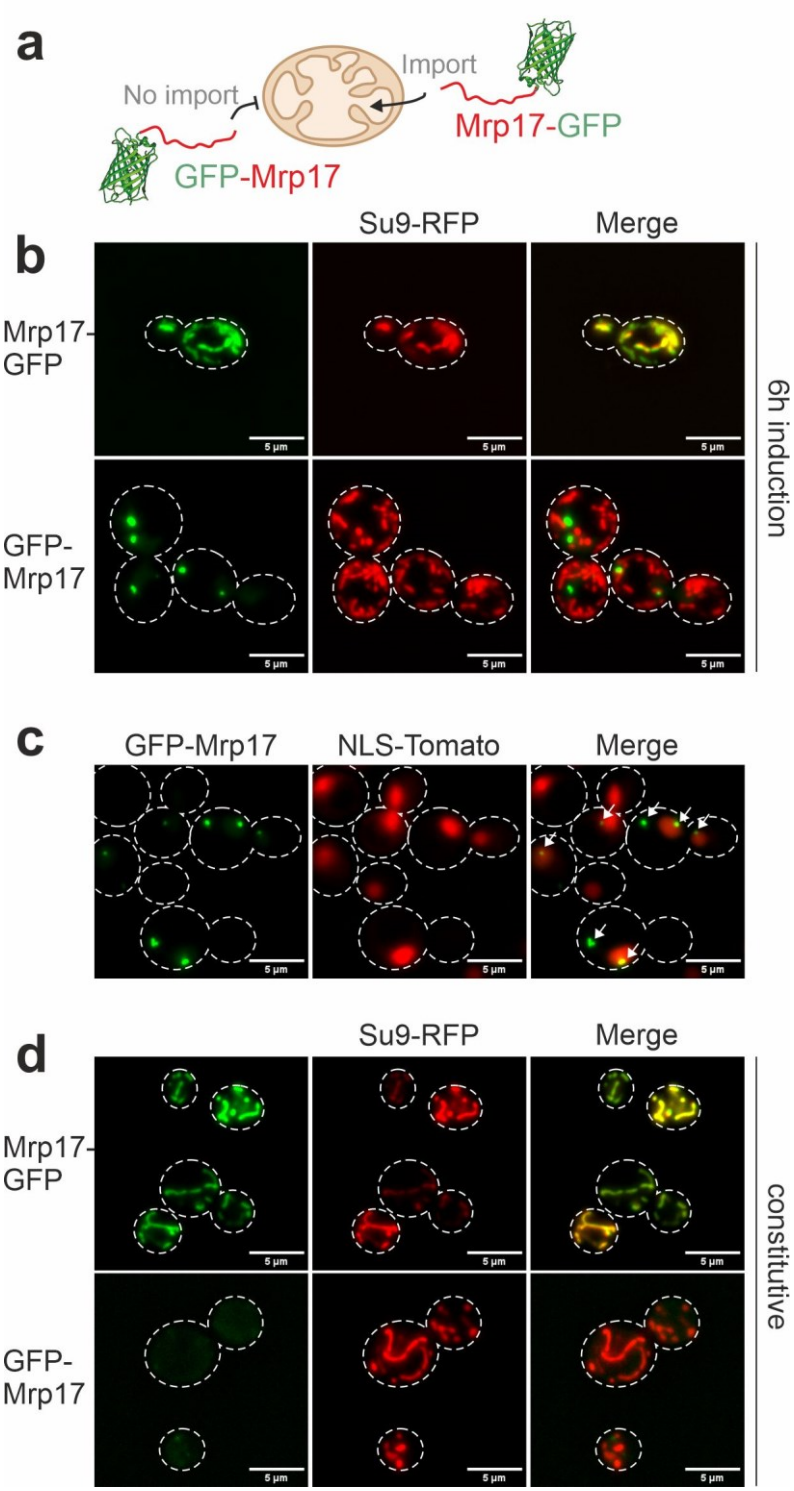

Fig. 29 | Non-imported Mrp17 partially localizes to the nucleus. (a) Mrp17-GFP can be imported into mitochondria. The N-terminal GFP prevents mitochondrial targeting of Mrp17. **(b, c)** Mrp17-GFP and GFP-Mrp17 were expressed from an inducible GAL10 promoter for 6 h and visualized by fluorescence microscopy. The mitochondrial network was stained by the expression of Su9-RFP, and the nucleus by the expression of NLS-Tomato. **(d)** Mrp17-GFP and GFP-Mrp17 were constitutively expressed from a *TPI1* promotor and visualized by fluorescence microscopy. Mitochondria were stained by the expression of Su9-RFP.

GFP-Mrp17 accumulated outside of mitochondria in one or two puncta per cell (Fig. 29b). To determine the localization of the puncta, I stained the nucleus by the expression of nucleus-targeted dtTomato. Fluorescence microscopy shows that at least one puncta per cell colocalizes with the nuclei. (Fig. 29c). To check if accumulated proteins in the puncta are stable, GFP-Mrp17 was constitutively expressed. In contrast, the constitutive expression of GFP-Mrp17 showed no fluorescence signal (Fig. 29d). Probably the fusion protein was degraded, or the cells quickly gave rise to suppressor strains in which GFP-Mrp17 was no longer expressed.

To identify interaction partners of the non-imported GFP-Mrp17, I expressed the fusion protein for 5 hours, purified it under native conditions on GFP nano trap beads and subjected the isolated fractions to mass spectrometry (Fig. 30 a).

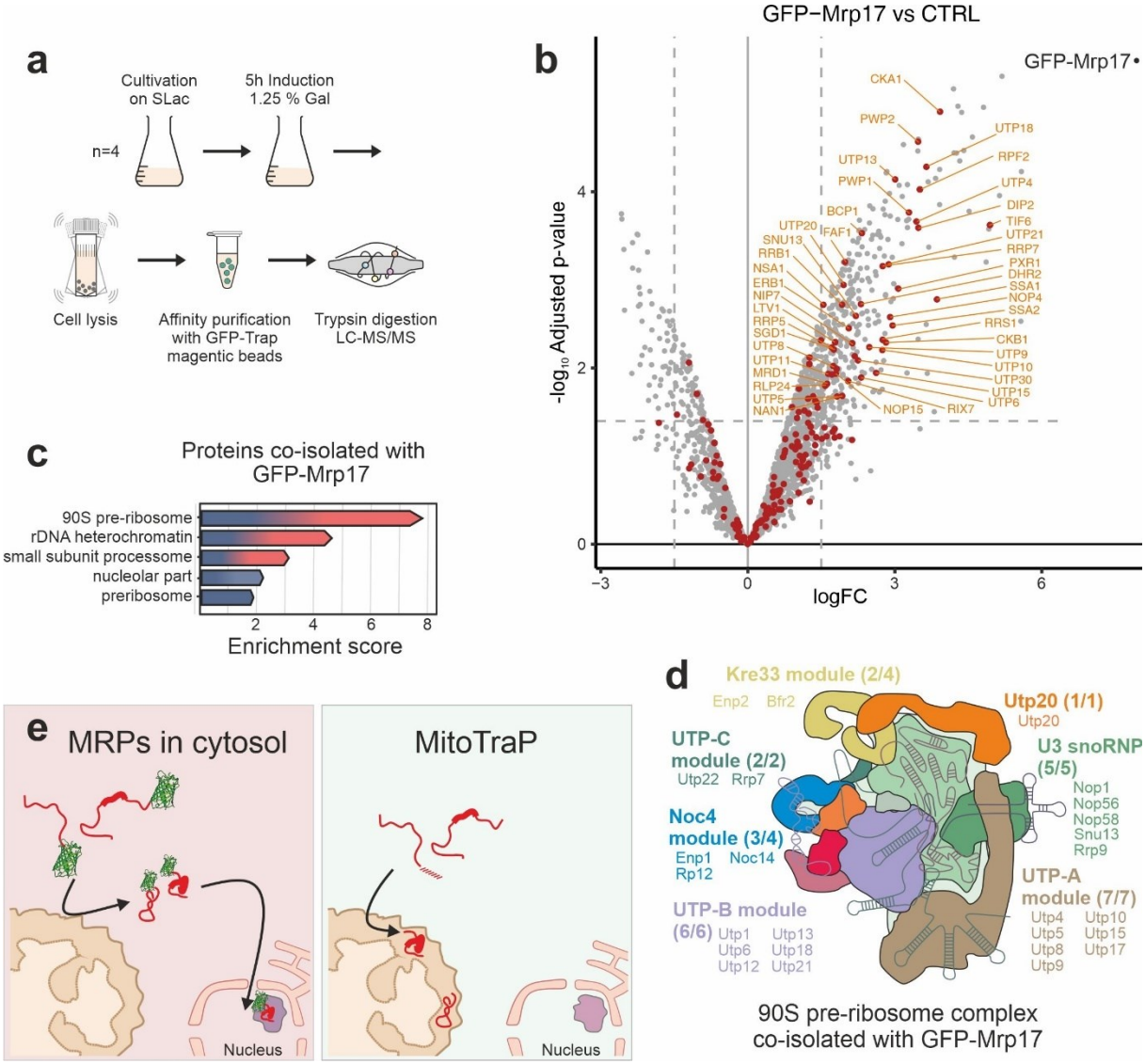

Fig. 30 | MitoTrap prevents the interference of Mrp17 with the 90S pre-ribosome. (a) Schematic representation of the GFP-Mrp17 purification. **(b)** GFP-Mrp17 was expressed for 5 h in wild type cells. GFP-Mrp17 was purified from cell extracts and co-isolated proteins were analyzed by mass spectrometry relative to proteins from a control sample (GFP). The log2 fold change (logFC) values were calculated from n=4 samples. **(c)** Enrichment of functional groups that were co-isolated with GFP-Mrp17. The proteins that were specifically enriched (logFC>1.5, p-value<0.05) in the GFP-Mrp17 pulldown were further analyzed by gene ontology (GO) enrichment, using the GOrilla tool (http://cbl-gorilla.cs.technion.ac.il/). **(d)** Schematic representation of the 90S pre-ribosomal complex of the nucleus **[116]**. Indicated are proteins of the different modules of the ribosome assembly complex that were found in the GFP-Mrp17 interactome. **(e)** Mitochondrial dysfunction leads to the trapping of MRPs in the IMS. The accumulation of MRPs in the IMS might prevent their targeting to the nucleus and, thus, their interference with the assembly of ribosomes in the nucleolus.

Analysis of the mass spectrometry data revealed many proteins of the nucleolus in the GFP-Mrp17 interactome, in particular proteins of the 90S pre-ribosome complex (Fig. 30 b, c). Almost the full complement of subunits of this assembly complex was coisolated with GFP-Mrp17 (Fig. 30 d). Thus, the non-imported GFP-Mrp17 is targeted into the nucleus or probably to the nucleolus, where it interferes with the biogenesis machinery for 80S ribosomes. Therefore, trapping Mrp17 into the IMS of compromised mitochondria might be a quality control mechanism to prevent Mrp17 or other MRPs from interfering with the assembly of the cytosolic ribosome.

All in all, I could show that low ATP conditions upon ATP synthase depletion reroute a subpopulation of mitochondrial matrix proteins into the IMS. Notably, one subgroup of matrix proteins stands out, namely mitoribosomal proteins. It seems that cells use this as a quality control mechanism to trap MRPs to prevent their interference with the cytosolic ribosome assembly (Fig. 30e). The mechanism of how matrix proteins get mislocalized into the IMS and why certain other matrix proteins are trapped in the IMS still is not clear and needs further investigation.

4 DISCUSSION

The aim of this work was to investigate how the import of mitochondrial proteins, especially mitoribosomal proteins is affected in compromised mitochondria upon ATP depletion. I could show that upon mitochondrial dysfunction such as upon inactivation of the mitochondrial ATPase, many matrix proteins, mostly mitoribosomal proteins were found to be mislocalized into the IMS. In the following, I would like to discuss this work's limitations and alternative hypotheses. Furthermore, I want to examine possible mechanisms and the relevance of MitoTraP (Mitochondrial Triage of Precursor proteins) for protein translocation and cellular and organellar proteostasis.

4.1 ATP-independent import of Mrp17 into the IMS

Most matrix proteins carry N-terminal presequences, however, many MRPs lack such presequences but use internal targeting sequences instead [24,25]. Why mitoribosomal proteins use such unconventional targeting signals is unknown. In this study, I used Mrp17 (bS6m) as a model protein that has an internal targeting information instead of a cleavable N-terminal MTS [25]. Mrp17 can be imported efficiently into energized mitochondria via the TOM and TIM23 complex, indicating that despite its unconventional targeting signal, Mrp17 takes the classical presequence pathway into the matrix (Fig. 9, 10). Moreover, the import of Mrp17 is highly dependent on the membrane potential (Fig. 11a). Surprisingly, depletion of mitochondrial ATP by incubation with the ATP-hydrolyzing enzyme apyrase, did not block Mrp17 import (Fig. 11c). This was unexpected as the import of matrix proteins is generally assumed to occur in a strictly ATP-dependent reaction [117,118]. Moreover, Mrp17 was also efficiently imported into mitochondria lacking functional Ssc1 (Fig. 11b). Nevertheless, both approaches can have secondary effects since ATP is involved in many mitochondrial processes and Ssc1 also has a matrix soluble pool. Therefore, the use of the CRISPRi-mediated depletion of the essential subunit Tim44, which couples mtHsp70 to the TIM23 complex, was crucial to determine the direct effect of the import motor loss. In consistency, the depletion of Tim44, did not prevent the translocation of Mrp17 into isolated mitochondria (Fig. 15). However, the quantification of the import of Atp1 into Tim44 depleted mitochondria showed that there is a high variance between the different replicates. Since the reduced protein levels of Tim44 were reproducible, this variance in the import rate was probably not caused by CRISPRi depletion. It is

more likely that the isolation process itself determines the quality of mitochondria. Thereby mitochondria of higher quality, might possess a higher membrane potential and therefore counteract the loss of Tim44. Since Atp1 showed reduced import rates and cells showed a clear growth defect upon depletion of Tim44, I expected marked changes in the mitochondrial proteome. While the depletion of Tim44 in whole cell lysates was verified by mass spectrometry data, other mitochondrial proteins showed no drastic changes (Appendix Fig. 1a, b). Already synthesized proteins may possess a longer half-life and a prolonged induction time is required to measure noticeable changes in protein levels of other mitochondrial proteins. The direct effect of Tim44 depletion might not be detectable with proteomics as Tim44 primarily plays a role in the recruitment and organization of the PAM complex [119]. Therefore, the depletion of Tim44 might not change the abundance of proteins but the availability. In the same line, the dataset shows that the level of Ssc1 is constant, but probably the ratio between soluble and membrane-bound Ssc1 changed (Appendix Fig. 1c). Nevertheless, the *in vitro* import shows that proteins have a varying dependence on Tim44 with Mrp17 being one of the proteins that does not need Tim44 and the import motor.

One limitation of *in vitro* import assays is that one cannot distinguish if the protein reaches the matrix or is stuck during the translocation. To overcome this problem and determine the subcompartmental localization of Mrp17, I established a new reporter assay. Unlike in a swelling approach, this reporter assay does not damage the OM and makes it possible to reliably distinguish protein targeting to the matrix from that to the IMS. To this end, two different viral proteases were expressed in mitochondria, one in the matrix and one in the IMS. Radiolabeled fusion proteins can be incubated with isolated mitochondria containing the protease and cleavage indicates the same localization. Cleavage of the proteases HCV and uTEV3 was highly efficient as imported proteins were cleaved (Fig. 18 b, c). In comparison to HCVP, uTEV3 cleavage was slightly more efficient, since no precursor and only the cleaved fragment is detectable (Fig. 18 b, c). uTEV3 is a modified TEV protease, with mutations to improve stability and activity, and was already optimized to work in yeast [120]. In contrast, HCVP was engineered to work in mammalian cells and therefore might have lower efficiency in yeast mitochondria [121]. Another advantage of this method over mitochondrial swelling is that this could be used *in vivo*. Cleavage can be analyzed via western blot with an antibody against the protein of interest that was tagged with the

respective cleavage site before. Accordingly, targeting the proteases in the nucleus or the ER might also be useful to determine the localization of proteins. Unfortunately, determination of the submitochondrial localization of Mrp17 *in vivo* was not possible since the antibody against Mrp17 was not sensitive enough to give a signal for endogenous and overexpressed protein in whole cells. Nevertheless, *in vitro*, this protease assay clearly showed that in energized mitochondria Atp1 and Mrp17 are localized to their correct destination but upon ATP depletion Mrp17 but also other MRPs are mislocalized into the IMS (Fig. 20c, d, Appendix Fig. 2). Still, this assay might need some further optimization, as in the control sample (20%), in which no protease is expressed, sometimes a faint band of the same size as the expected cleaved fragment is detectable (Fig. 21a). As the radiolabeled protein is synthesized with reticulocytes from rabbits the exact composition is not known. It cannot be excluded that this mix contains proteases that can recognize and cleave the proteins therefore resulting in the variable appearance of the fragment in the control sample. Otherwise, the presence of an alternative start codon could result in a fragment of this specific size. To address this issue, protease inhibitors could be added to the lysate, although this might interfere with the cleavage activity of the viral protease used in the assay. Alternatively, the cleavage sequence could be adjusted. By shortening or reorienting the cleavage sites, it may be possible to eliminate the extraneous band in the lysate control, thereby yielding clearer results.

Overall, the protease cleavage assay helped to follow the import route of Mrp17 and revealed that the translocation of Mrp17 into the IMS required the presence of the membrane potential while ATP levels were low. The import motor and the availability of ATP are only needed to pass the IM. Thus, the internal targeting information of Mrp17 is as functional as typical N-terminal MTS. However, the unconventional targeting of Mrp17 and the stronger dependence on the membrane potential may allow trapping in the IMS since the membrane potential is strong enough to pull the precursor protein into mitochondria. This difference in energy demand may be one of the requirements for trapping Mrp17 and other MRPs in the IMS.

4.2 Determination of mitochondrial subproteomes via APEX-labeling

The proteomes of the mitochondrial matrix and IMS have previously been analyzed based on biochemical fractionation experiments, in particular upon selective rupturing of the OM by hyperosmotic conditions or by employing proapoptotic factors [12,122]. As mentioned before, swelling can damage mitochondria and thereby introduce artifacts, such as background signals from other subcompartments. An alternative strategy is proximity labeling and thus I used an engineered and improved version of ascorbate peroxidase (APEX2). This worked out to be an excellent tool to biotinylate proteins with spatial and temporal control in mitochondrial subcompartments and proved to be particularly powerful in conjunction with mass spectrometry [13,109,110]. This kind of proximity labeling is well suited to label the whole subcompartment as biotin-phenol radicals generated by APEX2 can diffuse in the membrane-enclosed compartment. However, due to the impermeability of the cell wall in *S. cerevisiae*, in this study biotin-phenol and hydrogen peroxidase were added to isolated mitochondria. Strains in which APEX2 was targeted selectively to the IMS or the matrix were used (Fig. 23, 27). Both APEX reporters were highly specific: matrix proteins were predominantly biotinylated by the matrix-APEX enzyme and IMS and outer membrane proteins by the IMS-APEX enzyme (Fig. 25 b, c). Inner membrane proteins showed a mixed behavior, reflecting their individual topology in the inner membrane (Appendix Fig. 3).

However, the method has limitations which will be discussed in the following. In yeast, the cell wall is impermeable to biotin-phenol, and therefore only *in organello* assays are possible. The isolation process of mitochondria can impact the proteome and produce artifacts. This effect can be seen in the PCA plots of the different mitochondrial isolations. Here, the two biological replicates are similar but still distinguishable from each other, showing the high variance of the isolation process (Fig. 28a). Nonetheless, one advantage of the isolation process is the elimination of the cytosol. Studies with human cell lines have shown, that IMS-targeted APEX can also erroneously label cytosolic proteins due to the diffusion of biotin-phenol through the porins in the OM [13]. Another limitation of this method is that for the IMS-APEX in WT mitochondria, the coverage of IMS proteins was not high (Fig. 25c). Several reasons could explain this result. One limiting factor might be the steric accessibility of modifiable amino acid residues (e.g., tyrosine) to the biotin-phenol radical. Proteins could be inaccessible

because they are anchored in the OM or IM or assembled in protein complexes. Additionally, since many IMS proteins are small in size they might not have a large number of residues per se that can be modified. Also, during the isolation process, the OM of some mitochondria might have been ruptured and therefore lost a portion of the IMS proteome. Moreover, the protein annotation might be a problem, since proteins that have an IMS domain but are anchored in the IM, are annotated as IM proteins.

4.3 Matrix proteins are trapped in the IMS of compromised mitochondria

While Mrp17 mislocalizes into the IMS under low ATP conditions, the fate of other matrix proteins is still unknown. To gain a broader insight into the import behavior of matrix proteins in compromised mitochondria, I used APEX labeling to quickly label the entire proteome of the respective subcompartment. Since the general depletion of ATP is very artificial, I wanted to mimic a more physiological condition. Mitochondrial defects can arise from mutations in the mitochondrial genome, a widespread phenomenon in aging human cells [114]. Thus, I used a deletion mutant of *ATP6* as a model, since mutations in humans are associated with diseases like multiple sclerosis and Leber's hereditary optic neuropathy [123–125]. The protein compositions in the IMS of healthy (WT) and compromised (*⊿atp6*) mitochondria showed drastic differences since many matrix proteins accumulated in the IMS of the mutant (Fig. 28 b-d). Surprisingly, in *⊿atp6,* matrix proteins are not drastically depleted (Appendix Fig. 4). One explanation could be that the overall H_2O_2 level is higher in compromised mitochondria, therefore APEX labeling is more efficient. Furthermore, the mutant could have already adapted to the stress, and a small proportion of mislocalized proteins into the IMS can be imported into the matrix, albeit highly inefficient.

Further experiments show that the IMS mislocalization of matrix proteins is not restricted to cells with mitochondrial DNA mutations but was also found in mutants of nuclear-encoded proteins which impair the ATPase activity such as in cells lacking the ATPase biogenesis factor Atp23 (Appendix Fig. 5). The accumulation of matrix proteins in the IMS in *⊿atp23* is not as strong as in *⊿atp6* mitochondria but shows the same trend. This might be explained by the fact that Atp6 is a subunit of the F_0 part and therefore directly involved in the functionality of the ATP synthase [65]. In contrast, Atp23 is only indirectly involved in the functionality of the ATP synthase, as Atp23 is engaged in processing and assisting of the F_0 assembly [72].

The IMS accumulation is not simply the result of an import block of matrix proteins as the mislocalization affects mainly a specific subgroup of proteins, namely proteins of the small and large subunit of the mitochondrial ribosome. Many MRPs have untypical targeting sequences and only score low in prediction programs for mitochondrial targeting [24,25]. Analysis of the enriched MRPs in the IMS show that 58% have TargetP scores <0.8 and 35% have even scores lower than 0.5 (Appendix Table 2). Thus, fitting to the previous *in vitro* data, Mrp17 but also other MRPs, mainly with low TargetP prediction scores are mislocalized into the IMS upon impaired ATP synthase activity.

Mislocalized MRPs in the IMS are presumably non-functional due to the absence of rRNA in the IMS. Therefore, they are most likely degraded by proteases in the IMS. Studies showed that under stress conditions such as hydrogen peroxide stress, Yme1 increases ATP binding efficiency thereby potentially increasing proteolytic activity [126]. Thus, Yme1 could be the major protease in the IMS to degrade mislocalized matrix proteins under stress conditions to maintain mitochondrial proteostasis.

Another question is if under low ATP conditions proteins such as Mrp17 still are imported via the presequence pathway that is stopped in the IMS or if they take an IMS import pathway instead. A special import pathway via the IMS is known for one MRP, namely Mrp10. It has a low TargetP score and has no cleavable N-terminal MTS. Many proline residues at the N-terminus prevent rapid translocation through the TIM23 complex. This allows Mia40 to oxidize highly conserved cysteines of Mrp10 [127]. However, this import scenario is unlikely for Mrp17, as no cysteines are present in its sequence. However, Weckbecker was able to show that Atp23 was imported independently of cysteine residues in a mia40-dependent manner. They also show that Mia40 has a chaperone-like function and prevents Atp23 aggregation [128]. According to this, it can’t be excluded that Mrp17 may interact with Mia40 in the IMS.

Also, the mechanism that allows the trapping of MRPs in the IMS is unknown. The import of precursor proteins containing a typical N-terminal MTS leads to the formation of a continuous protein-conducting TOM-TIM23 supercomplex. However, the unconventional targeting information of MRPs might avoid the close interaction of the two translocases and prevent super complex formation [34,129]. Chacinska et al. showed that preproteins that get stuck in the supercomplex during import can be

chased into the matrix, which is accompanied by dissociation of the supercomplex [130]. Experiments to chase IMS located Mrp17 *in vitro* failed due to technical reasons. Therefore, it is not possible to conclude if Mrp17 might get stuck in the supercomplex and can be chased into the matrix. Also, it is unclear if the supercomplex can be stabilized or even generated under low ATP conditions. As the two mitochondrial translocases can function independently of each other, Mrp17 might be imported through the TOM complex but caused by unstable supercomplex formation in compromised mitochondria, Mrp17 escapes the import machinery and gets trapped in the IMS.

4.4 MitoTrap prevents interference of MRPs with ribosome assembly

Dysfunctional mitochondria have several quality control mechanisms to ensure mitochondrial and cellular proteostasis. Krämer et al. showed that competitive inhibition of mitochondrial import led to the formation of MitoStores in the cytosol. These are transiently stored precursor proteins of the matrix that are controlled by Hsp42 and Hsp104 [131]. Their study showed that mainly matrix proteins with an N-terminal MTS are sequestered in these dedicated granules. However, MRPs that often do not have a typical N-terminal MTS cannot be captured by MitoStores and are mislocalized into the IMS. Thus, MitoTrap is an additional mechanism to deal with precursor accumulation in the cytosol that is determined by the characteristics of the matrix targeting information.

Another mechanism in mitochondrial quality control is the formation of Var1-bodies in the matrix. Bertgen et al. showed the importance of one special MRP in maintaining the proteostasis in the matrix under acute stress situations such as heat stress or overexpression of misfolding proteins. The mitochondrially encoded MRP Var1 has poly-Asparagin stretches which makes it aggregation prone. Under acute stress conditions Var1-bodies are formed that function as nucleation seeds for intramitochondrial aggregates and thereby sequester misfolded matrix proteins [20].

With MitoStores in the cytosol, MitoTrap in the IMS, and Var1-bodies in the matrix, mitochondria have several quality control mechanisms that are spatially separated. These studies show that MRPs are highly sensitive to stress situations and are involved in several safeguard mechanisms in mitochondria, indicating that MRPs not

only function as constituents of the translation machinery but are also early reactors to stress conditions.

But what is the advantage of trapping MRPs in the IMS instead of storing or degrading them in the cytosol? One idea is that trapping MRPs in the IMS prevents translation in compromised mitochondria. The conditional sorting mechanism restricts mitoribosome biogenesis to mitochondria that contain functional respiratory chains. This could serve as an unknown quality control mechanism to prevent the synthesis of mitochondrial translation products in mitochondria that harbor compromised mitochondrial genomes.

Another idea is that accumulating MRPs in the cytosol might interfere with the assembly of the cytosolic ribosome. To address this hypothesis, I performed a pulldown of GFP-Mrp17 which cannot be imported into mitochondria and therefore is forced to stay in the cytosol after synthesis. The analysis of the pulldown experiment revealed a significant enrichment of assembly factors of the cytosolic ribosome, particularly those associated with the small subunit processome that consists of several subcomplexes such as Utp A, Utp B and UtpC. [132]. These three subcomplexes are involved in rRNA processing, transcription, stabilization and in recruiting other subcomplexes to the processome [133–135]. Overall, most of the assembly factors of the SSU processome were found in the pulldown, indicating that non-imported Mrp17 interferes with the SSU processome (Fig. 30d). This was rather unexpected as Mrp17 has homologs in mitochondria and bacteria, but no direct counterpart in the cytosolic ribosome of eukaryotes. However, the overall structural similarity of many MRPs with subunits of the 80S ribosome [56] and the fact that cells transport proteins with helical, positively charged sequences of RNA-binding segments into the nucleus might explain the observed findings.

Nevertheless, the efficient import of Mrp17 into mitochondria is indispensable as otherwise, Mrp17 could interfere with the early assembly stages of the cytosolic ribosome's small subunit. Such interference could have severe consequences as cytosolic translation is an essential cellular process. However, growth assays of cells expressing GFP-Mrp17 transient or constitutively did not show impaired growth or a toxic effect for the cells (Appendix Fig. 6). Thus, the accumulation of just one MRP might not be the problem. Microscopic analysis of constitutively expressed GFP-Mrp17 revealed no detectible GFP signal, indicating degradation of GFP-Mrp17 in the cytosol

(Fig. 29d). Accordingly, the cell is able to cope with non-imported Mrp17. One pathway to remove non-imported proteins is the mitochondrial protein translocation-associated degradation (mitoTAD). The cofactor Ubx2 interacts with the TOM complex and recruits Cdc48 to facilitate the removal of arrested precursor proteins from the TOM channel via ubiquitylation, and thereby initiates proteasomal degradation [80]. Indeed, Cdc48 was one of the top hits, indicating that GFP-Mrp17 was stuck in the TOM complex and removed and degraded via mitoTAD (Appendix Fig. 7a). In addition, several subunits of the proteasome were significantly enriched in the pulldown (Appendix Fig. 7b). Nevertheless, the protease cleavage assays as well as APEX labeling show that Mrp17 and other MRPs mislocalize into the IMS. Hence, the IMS might be a more suitable environment to degrade MRPs, as the interference with the cytoribosome assembly is excluded in this enclosed subcompartment (Fig. 31).

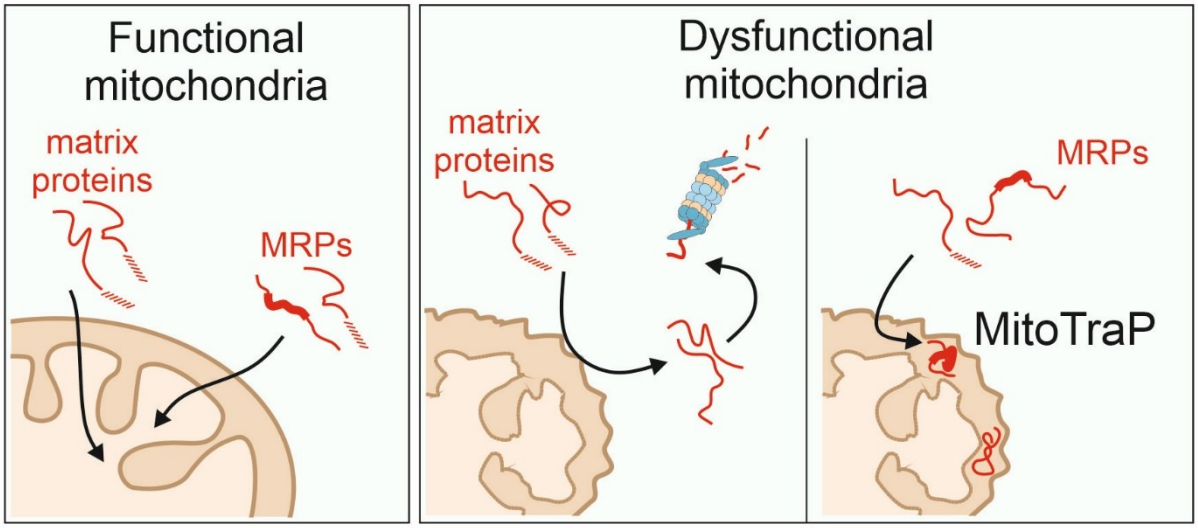

Fig. 31 | MitoTrap. Functional mitochondria efficiently import matrix proteins and MRPs into the matrix. Upon impaired ATPase, dysfunctional mitochondria do not import most matrix import which are degraded by the proteasome system. In contrast, many MRPs are trapped in the IMS, to prevent interference with the assembly of the cytosolic ribosome.

5 OUTLOOK

In this study, I used Mrp17 as a model protein to study the import process of proteins lacking typical MTSs. Despite its unconventional internal targeting signal, Mrp17 still takes the import pathway through the TOM and TIM23 complex. If the import motor is compromised upon ATP depletion most mitochondrial matrix proteins cannot be imported and stay outside of mitochondria. However, Mrp17 is deviated into the intermembrane space (IMS). Proximity Labeling showed that mitochondrial dysfunction such as upon inactivation of the mitochondrial ATPase, many matrix proteins were found to be mislocalized to the IMS, particularly constituents of the mitochondrial ribosome.

It is unclear what happens to Mrp17 after the mislocalization into the IMS. There are three options: (i) Mrp17 is directly degraded in the IMS, potentially by the IMS-localized i-AAA protease Yme1 (YME1L in humans) [136]. (ii) Mrp17 is retro-translocated to the cytosol and degraded by the proteasome [98] or (iii) Mrp17 is kept import competent in the IMS and can be further imported into the matrix under optimal conditions. Degradation by Yme1 is the most likely scenario. This could be tested with an *in vitro* import, using mitochondria of *Δyme1* cells, expressing the viral protease IMS-uTEV3. If Yme1 degrades Mrp17 in the IMS, the IMS fragment of Mrp17 should get less in the WT but should be stable in the Yme1 deletion mutant. The second scenario could be tested with a modified protease cleavage assay. After the import of Mrp17-cs in apyrase-treated mitochondria containing IMS-uTEV3, samples can be PK treated and afterward resuspended in a release buffer. After a distinct timepoint, mitochondria could be reisolated and proteins in the release buffer could be precipitated via TCA precipitation. If cleaved Mrp17-cs would be detectable in the release fraction this would indicate retransloaction out of the IMS. To test the third scenario a chase experiment as described in 4.3 could be done. As the first attempt did not work this assay would need optimization. Another possibility to address this question would be to search for interactors of IMS-trapped Mrp17 via cross-linking experiments. IMS proteins like Mia40 or the ATP-independent chaperone like small Tim proteins might interact with mislocalized proteins in the IMS and thereby keep them import-competent. Alternatively, mutant strains of small Tim proteins could be used to determine if they get essential under low ATP conditions.

Also, it remains unclear whether acute stress conditions lead to the same effect. In another study, the overexpression of mtDHFR^{mut} was utilized to induce mitochondrial proteostasis stress [137]. Under these acute conditions, it would be valuable to assess whether mitochondrial proteins are also localized into the IMS. Additionally, testing acute stress situations acting on the whole cell such as heat stress could provide further insights. Furthermore, it would be interesting to investigate whether already correctly imported matrix proteins can be translocated into the IMS under acute stress conditions. Again, a protease assay could be used. Therefore, a viral protease targeted to the matrix and IMS have to be expressed simultaneously. First, import of Mrp17-cs under normal conditions would lead to matrix cleavage, then non-imported proteins have to be degraded by PK. Afterwards, apyrase or oligomycin could be added. If Mrp17-cs, which was only processed once without stress, is suddenly processed twice, this would speak for the translocation from the matrix into the IMS. However, the attempt to express both proteases at the same time did not work, as cell growth was impaired, and mitochondria were no longer import-competent (Data not shown). Expressing both proteases under weaker promoters could solve this problem.

Another open question concerns the mechanism by which Mrp17 can escape the TOM-TIM supercomplex. One idea is that reduced ATP levels upon ATPase malfunction impair the function of the PAM complex, leading to the destabilization of the entire supercomplex. This destabilization could facilitate the release of proteins such as Mrp17 into the intermembrane space (IMS). To test this, the supercomplex can be purified and investigated with BN-PAGE [138] under normal and low ATP conditions. Comparisons between wild-type (WT) and *Δatp6* strains can be conducted to further elucidate the process.

This study used *S. cerevisiae* as a model organism to reveal the import mechanism of mitochondrial proteins. Whether the IMS targeting of MRPs in defective mitochondria is a peculiarity of fungi or whether this is a conserved feature of mitochondrial biology is unclear. To test this, APEX proximity labeling could be used in human cell lines.

Furthermore, methods such as APEX labeling could be adapted or optimized to get clearer results. In WT mitochondria only 43% (14 out of 32) of annotated IMS proteins were detected. The coverage for matrix proteins was much higher, with 81% (205 out of 252) identified. The reasons for this low coverage were already discussed in 4.2.

One of the reasons could be the process of mitochondria isolation that might damage the OM. Studies using APEX labeling with cell wall permeable reagents in yeast cells allow for labeling in whole cells, thereby reducing the chance of organelle disruption and potentially increasing the detection of IMS proteins [139]. This method could be one possibility to counteract the low coverage of IMS proteins.

While import routes into mitochondria appear to be well-studied, new details continue to emerge regularly. This study provides initial insights into how the mitochondrial import pathway can play a role in adaptation to stress conditions caused by a mitochondrial DNA mutation. Further research is necessary to fully understand the mechanisms of cellular and organelle adaptation to stress conditions.

6 MATERIAL AND METHODS

6.1 Genetic Methods

6.1.1 *E.coli* strains

For plasmid purification and isolation, the *Escherichia coli (E.coli)* strain MH1 and DH5α were used [140,141]. The strains are described in **Table 1**.

Table 1: Bacterial strains used in this study. Listed are the used *E. coli* strains with genotype and their references.

Strain	Genotype	Reference
MH1	MC1061 derivative; araD139, lacX74, galU, galK, hsr, hsm+, strA	[141]
DH5α	K12 derivative; F- φ80dlacZΔM15, Δ(lacZYAargF)U169, deoR, recA1, endA1, hsdR17(rk- mk+), phoA, supE44, λ -, thi-1, gyrA96, relA1	[140]

Bacterial plasmids used for *in vitro* translation are shown in **Table 2**.

Table 2: Bacterial plasmids used in this study

Plasmid	Characteristics	Reference
pGem4-Mrp17-DHFR^{mut}	Mrp17 with dihydrofolate reductase that cannot fold, *in vitro* expression	[25]
pGem4-Mrp17-DHFR	Mrp17 with dihydrofolate reductase, *in vitro* expression	This study
pGem4-Mrp17	Mrp17, *in vitro* expression	[25]
pGem4-Hsp60	Hsp60, *in vitro* expression	Herrmann lab
pGem4-Atp1	Atp1, *in vitro* expression	[25]
pGem4-Mix23	Mix23, *in vitro* expression	Herrmann lab
pGem4-Aac1	Aac1, *in vitro* expression	Herrmann lab
pGem4-Mrp17-cs	Mrp17 with cleavage sites for viral proteases, *in vitro* expression	This study
pGem4-Atp1-cs	Atp1 with cleavage sites for viral proteases, *in vitro* expression	This study
pGem4-b2-DHFR-cs	Cytochrome b2-DHFR with cleavage sites for viral proteases, *in vitro* expression	This study
pGem4-Oxa1	Oxa1, *in vitro* expression	[142]
pGem-Mrpl40-cs	Mrpl40 with cleavage sites for viral proteases, *in vitro* expression	This study
pGem4-Mrpl28-cs	Mrpl28 with cleavage sites for viral proteases, *in vitro* expression	This study

6.1.2 Transformation of chemo-competent *E.coli* cells

50 µl chemically competent *E. coli* cells were transformed for the amplification of plasmid DNA. Therefore, the cells were thawed slowly on ice and 10 µl of a ligation or 5 µl Gibson assembly or 1 µl plasmid DNA were added. The mixture was incubated on ice for 20 min, subjected to heat shock treatment at 42°C for 1 min 30 sec and cooled down on ice for 2 min. Next, 800 µl LB medium was added to the cells, followed by incubation for 30-60 min at 37°C and 850 rpm. Transformed cells were plated onto LB agar plates containing 100 µg/ml ampicillin (Amp) or 25 µg/ml chloramphenicol (Cam), or 30 µg/ml kanamycin (Kan) depending on the used resistance cassette and incubated overnight at 37°C.

6.1.3 *S. cerevisiae* strains, plasmids, and primers

Saccharomyces cerevisiae (*S. cerevisiae*) strains are stored in glycerol stocks and were plated onto agar plates. Cultures were inoculated from plates in liquid media and cultivated shaking at 130 rpm and 30°C. Temperature-sensitive mutants were grown at 25°C and shifted overnight to 33°C. The strains and plasmids used in this study are shown in **Table 3** and **Table 4**.

Table 3 Overview of *S. cerevisiae* strains used in this study. Listed are the background strains, strains obtained by homologous recombination and by transformation, together with their phenotype and references.

Database	Strain	Genotype	Reference
HHY0003	YPH499	MATa ura3-52 lys2-801 ade2-101 trp1-Δ63 his3-Δ200 leu2-Δ1	[143]
HHY0084	W303	MATα {leu2-3,112 trp1-1 can1-100 ura3-1 ade2-1 his3-11,15} [phi$^+$]	[144]
HHY3715	W303 *rho^0*		[20]
HHY3182	Δtom22	YPH499 *rho-* TOM22::HIS3	[145]
HHY3181	YPH499 (WT of *Δtom22*)	MATa {*ura3-52 lys2-801 ade2-101 trp1-Δ63 his3-Δ200 leu2-Δ1} rho-*	[145]
HHY1765	tom40ts-18	YPH499 TOM40::ADE2 pFL39-Tom40-18	[146]
HHY1764	YPH499-Tom40	YPH499 Tom40::ADE2 pFL39-Tom40-WT	[146]
HHY1768	Δtom5	YPH500 TOM5::HIS3	[31]
HHY1767	YPH500	YPH500	[143]
HHY1326	tim17-ts5	MATa {ade2-101 his3-Δ200 leu2-Δ1 ura3-52 trp1-Δ63 lys2-801 tim17-5}	[130]
HHY1821	tim22-14 ts	YPH499 tim22-M4	[147]
HHY1653	ssc1-3	MATα ade2-101, lys2, ura3-52, leu2-3, Dtrp1 ssc1-3(LEU2)	[148]
HHY3373	CRISPRi-ev	YPH499, pKR366-dCas9-Mxi	This study
HHY3374	CRISPRi-Tim16	YPH499, pKR366-dCas9-Mxi-Tim16	This study
HHY3375	CRISPRi-Tim14	YPH499, pKR366-dCas9-Mxi-Tim14	This study

HHY3376	CRISPRi-TIM44	YPH499, pKR366-dCas9-Mxi-Tim44	This study
HHY3350	W303 Su9-SMVPZ	W303 YPRCΔ15C::Su9-SMVPZ-Hygromycin	This study
HHY3351	W303 Su9-HCVP	W303 YPRCΔ15C::Su9-HCVP-Hygromycin	This study
HHY3352	W303 Su9-3C	W303 YPRCΔ15C::Su9-3C-Hygromycin	This study
HHY3353	W303 Su9-uTEV3	W303 YPRCΔ15C::Su9-uTEV-Hygromycin	This study
HHY3473	W303 IMS-uTEV3	W303 YPRCΔ15C::IMS-uTEV-Hygromycin	This study
HHY3474	W303 IMS-HCVP	W303 YPRCΔ15C::IMS-HCVP-Hygromycin	This study
HHY0730	Δatp23	W303-1B MATα ATP23::HIS3MX	[72]
HHY3979	*Δatp23* Su9-HCVP	*Δatp23* YPRCΔ15C::Su9-HCVP-Hygromycin	This study
HHY3980	*Δatp23* IMS-uTEV3	*Δatp23* YPRCΔ15C::IMS-uTEV-Hygromycin	This study
HHY3713	W303 Su9-APEX2-FLAG	W303 YPRCΔ15C::Su9-APEX2-FLAG-Hygromycin	This study
HHY3714	W303 IMS-APEX2-FLAG	W303 YPRCΔ15C::IMS-APEX2-FLAG-Hygromycin	This study
HHY0621	MR6	D273-10B MATα ade2-1 his3-11,15 trp1-1 leu2-3,112 ura3-1 CAN1 arg8::HIS3 rho+	[149]
HHY3886	MR6 Su9-APEX2-FLAG	MR6 YPRCΔ15C::Su9-APEX2-FLAG-Hygromycin	This study
HHY3887	MR6 IMS-APEX2-FLAG	MR6 YPRCΔ15C::IMS-APEX2-FLAG-Hygromycin	This study
HHY0622	MR10	D273-10B MATα ade2-1 his3-11,15 trp1-1 leu2-3,112 ura3-1 CAN1 arg8::HIS3; atp6::ARG8m rho+	[149]
HHY3888	MR10 *Δatp6* Su9-APEX2-FLAG	MR10 YPRCΔ15C::Su9-APEX2-FLAG-Hygromycin	This study
HHY3889	MR10 *Δatp6* IMS-APEX2-FLAG	MR10 YPRCΔ15C::IMS-APEX2-FLAG-Hygromycin	This study
HHY3890	*Δatp23* Su9-APEX2-FLAG	*Δatp23* YPRCΔ15C::Su9-APEX2-FLAG-Hygromycin	This study
HHY3891	*Δatp23* IMS-APEX2-FLAG	*Δatp23* YPRCΔ15C::IMS-APEX2-FLAG-Hygromycin	This study
HHY3989	IMS-APEX-GFP11, IMS-GFP1-10	W303, cHHYTK257-IMS-APEX-GFP11_IMS-GFP1-10	This study
HHY3990	IMS-APEX-GFP11, Su9-GFP1-10	W303, cHHYTK258-IMS-APEX-GFP11_Su9-GFP1-10	This study
HHY3992	Su9-APEX-GFP11, IMS-GFP1-10	W303, cHHYTK260-Su9-APEX-GFP11_IMS-GFP1-10	This study
HHY3993	Su9-APEX-GFP11, Su9-GFP1-10	W303, cHHYTK261-Su9-APEX-GFP11_Su9-GFP1-10	This study
HHY4407	MR10 IMS-APEX-GFP11, IMS-GFP1-10	MR10, cHHYTK257-IMS-APEX-GFP11_IMS-GFP1-10	This study
HHY4408	MR10 IMS-APEX-GFP11, Su9-GFP1-10	MR10, cHHYTK258-IMS-APEX-GFP11_Su9-GFP1-10	This study
HHY4409	MR10 Su9-APEX-GFP11, IMS-GFP1-10	MR10, cHHYTK260-Su9-APEX-GFP11_IMS-GFP1-10	This study
HHY4410	MR10 Su9-APEX-GFP11, Su9-GFP1-10	MR10, cHHYTK261-Su9-APEX-GFP11_Su9-GFP1-10	This study
HHY4411	W303 Mrp17-GFP, Su9-RFP	W303 pYX233-Mrp17-GFP, pYX112-Su9-RFP	This study
HHY4412	W303 GFP-Mrp17, Su9-RFP	W303 pYX233-GFP-Mrp17, pYX112-Su9-RFP	This study
HHY4413	W303 GFP-Mrp17, NLS-Tomato	W303 pYX233-GFP-Mrp17, pYX112-NLS-Tomato	This study

HHY4414	W303 GFP-Mrp17	W303 pYX233-GFP-Mrp17	This study
HHY4415	W303 GFP	W303 pYX233-GFP	This study
HHY	W303 ev	W303 pYX233-ev	This study
HHY	W303 Mrp17-GFP	W303 pYX233-Mrp17-GFP	This study
HHY	W303 GFP-Mrp17	W303 pYX142-GFP-Mrp17	This study
HHY	W303 GFP	W303 pYX142-GFP	This study
HHY	W303 ev	W303 pYX142-ev	This study
HHY	W303 Mrp17-GFP	W303 pYX142-Mrp17-GFP	This study
HHY4416	W303 Mrp17-GFP, Su9-RFP	W303 pYX142-Mrp17-GFP, pYX112-Su9-RFP	This study
HHY4417	W303 GFP-Mrp17, Su9-RFP	W303 pYX142-GFP-Mrp17, pYX112-Su9-RFP	This study

Table 4: Yeast plasmids used in this study. Listed below are the plasmids used in this work. The selection marker for yeast and promotors are given.

Database	Plasmid	Description	Reference
HHB1817	pKR366-dCas9-Mxi	CEN/ARS, URA3, AmpR, *pTEF* NLS-dCas9-NLS-Mxi1, *pGPM1* TetR, *pRPR1*-gRNA	[150,151]
HHB2181	pKR366-dCas9-Mxi-Tim16	pKR366 *pRPR1*-TIM16 gRNA	This study
HHB2182	pKR366-dCas9-Mxi-Tim14	pKR366 *pRPR1*-TIM14 gRNA	This study
HHB2180	pKR366-dCas9-Mxi-Tim44	pKR366 *pRPR1*-TIM44 gRNA	This study
HHB2191	Ω2-Su9-SMVPZ-Hygro	HygroR, SpecR, YPRCΔ15, *pTDH3*-Su9-SMVPZ-*tTDH2*	This study
HHB2192	Ω2-Su9-HCVP-Hygro	HygroR, SpecR, YPRCΔ15, *pTDH3*-Su9-HCVP-*tTDH2*	This study
HHB2193	Ω2-Su9-3C-Hygro	HygroR, SpecR, YPRCΔ15, *pTDH3*-Su9-3C-*tTDH2*	This study
HHB2194	Ω2-Su9-uTEV3-Hygro	HygroR, SpecR, YPRCΔ15, *pTDH3*-Su9-uTEV3-*tTDH2*	This study
HHB2195	Ω2-IMS-uTEV3-Hygro	HygroR, SpecR, YPRCΔ15, *pTDH3*-IMS-uTEV3-*tTDH2*	This study
HHB2196	Ω2-IMS-HCVP-Hygro	HygroR, SpecR, YPRCΔ15, *pTDH3*-IMS-HCVP-*tTDH2*	This study
HHB1952	mito-V5-APEX2		[110]
HHB2209	IMS-APEX2-FLAG	HygroR, KanR, YPRCΔ15, *pRNR1*-IMS-APEX2-FLAG-*tTDH1*	This study
HHB2210	Su9-APEX2-FLAG	HygroR, KanR, YPRCΔ15, *pRNR1*-Su9-APEX2-FLAG-*tTDH1*	This study
cHHYTK257	IMS-APEX-GFP11, IMS-GFP1-10	CEN/ARS, URA3, KanR, *pRNR2*-IMS-APEX-GFP11-*tENO2, pRNR1*-IMS-GFP1-10-*tADH1*	This study
cHHYTK258	IMS-APEX-GFP11, Su9-GFP1-10	CEN/ARS, URA3, KanR, *pRNR2*-IMS-APEX-GFP11-*tENO2, pRNR1*-Su9-GFP1-10-*tADH1*	This study
cHHYTK260	Su9-APEX-GFP11, IMS-GFP1-10	CEN/ARS, URA3, KanR, *pRNR2*-Su9-APEX-GFP11-*tENO2, pRNR1*-IMS-GFP1-10-*tADH1*	This study
cHHYTK261	Su9-APEX-GFP11, Su9-GFP1-10	CEN/ARS, URA3, KanR, *pRNR2*-Su9-APEX-GFP11-*tENO2, pRNR1*-Su9-GFP1-10-*tADH1*	This study
HHB2369	pYX233-Mrp17-GFP	2µ, pGAL-Mrp17-GFP, TRP1	This study
HHB2370	pYX233-GFP-Mrp17	2µ, pGAL-GFP-Mrp17, TRP1	This study
HHB2371	pYX233-GFP	2µ, pGAL-GFP, TRP1, Control for GFP-Mrp17 Pulldown	This study
HHB2165	pYX112-Su9-RFP	ARS/CEN, pTPI-Su9-RFP, URA3	This study

HHB2381	NLS-Tomato	CEN/ARS, pGPD-NLS-Tomato, URA3	This study
HHB2372	pYX142-Mrp17-GFP	ARS/CEN, pTPI-Mrp17-GFP, LEU2	This study
HHB2373	pYX142-GFP-Mrp17	ARS/CEN, pTPI-GFP-Mrp17, LEU2	This study
HHB	pYX142-GFP	ARS/CEN, pTPI-GFP, LEU2	This study

Table 5 lists all primers used to generate plasmids of **Table 2** and **Table 4**.

Table 5 | Primers used in this work. Plasmids were used for cloning or qPCR.

No.	Primer	Sequenz (5' → 3')	Used for
TF60	Tim44-Cri1-F	aggGAAGACTGGTTGAGTAGCAT	Cloning of pKR366-dCas9-Mxi-Tim44
TF61	Tim44-Cri1-R	aacATGCTACTCAACCAGTCTTC	
TF66	Pam18-Cri1-F	aggTTTTCACTCCGCTGAGTTCG	Cloning of pKR366-dCas9-Mxi-Tim14
TF67	Pam18-Cri1-R	aacCGAACTCAGCGGAGTGAAAA	
TF68	Pam18-Cri2-F	aggTCCGCTGAGTTCGAGGCGAG	
TF69	Pam18-Cri2-R	aacCTCGCCTCGAACTCAGCGGA	
TF72	Pam16-Cri1-F	aggGTCAGCTGAAATATGTGAAT	Cloning of pKR366-dCas9-Mxi-Tim16
TF73	Pam16-Cri1-R	aacATTCACATATTTCAGCTGAC	
TF76	Pam16-Cri3-F	aggCTTATTTGATATGAAGAGTG	
TF77	Pam16-Cri3-R	aacCACTCTTCATATCAAATAAG	
TF84	Tim44-F_qPCR1	CACGAAAGAGCAAAGGAGAC	qPCR
TF85	Tim44-R_qPCR1	ATCCTCCACTTTCTTACCAAAC	qPCR
TF86	Tim44-F_qPCR2	TTATTCTCCACCTCTACGACC	qPCR
TF87	Tim44-R_qPCR2	TCAGACTCGCCTAACTTTCC	qPCR
TF88	Pam18-F_qPCR1	GCACCACAACTACCCATTC	qPCR
TF89	Pam18-R_qPCR1	TCCACCGTTAAGTCCCTTC	qPCR
TF90	Pam18-R_qPCR2	TCTTTTGACCCTGCGAACC	qPCR
TF91	Pam16-F_qPCR1	ACAAGCGGCTTCACAATC	qPCR
TF92	Pam16-R_qPCR1	TTCGCCTTCGCATTTTTTTC	qPCR
TF93	Pam16-R_qPCR2	CGCCTTCGCATTTTTTTCTC	qPCR
TF115	SMVPZ fwd	GCGCCGTCTCGCTCGAATGGGATCCAAATCCGTATAC	Part domestication
TF116	SMVPZ rev	GCGCCGTCTCGCTCAAAGCTTACTGAACCGTTACAGTGTTG	Part domestication
TF121	HCV fwd	GCGCCGTCTCGCTCGAATGGGATCCGGCTCTG	Part domestication
TF122	HCV rev	GCGCCGTCTCGCTCAAAGCCTAGCTGACAGCCGGAG	Part domestication
TF123	3CProtease fwd	GCGCCGTCTCGCTCGAATGGGACCAAACACAGAATTTG	Part domestication
TF124	3CProtease rev	GCGCCGTCTCGCTCAAAGCTTATTGTTTCTCTACAAAATATTGTTTTTTAA	Part domestication
TF129	TEV3 fwd	GCGCCGTCTCGCTCGAATGGGAGAAAGCTTGTTTAAGG	Part domestication
TF130	TEV3 rev	GCGCCGTCTCGCTCAAAGCTTAATTCATGAGTTGAGTCGCTTC	Part domestication

TF141	fwd_5'homol armYPRCΔ15	GAGCTTGTAGCACAATAATAC	Verification, binding in 5' homology arm YPRCΔ15α1
TF142	rev_3'homol armYPRCΔ15	CAGAAGTCCAAATCACGTC	Verification, binding in 3' homology arm YPRCΔ15α1
TF145	w/otom20bm1_ fwd	TGACACTATAGAATACACGGAATTCATGC TTTATGAGCTGATCG	Gibson assembly of pGem4-Mrp17-cs
TF163	Mrp17-consensus rev	TACCACCCATAATGGATTGATAATCTTCA TTCAC	
TF164	Mrp17 consensus fwd	TCAATCCATTATGGGTGGTATGGCTGGT ATG	
TF165	consensus-pGem4 rev	CTCACTATAGGGAGACCGGAAGCTTTCA TCCGCCAGCACCAGC	Gibson assembly of pGem4-Mrp17/Atp1-cs
TF188	pGem4-Atp1_fwd	TGACACTATAGAATACACGGAATTCATGT TGGCTCGTACTGCTG	Gibson assembly of pGem4-Atp1-cs
TF189	Atp1-consensus_rev	TACCACCCATAAAAGTGGCAACAAATGAT TCAG	
TF190	Atp1-consensus_fwd	TGCCACTTTTATGGGTGGTATGGCTGGT ATG	
TF196	pGem4-Mrpl40_fwd	TGACACTATAGAATACACGGAATTCAACA TGTCTGGAAGCTATC	Gibson assembly of pGem4-Mrpl40-cs
TF197	Mrpl40-consensus_rev	TACCACCCATTTCTCTTTTTTGTTTTTCCA AAAATTC	
TF198	Mrpl40-consensus_fwd	AAAAAGAGAAATGGGTGGTATGGCTGGT ATG	
TF199	pGem4-Mrpl28_fwd	TGACACTATAGAATACACGGAATTCAACA TGCTGGCACAAACATTC	Gibson assembly of pGem4-Mrpl28-cs
TF200	Mrpl28-consensus_rev	TACCACCCATTTTTCGGAAGTTATAATGC CATAAC	
TF201	Mrpl28-consensus_fwd	CTTCCGAAAAATGGGTGGTATGGCTGGT ATG	
TF231	omega2-pTDH3_fwd	TGACGGGCTGATACTGGGCCGGCAGGC GCTCCATTGCCCAG	Cloning of omega2-pTDH3-IMS-uTEV3-tTDH2-Hygro
TF232	omega2-pTDH3_rev	TGCGAAGCATTTTGTTTGTTTATGTGTGT TTATTCGAAACTAAGTTCTTGG	
TF233	Mi40 N-term_fwd	AACAAACAAAATGCTTCGCAACTTAGTC	
TF234	Mi40 N-term_rev	TTTCTCCCATATCGGATTCTACCTTCCTT G	
TF235	uTEV3-tTDH2-Hyg_fwd	AGAATCCGATATGGGAGAAAGCTTGTTTA AG	
TF236	uTEV3-tTDH2-Hyg_rev	AATAGGTCAGGCTCTCGCTGAATTCCCC AATGTCAAGCACTTC	
TF237	omega2-pTDH3_fwd	TCCAGTGTCGAAAACGAGCTCTCGAGAA CCCTTAATATAAC	Cloning of omega2-pTDH3-IMS-HCVP-tTDH2-Hygro
TF238	omega2-pTDH3_rev	TGCGAAGCATTTTGTTTGTTTATGTGTGT TTATTC	
TF239	Mi40 N-term_rev	CTACAAGCACCACAGAGCCGGATCCCAT ATCGGATTCTACCTTCCTTG	
TF283	TF283_Apex2_ Pr1 fwd	GCATCGTCTCATCGGTCTCATTCTGGAAA GTCTTACCCAACTGTGAG	MoClo-Part domestication APEX2
TF284	TF284_Apex2_ Pr2 rev	TCGTCTCATAGACCTTCCTTCTCACCACT CAACAAC	
TF285	TF285_Apex2_ Pr3 fwd	TCGTCTCATCTACTTCAGCTACCTTCTGA CAAGG	
TF286	TF286_Apex2_ Pr4 rev	ATGCCGTCTCAGGTCTCAGGATCCGGCA TCAGCAAACCCAAG	

TF287	TF287_Apex2-FLAG fwd	GCGCCGTCTCGCTCGAGGAAAGTCTTACCCAACTG	Goldenbraid Domestication Apex2-FLAG
TF288	TF288_Apex2-FLAG rev	GCGCCGTCTCGCTCAAAGCTTACTTGTCATCGTCATCTTTATAATCGGCATCAGCAAACCCAAG	
TF289	TF289_Ver Apex2-FLAG fwd	GGAAAGTCTTACCCAAC	Ver. Domestication Apex2-FLAG
TF290	TF290_Ver Apex2-FLAG rev	TTACTTGTCATCGTCATCT	
TF350	TF350_b2-DHFR_fwd	TGACACTATAGAATACACGGATGCTAAAATACAAACCTTTAC	Gibson assembly pGem4-b2-DHFR-consensus
TF351	TF351_b2-DHFR_rev	TACCACCCATGTCTTTCTTCTCGTAGAC	
LP1	Mrp17 fwd EcoRI	GGG GAATTC ATGCTTTATG AGCTGATC	Cloning of pYX233-/pYX142-Mrp17-GFP and pYX233-/pYX142-GFP
TF220	GFP-HindIII rev	CCCAAGCTTTTATTTGTATAGTTCATCCATGC	
TF218	TF218 EcoRI-GFP fwd	GGGGAATTCATGAGTAAGGGTGAAGAACTTTTCACTG	Cloning of pYX233-/pYX142-GFP-Mrp17 and pYX233-/pYX142-GFP
TF364	TF364_GFP wo Stop rev	CCCGGATCCTTTGTATAGTTCATCCATGCCATG	
TF3	TF3 BamHI+Mrp17 fwd	CCCGGATCCATGCTTTATGAGCTGATC	
TF365	Mrp17_Hind rev	CCCAAGCTTCTAAATGGATTGATAATCTTCATTCAC	

6.1.4 *S. cerevisiae* transformation

S. cerevisiae cells were grown to exponential phase, and 1.5 ml culture was harvested by centrifugation for 1 min at 17,000 g at room temperature (RT). The cell pellet was washed with 1 ml ddH_2O. The cells were resuspended with 1 ml of 0.1 M lithium acetate and incubated for 10 min at 30°C and 1,000 rpm. After centrifugation (1 min at 17,000 g at RT), the cell pellet was resuspended in 74 µl ddH_2O, 5 µl salmon sperm DNA (ssDNA, denatured at 96°C for 10 min and cooled down), 5 µl 100 ng/µl plasmid DNA, 36 µl 1 M lithium acetate (final concentration 0.1 M) and 240 µl 50% (w/v) polyethylene glycol (PEG) 3350. The mixture was vortexed for 1 min and incubated for 30 min at 30°C, followed by a heat shock for 25 min at 42°C. For temperature-sensitive (ts) mutants, the incubation for the heat shock was done at 30°C. Afterward, the cells were pelleted (1 min at 17,000 g at RT) and resuspended in 100 µl sterile ddH_2O. The suspension was plated on selective media and incubated 2 days at 30°C or 25°C for ts strains.

For homologous recombination to genomically integrate a DNA cassette, 1 µg of DNA was used. Integrating plasmids were linearized (HHB2191-2196 with SceI and HHB2209, 2210 with NotI) and purified before transformation. The residual procedure was the same as described above. For homologous recombination with antibiotic cassettes, the cells were first plated on YPD media and incubated overnight at 30°C to allow the expression of the resistance cassette and afterward stamped with a velvet onto the media containing the respective antibiotic.

6.2 Molecular Biology Methods

6.2.1 Isolation of plasmid DNA from *E. coli*

Plasmid DNA was isolated from *E. coli* cells in small (Mini-prep) or large scale (Midi-prep). For small-scale isolation of plasmids, 5 ml selective $LB_{Amp/\ Cam/\ Kan\ /Spec}$-media were inoculated with a single bacterial colony and incubated overnight. To isolate plasmid DNA, 5 ml of culture was harvested, and the DNA was extracted using the NucleoSpin® Plasmid EasyPure Kit (Macherey-Nagel) according to the manufacturer's instructions.

For large-scale isolation, 100 ml selective $LB_{Amp\ Cam/\ Kan\ /Spec}$-media were inoculated with bacteria. The cells were cultured overnight before the plasmid DNA of the whole culture was isolated using the *PureYield™* Plasmid Midiprep System (Promega) as described by the manufacturer.

6.2.2 Determination of DNA concentration

The Spectrophotometer/Fluorometer DS-11 FX+ (DeNovix) was used to determine the DNA concentration and purity. After calibration with 1 µl of water, 1 µl of DNA was used for the measurement. The absorbance was measured at 230 nm, 260 nm, and 280 nm. The ratio of the absorbance at 260 and 280 nm indicates the degree of contamination with proteins (< 1.8) or RNA (> 1.8). The 260/230 values should be between 2.0 and 2.2. If the ratio is lower, it may indicate the presence of organic compounds.

6.2.3 Polymerase Chain Reaction

DNA amplification for plasmid construction was achieved by polymerase chain reaction (PCR). One reaction had a volume of 50 µl containing 1x Q5® reaction buffer, 1x Q5

High GC enhancer, 0.2 mM dNTPs (deoxyriboNucleoside Triphosphates), 0.5 µM of each primer, 50 ng template DNA and 1 U Q5® High-Fidelity (HF) polymerase.

Table 6 displays the PCR program for the DNA amplification with the Q5 polymerase. Annealing temperature was calculated with the NEB Tm calculator (https://tmcalculator.neb.com), elongation time was determined by the insert length.

Table 6: PCR Program. Protocol for DNA amplification by standard PCR

Temperature [°C]	Time	Cycle Number	Reaction
98°C	30 sec		Initial denaturation of DNA and nuclease inactivation
98°C 50-72°C 72°C	10 sec 30 sec 20-30 sec/kb	30-35x	DNA denaturation Primer annealing Elongation
72°C	2 min		Final elongation
4°C	∞		Cooling

6.2.3.1 Colony PCR and genomic DNA preparation

Colony PCR was used for the verification of successful homologous recombination. Therefore, one colony was inoculated in 15 ml liquid culture and grown overnight. Cells were harvested (5 000 g, 5 min, RT). Pellet was washed with 1 ml water and resuspended in 500 µl lysis buffer (100 mM Tris/HCl pH8, 50 mM EDTA/NaOH pH8, 1% SDS). 5-6 glas beads (1 mm) were added and sample was harshly vortexed for 2 min. After 5 min of incubation on ice sample was centrifuged for 1 min at 13 000 rpm. The supernatant was taken into a new tube, the pellet was discarded. 275 µl ammonium acetate (7M, pH 7) was added to supernatant and incubated for 5 min at 65°C, afterwards sample were incubated 5 min on ice. 500 µl chloroform was added to sample, vortexed and centrifuged for 2 min at 13 000 rpm. The upper part of the supernatant was transferred into a new tube and DNA was precipitated by addition of 1 ml isopropanol and incubation for 5 min at RT. Sample were centrifuged for 5 min at 13 000 rpm, pellet was washed in 70% ethanol and evaporated. DNA was solubilized with 50 µl water. 50 ng of the genomic DNA was added as template DNA to a 25 µl PCR reaction.

6.2.4 Restriction digest of DNA

Restriction digest was performed to prepare insert DNA and vectors for ligation, verify successful ligation or linearize plasmids for homologous recombination. The 50 µl reaction mix contained 15 U of the specific restriction enzyme, specific restriction buffer, and 2 µg of DNA. The reaction mixture was incubated for 15-60 min at 37°C, analyzed by agarose gel electrophoresis, or directly purified using the Monarch® PCR & Cleanup Kit (NEB) according to the manufacturer's instructions.

6.2.5 Ligation of DNA

Insert fragments were ligated into vector plasmid DNA in a 20 µl reaction volume. Therefore, 3:1 (5:1, if the length of the insert was smaller than 200 bp) molar ratios of the insert to vector (50-100 ng), 1 µl T4 DNA ligase, and 2 µl 10x ligase buffer were mixed. To molar ratios were calculated with the NEB web tool (https://nebiocalculator.neb.com/#!/ligation). The reaction was incubated at room temperature (RT) for 30-60 min. 10 µl of the ligation reaction was used to transform *E. coli* cells. Single colonies were selected and inoculated in a small volume (5 ml) of selective LB media and subjected to plasmid DNA isolation as described in 6.2.1 and analyzed with a restriction digest (6.2.4) for successful ligation.

6.2.6 Agarose gel electrophoresis

Agarose gel electrophoresis was used for analytic (test of successful ligation) and preparative purposes (isolation of DNA fragments). This method allows the size-dependent separation of DNA fragments in an electric field. The negatively charged DNA migrates in an electrical field through a polysaccharide agarose matrix towards a positive electrode. To cast the gel matrix, 1% agarose (w/v) was dissolved entirely in TAE buffer (40 mM Tris, 1.14% acetic acid, ten mM EDTA pH 8.0) by heating the solution in the microwave. After cooling down the agarose solution, 0.5 µg/ml ethidium bromide was added to visualize DNA under ultraviolet light. Before loading, samples were supplemented with 6x loading dye (60 mM Tris/HCl pH 7.5, 30 mM sodium acetate, 12 mM EDTA, 60% (v/v) glycerol, 0.36% (w/v) orange G). A molecular weight ladder (a mix of DNA fragments of known lengths) was loaded alongside the samples to determine the size of the DNA fragments. The electrophoresis was performed in 1x TAE buffer at 10 V/cm. The separation of DNA fragments was analyzed under

ultraviolet light. To isolate DNA fragments of interest (for preparative purposes), the respective DNA band was cut out using a scalpel and purified with the Monarch® PCR & Cleanup Kit (NEB) according to the manufacturer's instructions.

6.2.7 Gibson Assembly

Several plasmids were cloned by Gibson Assembly. To integrate the DNA fragments generated by PCR into the digested vector, the HiFi DNA Assembly Master Mix from NEB was used. The ligation was prepared in a 20 µl reaction mixture and incubated for 60 min at 50 °C. The reaction mixture contained 10 µl of the NEBuilder HiFi DNA Assembly Mix, 100 ng of the vector, PCR fragments (each 1:5 molar ratio) and reaction mixed was filled up with water.

6.2.8 Goldenbraid and Modular Cloning

Plasmids for the protease assay were cloned with GoldenBraid. Therefore protease expression plasmids were used as templates for PCR reactions to amplify protease sequences with overhangs needed for domestication into pUPD2 plasmid. Therfore the restriction enzyme Esp3I was used. Afterwards, alpha1 (YPRΔ15α1-pTDH3-MTS-Protese-tTDH2) and alpha2 (YPRΔ15α2-resistance cassette) plasmids were generated using the restriction enzyme BsaI. For assembly of the final plasmid (omega2), omega2, alpha1 and alpha2 plasmids were digested with Esp3I and afterward ligated with T4 ligase.

Plasmids for the expression of APEX were clones via Modular Cloning. For level 0 assembly/part domestication, the NEB BsmBI-v2 enzyme mix was used. For Level 1 assembly the NEB BsaI-HFv2 enzyme mix was used.

6.2.9 Real-time quantitative polymerase chain reaction and RNA isolation

For total RNA extraction, yeast strains were cultivated in synthetic media to mid-log phase. 4 OD_{600} cells were harvested and used for RNA extraction using the RNeasy Mini Kit (Qiagen) in conjunction with the RNase-Free DNase Set (Qiagen) according to the manufacturer’s instructions. Yield and purity of the obtained RNA was determined with a Spectrophotometer/Fluorometer DS-11 FX+ (DeNovix). According to the manufacturer's instructions, 500 ng RNA was reverse transcribed into cDNA using the qScript cDNA Synthesis Kit (Quanta Biosciences). The iTaq Universal SYBR

Green Supermix (BioRad) was used with 2 µl of a 1:10 dilution of the cDNA sample to measure relative mRNA levels. Measurements were performed in technical triplicates with the CFX96 Touch Real-Time PCR Detection System (BioRad). The relative mRNA expressions were calculated using the 2-ΔΔCt method [152]. For normalization, the housekeeping gene *ACT1* was used due to its stability. See **Table 5** for primer sequences.

6.3 Cell Biology Methods

6.3.1 *E. coli* cultivation media

E. coli cells were grown on LB-medium or LB plates. 1% bacto-tryptone, 0.5% yeast extract, and 1% sodium chloride were used for liquid culture. The pH was adjusted to 7.5 with NaOH. LB medium was supplemented with 2% bacto-agar (w/v) for agar plates and autoclaved. For plasmid selection 100 µg/ml ampicillin (Amp), or 30 µg/ml chloramphenicol (Cam), or 50 µg/ml Kanamycin (Kan), or 50 µg/ml Spectinomycin (Spec) was used.

6.3.2 *S. cerevisiae* cultivation media

Yeast cells were grown at 30°C in non-selective yeast complete (YP) medium, containing 1% (w/v) yeast extract, 2% (w/v) peptone and 2% (w/v) of the respective carbon source (D, glucose; Gal, galactose, G, glycerol). The pH was adjusted to 5.5 with HCl. For plates 2% (w/v) agar was added to YP medium and autoclaved. For selection 300µg/ml hygromycin b were added. To induce expression of the gRNA for CRISPRi 960 ng/ml ATc was added.

Cells harboring plasmids were cultured in minimal synthetic media (S-medium) or lactic acid-based media (SLac-medium). For this purpose, 1.7 g/l yeast nitrogen base 5 g/l ammonium sulfate was mixed with a drop-out mix lacking auxotrophic markers and 2% of the respective carbon source (D, glucose; Gal, galactose; G, glycerol). For SLac medium, 1.7 g/l yeast nitrogen base, five g/l ammonium sulfate, and 2.2% lactic acid (90%(v/v)) were mixed with drop-out mix lacking auxotrophic markers and could be supplemented with 0.5% or 2% galactose to induce protein expression from a GAL-promotor. In **Table 7**, the components of the 20x drop-out mix are listed. For plates containing selective media, water was supplemented with 2% (w/v) agar

and autoclaved. The agar solution was mixed with S-medium or SLac-medium, dropout-mix, and carbon source.

6.3.3 Dropout-Mix

The dropout mix contains all amino acids. For plasmid selection, the respective amino acids were left out.

Table 7: **Composition of the Dropout-Mix**. Depending on the selection marker, amino acids were left out.

Amino acids/Nucleobase	20x (mg/ml)
L-adenine hemisulfate salt	400
L-Arginine	400
L-Histidine HCl Monohydrate	400
L-Isoleucine	600
L-Leucine	2000
L-Lysin HCl	600
L-Methionine	400
L-Phenylalanine	1000
L-Threonine	400
L-Tryptophan	400
L-Tyrosine	400
L-Uracil	400
L-Valine	3000

6.3.4 Growth assays

Growth curves were performed in a 96-well plate using the automated SPECTROstar^{Nano} plate reader (BMG Labtech). Yeast cells were grown to mid-log phase in liquid rich or synthetic media. The growth curves started at 0.1 OD_{600} and the OD_{600} was measured every 10 min for 72 h at 30°C. The mean of three technical replicates was calculated and plotted in R.

For drop dilutiom analysis, the respective yeast strains were grown in liquid media. Yeast cells equivalent to 0.5 OD600 were harvested at the exponential phase. The cells were washed in sterile water and 3 µl of ten-fold serial dilutions were spotted on the respective media followed by incubation at 30°C. Pictures were taken after different days of the incubation.

6.3.5 Isolation of mitochondria

For the isolation of mitochondria, cells were grown in rich or selective galactose media to exponential phase. Cultures for CRISPRi samples were additionally treated with ATc (960 ng/ml final) for 18 h. For APEX Labeling, cultures were grown in SGal full media, diluted into SGal full media without Biotin and harvested after 18h. Cells were harvested (2,800 g, 5 min, RT) in the exponential phase. After a washing step, cells were treated for 10 min with 2 ml per g wet weight MP1 buffer (100 mM DTT, 10 mM Tris pH unadjusted) at 30°C. After washing with 1.2 M sorbitol, yeast cells were resuspended in 6.7 ml per g wet weight MP2 buffer (20 mM KPi buffer pH 7.4, 1.2 M sorbitol, 3 mg per g wet weight zymolyase 20T from Seikagaku Biobusiness) and incubated for 1 h at 30°C. Spheroplasts were collected via centrifugation at 4°C and resuspended in ice-cold homogenization buffer (13.4 ml/g wet weight) (10 mM Tris pH 7.4, 1 mM EDTA pH 8, 0.2% fatty acids free bovine serum albumin (BSA), 1 mM PMSF, 0.6 M sorbitol). Spheroplasts were disrupted by 12 strokes with a cooled glass potter. Cell debris was removed via centrifugation at 1,900 g for 5 min at 4°C. The supernatant was centrifuged for 12 min at 17,700 g at 4°C to collect mitochondria. Mitochondria were resuspended in 600 µl of ice-cold SH-buffer (0.6 M sorbitol, 20 mM Hepes pH 7.4). Protein concentration was measured by Bradford assay or the Spectrophotometer/Fluorometer DS-11 FX+ (DeNovix). The mitochondria were diluted to a protein concentration of 10 mg/ml.

6.4 Protein Biochemistry Methods

6.4.1 Whole cell lysates

For whole cell lysates, yeast strains were cultivated in liquid media to mid-log phase. 2 OD_{600} were harvested by centrifugation (17,000 g, 1 min at RT) and resuspended in 100 µl (50 µl/1 OD_{600}) reducing loading buffer. Cells were transferred to screw-cap tubes containing 1 mm glass beads. Samples were boiled at 96°C for 10 min. Cell lysis was performed using a FastPrep-24 5G homogenizer (MP Biomedicals, Heidelberg, Germany) with 3 cycles of 20 s, speed 6.0 m/s, 120 s breaks. Lysates were centrifuged (25,000g, 5 min, 4°C) and stored at -20°C until further use. Equal amounts were resolved via SDS-PAGE.

6.4.2 SDS-polyacrylamide gel electrophoresis

Sodiumdodecylsulfate polyacrylamide gel electrophoresis (SDS-PAGE) allows the separation of proteins by size [153]. In this method, proteins are denatured and negatively charged through the detergent SDS. This allows the migration through an electric field put on a polyacrylamide gel matrix. The network of acrylamide fibers leads to a slow migration of unfolded and large proteins. In contrast, small or partially folded proteins (for example, folded because of preserved disulfide bridges) run faster through the gel. In this study, a self-made vertical one-dimensional gel system was used. For the standard gel system, glass plates with a size of 160 x 180 mm and spacers with 1 mm thickness were sealed using a base gel, on top of which first the separation gel and then the stacking gel was placed. The concentration of acrylamide and bis-acrylamide in the separation gel depends on the molecular size of the proteins of interest. The composition of the gels is represented in **Table 8**. Before loading, samples were supplemented with reducing sample (Laemmli) buffer (50 mM Tris-HCl pH 6.8, 10% glycerin, 2% SDS, 0.01% bromophenol blue, 100 mM DTT). To determine the protein size, the unstained marker from peQLab was used. The electrophoresis was conducted at 25 mA for 2.45 h in SDS running buffer (25 mM Tris-HCl pH 8.3, 190 mM glycine, 0.1% SDS).

Table 8: Gel composition for SDS-PAGE. Composition of the running, stacking, and base gel.

Gel	Composition
Running gel	16% acrylamide 0.11% bisacrylamide 375 mM Tris-HCl pH 8.8 0.1% SDS 0.1% ammonium persulfate (APS) 0.03%N,N,N',N'-Tetramethylethylenediamine (TEMED)
Stacking gel	5% acrylamide 0.03% bisacrylamide 60 mM Tris-HCl pH 6.8 0.1% SDS 0.05% ammonium persulfate (APS) 0.1%N,N,N',N'-Tetramethylethylenediamine (TEMED)
Base gel	20% acrylamide 0.13% bisacrylamide 375 mM Tris-HCl pH 8.8 0.1% SDS 0.05% ammonium persulfate (APS) 0.1%N,N,N',N'-Tetramethylethylenediamine (TEMED)

6.4.3 Transfer of proteins to a nitrocellulose membrane (Western Blot)

Proteins separated by SDS-PAGE were transferred from a gel onto a nitrocellulose membrane using a semi-dry blotting method [154]. Therefore, the SDS-gel was placed onto a nitrocellulose membrane. It was covered with 2 Whatman papers below and one Whatman paper on top of it. The stack was soaked in blotting buffer (20 mM Tris, 150 mM glycine, 0.08% SDS, 20% methanol), arranged in this order on the anode transfer module, and covered with the cathode transfer module. The transfer of proteins from the gel onto the membrane was performed for 1.5 h at 1.3 mA/cm^2. To detect proteins on the nitrocellulose membrane, it was stained with Ponceau S solution (0.2% (w/v) Ponceau S, 3% (w/v) acetic acid) for 5 min.

6.4.4 Radioactive *in organello* labeling of mitochondrial translation products

Isolated mitochondria (100 µg) were incubated in 1.5x *in organello* translation buffer (ioTL buffer, 20 mM Hepes/KOH pH 7.4, 15 mM KPi, 0.6 M Sorbitol, 150 mM KCl, 12.66 mM $MgSO_4$, 12.13µg/ml Amino acid mix, 66.66µM Cys, 12.13 µg/ml Tyrosine, 7.5 mM Phosphoenolpyruvate, six mM ATP, 0.75 mM GTP, five mM α-Ketoglutarate, 10 µg/ml Pyruvat-Kinase) together with 1µl ^{35}S-methionine (of a 11 µCi solution) and incubated at 30°C for 10 min shaking at 600 rpm. The incorporation of radioactive methionine was quenched by adding 8 mM cold methionine, and the reaction was stopped by adding 1 ml ice-cold SH buffer (0.6 M Sorbitol, 20 mM Hepes). Mitochondria were pelleted by centrifugation (20000 x g, 10 min, 4°C), resuspended in loading buffer, and analyzed by SDS-PAGE and autoradiography.

6.4.5 Protein import into mitochondria

The TNT® Quick Coupled Transcription/Translation Kit from Promega was for synthesis of ^{35}S-methionine labeled proteins in reticulocyte lysate. 50 µg mitochondria were taken in import buffer (500 mM sorbitol, 50 mM Hepes pH 7.4, 80 mM KCl, 10 mM $Mg(OAc)_2$ and 2 mM KH_2PO_4), 2 mM ATP and 2 mM NADH. Indicated concentrations of CCCP were added into the reaction mix to disturb the membrane potential. VAO (55.6 µg/mL Valinomycin, 440 µg/mL Antimycin A, 850 µg/mL Oligomycin in ethanol (>99.8 %, p.a.) was added to make mitochondria import incompetent. In samples where all ATP should be depleted, 40 U/ml Apyrase was added instead of ATP and NADH. Samples were incubated for 10 min at 30°C unless

indicated otherwise. The import reaction was started by addition of 1% (v/v) reticulocyte lysate. Samples were taken after the indicated time points and the reaction was stopped by a 1:10 dilution in ice-cold SH buffer supplemented with 100 µg/ml Proteinase K. The samples were incubated on ice for 30 min to remove precursors which were not imported. The protease treatment was stopped by addition of 2 mM PMSF. The samples were centrifuged 15 min at 25,000 g and 4°C. The mitochondria were washed with 500 µl SH/KCl-buffer (0.6 M sorbitol, 20 mM HEPES/KOH pH 7.4, 150 mM KCl) and 2 mM PMSF. The mitochondria were reisolated by centrifugation for 15 min at 25,000 g and 4°C, resuspended in sample buffer and analyzed by SDS-PAGE and autoradiography.

6.4.6 Autoradiography

Radioactive proteins can be detected by autoradiography. Therefore, the signals were detected on Super RX Medical X-Ray Films (Fuji) using the Optimax Type TR-developer (MS Laborgeräte). Quantification was done with the Image Lab 6.1 Software (BioRad). Alternatively, the dried cellulose membrane was exposed to an imaging plate (Fujifilm) for phospho-imaging with the Typhoon FLA 7000 from GE Healthcare. The films were scanned in a grey-scale 8-bit format for quantification, and the quantification was performed using the ImageQuant software.

6.4.7 Proteinase K digest

100 µg isolated mitochondria are taken in SH buffer with or without 0.2 mg/ml Proteinase K. Samples were incubated on ice for 30 min. To stop the digest 1 ml SH buffer with 2 mM PMSF was added. To reisolate mitochondria samples were centrifuged 10 min at 25,000 g at 4°C. Pellet was resuspended in 50 µl loading buffer and boiled for 5 min at 96°C. Samples were analyzed by SDS-PAGE.

6.4.8 APEX-Labeling and affinity purification on streptavidin beads

100 µg isolated mitochondria were taken in SH buffer (0.6 M sorbitol, 20 mM Hepes pH 7.4) and 100 µM biotin-phenol. Samples were incubated for 30 min at 30°C. To start the Labeling reaction 1 mM H_2O_2 was added. After 2 or 5 minutes the reaction was stopped by adding the equal amount of ice-cold quencher solution (10 mM sodium ascorbate, 10 mM sodium azide, 5mM Trolox in SH buffer) to the sample and put on ice. To reisolate mitochondria samples were centrifuged for 10 min at 25,000 g at 4°C.

Pellets were washed with ice cold quencher solution and again centrifuged for 10 min at 25,000 g at 4°C. Pellets were resuspended in loading buffer, boiled for 5 min, and analyzed by SDS-PAGE.

For Streptavidin pulldown, after adding quencher solution to wash mitochondria, samples were divided into two samples (Total and IP). Both were centrifuged for 10 min at 25,000 g at 4°C. The pellet of the Total sample was resolved in loading buffer and boiled for 5min. To lyse mitochondria, the IP sample was resuspended in RIPA buffer (20 mM NaPi ph7.4, 150 mM NaCl, 1% NP-40 (IGEPAL), 0.5% (w/v) Deoxycholate, 0.1 % SDS, 1x Protease Inhibitor (cOmplete Tablets, Roche, 04 693 159 001) and incubated 30 minutes at 4°C on a rotator. Lysed IP samples were added onto equilibrated Streptavidin beads (PierceTM Streptavidin magnetic beads, Thermo Scientific, 815-968-0747) and incubated for 1h at 4°C on a rotator. Beads were separated on a magnetic rack and washed two times with RIPA buffer und two times with TBS-T (1x TBS, 0.1% Tween). Samples were eluted by addition of 30 µl loading buffer and boiling for 5 min. Samples were analyzed by SDS-PAGE.

6.4.9 Sample preparation and mass spectrometric identification of proteins

For Streptavidin pulldown cells were grown in SGal full media. Cells were diluted into SGal full media without Biotin and mitochondria were isolated after 18h. For APEX Labeling 500 µg isolated mitochondria were taken in SH buffer (20 mM Hepes pH7.4, 0.6 M Sorbitol) and 100 µM biotin-phenol. After incubation on 30°C for 30 min, 1 mM H_2O_2 was added. After 5 min, the labeling reaction was stopped by addition of an equal amount of ice-cold quencher solution (10 mM sodium ascorbate, 10 mM sodium azide, 5mM Trolox, SH) and samples were put on ice. After centrifugation for 10 min, 25 000g, 4°C the pellets were washed with quencher solution. After another centrifugation step (10 min, 25 000g, 4°C) pellets were resuspended in ice-cold RIPA buffer (20 mM NaPi pH7.4, 150 mM NaCl, 1% NP-40, 0.5% Deoxycholate, 0.1% SDS, 1x Protease inhibitor). To lyse mitochondria, samples were incubated 30 min at 4°C. Cleared lysates (20,000 g, 10 min, 4°C) were incubated with activated beads (PierceTM Streptavidin magnetic beads) and tumbled end-over-end for 1 h at 4°C. Streptavidin beads were washed three times with RIPA buffer and two times with 20 mM Tris.

For the co-immunoprecipitation of GFP-Mrp17 and mass spectrometry cells were grown in SLac media and expression was induced by 1.25% galactose. After 5 h of

induction 20 OD_{600} of cells were harvested by centrifugation (5,000 g, 5 min). Cell lysates were prepared in lysis buffer (10 mM Tris pH7.4, 150 mM NaCl, 0.5 mM EDTA, 0.5% Triton, 1 mM PMSF, 1x Protease inhibitor) using a FastPrep-24 5G homogenizer (MP Biomedicals, Heidelberg, Germany) with 3 cycles of 20 s, speed 6.0 m/s, 120 s breaks, glass beads. Lysates were cleared by centrifugation (12 000 g, 5 min, 4°C). Washed GFP-Trap-magnetic beads were added to lysed samples and incubated 1 h tumbling at 4°C. The beads were washed 2x with wash buffer I (150 mM NaCl, 50 mM Tris pH 7.5,5% glycerol, 0.05% Tx-100) and 2x with wash buffer II (150 mM NaCl, 50 mM Trish pH 7.5, 5% glycerol).

Peptides were digested on-bead with Elution buffer I (2 M urea, 50 mM Tris-HCl, pH 7.5, 1 mM DTT, 5 ng/µl trypsin (Promega, #V5111)) for 1 h at room temperature. Eluted peptides were transferred to a fresh tube. For a second elution step 50 µl Elution buffer II (2 M Urea, 50 mM Tris pH 7.5, 5 mM CAA, 5 ng/µl trypsin) was again added to the beads. After 30 min at room temperature the supernatant was combined with the first elution. Samples incubated overnight in the dark at 37°C. Peptides were acidified to pH <2 with Tri-flouracetic acid and desalted on home-made StageTips containing Empore C18 disks [155]. C18 stage tips were activated with 100 µl methanol, 100 µl buffer B (0.1% formic acid, 80% acetonitrile) and twice with 100 µl buffer A (0.1% formic acid). The acidified peptides were added onto the stage tips and washed with 100 µl buffer A. Peptides were eluted with 40 µl buffer B and dried-down in a speed vac and resolubilized in 9 µl buffer A (0.1 % formic acid in MS grade water) and 1 µl buffer A* (2 % acetonitrile, 0.1 % tri-flouracetic acid in MS grade water). Peptides were separated using an Easy-nLC 1200 system (Thermo Scientific) coupled to a Q Exactive HF mass spectrometer via a Nanospray-Flex ion source. The analytical column (50 cm, 75 µm inner diameter (NewObjective) packed in-house with C18 resin ReproSilPur 120, 1.9 µm diameter Dr. Maisch) was operated at a constant flow rate of 250 nl/min. Gradients of 90 minutes were used to elute peptides (Solvent A: aqueous 0.1% formic acid; Solvent B: 80 % acetonitrile, 0.1% formic acid). MS spectra with a mass range of 300–1.650 m/z were acquired in profile mode using a resolution of 60.000 [maximum fill time of 20 ms or a maximum of 3e6 ions (automatic gain control, AGC)]. Fragmentation was triggered for the top 15 peaks with charge 2–8 on the MS scan (data-dependent acquisition) with a 30 s dynamic exclusion window (normalized collision energy was 28). Precursors were isolated with a 1.4 m/z window and MS/MS

spectra were acquired in profile mode with a resolution of 15,000 (maximum fill time of 80 ms, AGC target of 2e4 ions).

6.4.10 Analysis of mass spectrometry data

Peptide and protein identification and quantification was done using the MaxQuant software (version 2.0.1.0) 41-43 and a *S. cerevisiae* proteome database obtained from Uniprot. Protein N-terminal acetylation and Met oxidation were specified as variable modifications and Cys carbamidomethylation as fixed modification. The “Requantify” and “Second Peptides” options were deactivated. False discovery rate was set at 1% for peptides, proteins and sites, minimal peptide length was 7 amino acids. For label-free data, the LFQ normalization algorithm and second peptides was enabled. Match between run was applied within each group of replicates.

The protein groups identified in each mass spectrometry data set were processed and analyzed in parallel using the R programming language (version 4.2.1, R Core Team (2018). R: A language and environment for statistical computing. R Foundation for Statistical Computing, Vienna, Austria. Available online at https://www.R-project.org/.). First, the MaxQuant output was filtered to remove contaminants, reverse hits, proteins identified by site only as well as proteins that were identified in less than three replicates (N = 4) of every condition. This resulted in 1744 (GFP-pulldown), 1341 (Streptavidin-pulldowns) robustly identified protein groups whose label-free quantification (LFQ) intensities were log2-transformed subsequently. Lastly, in the GFP-Mrp17 Pulldown missing values in the Control samples were imputed by sampling n=4 values from a normal distribution and using them whenever there are no valid values in a quadruplicate of a condition. Different for each data set, the mean of this normal distribution corresponds to the 1% percentile of LFQ intensities, and its standard deviation is determined as the median of LFQ intensity sample standard deviations calculated within and then averaged over each quadruplicate.

Principal component analysis was carried out for each data set using the processed and standardized LFQ intensities of those protein groups with an ANOVA F-statistic p-value < 0.05 between all replicate groups to filter for proteins with a discernable degree of variance between conditions.

For the calculation of fold changes and p-values, the limma package within the R programming language was used 44. Protein groups were statistically analyzed using pairwise, two-sided Welch's t-tests on the processed LFQ intensities between the replicates of respective control and treatment conditions. Only proteins with valid values in the bait pull-down were considered for comparison. Log2 fold changes were derived as the tested difference of means and the resulting p-values were adjusted for multiple testing using the Benjamini-Hochberg procedure.

For gene ontology (GO) enrichment analysis, proteins with smaller than −0.5 log2 fold change were used as target set and analyzed by using the GOrilla tool (http://cbl-gorilla.cs.technion.ac.il/) with all quantified proteins as background set.

6.5 Immunology Methods

6.5.1 Immune decoration of cellulose membranes

Proteins transferred onto a nitrocellulose membrane were visualized by immunodecoration with specific antibodies. After staining the membrane with Ponceau S, it was incubated 30 min at RT with 5% (w/v) milk or 3% (w/v) BSA in TBS buffer (10 mM Tris/HCl pH 7.5, 150 mM NaCl) to block non-specific protein binding sites. Then, the blocking solution was replaced by a solution containing the specific primary antibody (1:125 to 1:10,000 in 5% milk or 3% BSA in TBS, prepared by immunization in rabbits). The membrane was incubated in this solution overnight at 4°C, washed three times (each 5 min) with TBS, followed by incubation with the secondary antibody (goat anti-rabbit, anti-mouse) coupled to horseradish peroxidase (1: 10,000 in 5% milk in TBS, BioRad) for 1 h 30 min at RT. After the washing procedure with TBS, the membrane was coated with a 1:1 mix of ECL solutions (ECL 1: 100 mM Tris/HCl pH 8.5, 0.044% (w/v) luminol, 0.0066% p-coumaric acid; ECL 2: 100 mM Tris/HCl pH 8.5, 0.03% H_2O_2). Luminescence signals were detected using the ChemiDoc™ MP (BioRAD) or on Super RX Medical X-Ray Films (Fuji) using the Optimax Type TR-developer (MS Laborgeräte). No secondary antibody was needed for the horseradish peroxidase coupled HA-antibody, and the films could be exposed directly after washing the primary antibody.

6.5.2 Antibodies

The antibodies against Hsp60, Mia40, Erv1, Ilv5, Tom70 were raised in rabbits using recombinant purified proteins. The antibody against Tim44 and Tim16 were kindly gifted by Dejana Mokranjac (LMU Munich, Germany). The FLAG antibody was ordered from Sigma (Monoclonal ANTI-FLAG M2, F3165-1MG). The horseradish-peroxidase coupled Streptavidin was ordered from Abcam (ab7403). The secondary antibodies were ordered from BioRad (Goat Anti-Rabbit IgG (H+L)-HRP Conjugate #172-1019, Goat Anti-Mouse IgG (H+L)-HRP Conjugate #172-1011) and used in a 1:10000 dilution. Antibodies were diluted in 5% (w/v) nonfat dry milk-TBS (Roth T145.2) as listed in **Table 9**. Streptavidin was diluted 1:3333 in 3% BSA-TBS (Roth 8076.2).

Table 9: Antibodies used in this study.

Name	Dilution
a-Tim44	1:500
a-Tim16	1:500
a-Hsp60	1:500
a-FLAG	1:2000
a-Tom70	1:2500
Streptavidin	1:3333
a-Mia40	1:5000
a-Erv1	1:1000
a-Ilv5	1:5000

6.6 Microscopy

6.6.1 Fluorescence microscopy

For microscopy, cells were grown to the mid-log phase and 1 OD_{600} was harvested via centrifugation (17000g, 1 min, RT). Cell pellets were resuspended in 30 µl of H_2O. 3 µl were pipetted onto a glass slide and covered with a cover slip. Manual microscopy was performed using a Leica Dmi8 Thunder Imager. Images were acquired using an HC PL APO100x/1,44 Oil UV objective with Immersion Oil Type A 518 F for excitation of GFP 475 nm and RFP 575nm was used. All images were taken as Z-stacks. Image analysis was done with the LAS X software, and images were further processed in Fiji/ImageJ.

ABBREVIATIONS

°C	Grade Celsius
µg	Microgram
µl	Microliter
µM	Micromolar
AAA+	ATPases Associated with diverse cellular Activities
Amp	Ampicillin
ATc	Anhydrotetracycline
ATP	Adenosine triphosphate
CCCP	Carbonylcyanid-m-chlorphenylhydrazon
CIP	Calf intestine alkaline phosphatase
dCas9	Catalytically dead Cas9
DMSO	Dimethyl sulfoxide
DNA	Deoxyribonucleic acid
DTT	Dithiothreitol
E. coli	*Escherichia coli*
ECL	Enhanced chemiluminescence
EDTA	Ethylene diamine tetraacetate
ER	Endoplasmic reticulum
ERAD	ER-associated degradation
EtOH	Ethanol
g	Gravity of earth
GFP	Green fluorescent protein
GO	Gene Ontology
gRNA	guide ribonucleic acid
h	Hours

HA	Hemagglutinin
HEPES	4-(2-hydroxyethyl)-1-piperazine-ethane sulfonic acid
HF	High fidelity
HSE	Heat shock element
IM	Inner mitochondrial membrane
IMS	Intermembrane space
kDa	Kilodalton
LB	Lysogeny broth media
M	Molarity
MAD	Mitochondria-associated degradation
mg	Milligram
min	Minute
ml	Milliliter
mM	Millimolar
mtDNA	mitochondrial DNA
MTS	Matrix targeting signal
nm	Nanometer
OD_{600}	Optical density at 600 nm
OM	Outer mitochondrial membrane
PAGE	Polyacrylamide gel electrophoresis
PAM	Presequence translocase-associated motor
PCR	Polymerase chain reaction
PEG	Polyethylene glycol
PK	Proteinase K
RNA	Ribonucleic acid
rpm	Revolutions per minute
RT	Room temperature

s	Seconds
SAM	Sorting and assembly machinery
S. cerevisiae	*Saccharomyces cerevisiae*
SDS	Sodium dodecyl sulfate
SS	Signal-sequence
T	Total
TA	Tail-anchored
TBS	Tris buffered saline
TCA	Trichloroacetic acid
TIM	Translocase of the inner membrane
TMD	Transmembrane domain
TOM	Translocase of the outer membrane
Tris	Tris-(hydroxymethyl)-aminomethane
U	Units
UPR	Unfolded protein response
w/v	Weight per volume
WT	Wild type

APPENDIX

Appendix Table 1 | Viral proteases used in this study.

Viral proteases used in this study

	SMVPZ	HCVP	3C	uTEV3
Name	Soybean mosaic virus NIa-Pro protease	Hepatitis C virus NS3 protease	3C protease	*proximity-dependent* tobacco etch virus protease, version 3
Source	Soybean mosaic virus	Hepatitis C virus	Rhinovirus B14	Tobacco etch virus
Reference	Ghabrial et al., 1990 PMID: 2212987	Yang and Ding, 2021 PMID: 34589286	Callahan et al., 1985 PMID: 2983312	Sanchez and Ting, 2020
Protein	NP_734202.1	QSL83343.1	NP_740524.1	Q0GDU8 (modified) I138T, S153N, T180A, S219V
Properties	28 kDa, 245 res. pI 7.13	22 kDa, 213 res. pI 9.25	20 kDa, 183 res. pI 8.43	27 kDa, 237 res. pI 8.90
Type	Cysteine-type endopeptidase	Cysteine-type endopeptidase	Cysteine-type endopeptidase	Cysteine-type endopeptidase
Recognition and cleavage site	E/NxVxxQ|S/G	DTEDVVCC| SMSYTWTGK	DSLETLFQ| GPVYKDL	ENLYFQ|S
Cleavage sites in the yeast proteome	none	none	none	none

Appendix Table 2 | All significantly enriched MRPs in the IMS of *Δatp6* mitochondria. TargetP scores from Bykov, Flohr et. al were used [25]. Scores >0.8 are labeled in red, between 0.5 to 0.8 are labeled in yellow, and scores <0.5 are labeled in red.

Gene	Uniprot	SysName	logFC	pvalue	Subunit	TargetP2
MRPS17	Q03246	YMR188C	5.81420094	0.00000000094	S	0.002612
YML6	P51998	YML025C	5.5390605	0.00000000000	L	0.642226
NAM9	P27929	YNL137C	5.04375718	0.00000000008	S	0.413285
IMG2	P25642	YCR071C	4.75635574	0.00000000097	L	0.99183
MRPL13	Q02204	YKR006C	4.45340117	0.00000000000	L	0.85362
EHD3	P28817	YDR036C	4.40604495	0.00000000010	S	0.993935
MRPL11	P36521	YDL202W	4.31490238	0.00000002764	L	0.933532
MRPL1	Q04599	YDR116C	4.31480946	0.00000000001	L	0.981095
MRPL15	P36523	YLR312W-A	4.05316238	0.00000000001	L	0.767748
RSM24	Q03976	YDR175C	4.04931317	0.00000002114	S	0.895192
RSM10	Q03201	YDR041W	3.93526506	0.00000001540	S	0.964673

RSM25	P40496	YIL093C	3.9043075	0.00000000099	S	0.420965
MRP21	P38175	YBL090W	3.81035901	0.00000000005	S	0.90686
MRPL24	P36525	YMR193W	3.73095016	0.00000008385	L	0.886739
MRPL10	P36520	YNL284C	3.70498893	0.00000015997	L	0.452517
MRPL3	P36516	YMR024W	3.67370599	0.00000000001	L	0.836676
MRPS28	P21771	YDR337W	3.62404163	0.00000000025	S	0.906329
MRPS35	P53292	YGR165W	3.55216025	0.00000002106	S	0.63736
MRPS9	P38120	YBR146W	3.53525259	0.00000006746	S	0.987643
MRP4	P32902	YHL004W	3.52122068	0.00000008660	S	0.86384
MRPS18	P42847	YNL306W	3.38348249	0.00000000017	S	0.983606
RSM26	P47141	YJR101W	3.34306776	0.00000000057	S	0.282338
MRPL22	P53881	YNL177C	3.3309454	0.00000000147	L	0.85127
MRPL20	P22354	YKR085C	3.31038865	0.00000000001	L	0.793393
RSM7	P47150	YJR113C	3.2961522	0.00000001843	S	0.997289
MRPL35	Q06678	YDR322W	3.19053329	0.00000000169	L	0.837573
MRP1	P10662	YDR347W	3.18846942	0.00000000000	S	0.514647
MRPL49	P40858	YJL096W	3.16878807	0.00000012707	L	0.950123
IMG1	P25626	YCR046C	3.16708814	0.00000000389	L	0.962959
MRPL4	P36517	YLR439W	3.15439452	0.00000000209	L	0.618245
MRP51	Q02950	YPL118W	3.06075065	0.00000000034	S	0.214005
MRPL51	Q06090	YPR100W	2.99463897	0.00000000023	L	0.342965
MRPL25	P23369	YGR076C	2.92338458	0.00000001521	L	0.176489
PET123	P17558	YOR158W	2.90074718	0.00000001329	S	0.037595
MRP13	P12686	YGR084C	2.90064147	0.00000008467	S	0.786957
MRPL33	P20084	YMR286W	2.88868881	0.00000046920	L	0.589278
MRPL23	Q12487	YOR150W	2.79352084	0.00001347700	L	0.056579
MRPS8	Q03799	YMR158W	2.76831269	0.00000041110	S	0.485669
MRPL6	P32904	YHR147C	2.72646365	0.00000237781	L	0.912033
MRP7	P12687	YNL005C	2.72054481	0.00000000543	L	0.771788
MRPL8	P22353	YJL063C	2.66799367	0.00000006808	L	0.011669
RSM23	Q01163	YGL129C	2.61085812	0.00006186601	S	0.997582
MRPL17	P36528	YNL252C	2.57569593	0.00000208473	L	0.790467
MRPL7	P36519	YDR237W	2.51137126	0.00433610142	L	0.909013
MRPL40	P36534	YPL173W	2.46175601	0.00000001321	L	0.023298
MNP1	P53163	YGL068W	2.40974167	0.00000144971	L	0.996971
MRP20	P32387	YDR405W	2.37398593	0.00000001108	L	0.489768
RSM18	P40033	YER050C	2.34212066	0.00000012164	S	0.084164
MRPS5	P33759	YBR251W	2.31078355	0.00000072964	S	0.565142
MHR1	Q06630	YDR296W	2.30215375	0.00002815982	L	0.085649
MRPL27	P36526	YBR282W	2.29371891	0.00000623052	L	0.53119
MRPL19	P53875	YNL185C	2.22056573	0.00000058403	L	0.404846
MRP17	P28778	YKL003C	2.17583698	0.00006516933	S	0.085661
MRPL9	P31334	YGR220C	2.11812667	0.00000168384	L	0.930767
MRPL39	P36533	YML009C	2.0842858	0.00001385846	L	0.3143
MRPL16	P38064	YBL038W	1.94304009	0.00008456330	L	0.934198
MRPL36	P36531	YBR122C	1.84409911	0.00000255595	L	0.904509
MRPL38	P35996	YKL170W	1.78819003	0.00004119885	L	0.010607
VAR1	P02381	Q0140	1.73557523	0.00001897976	S	0.06319
MRPS12	P53732	YNR036C	1.65312918	0.00008113662	S	0.994453
MRPL44	P19956	YMR225C	1.53891383	0.00087759952	L	0.322631
MRPL31	P14063	YKL138C	1.44812051	0.00499866280	L	0.831937

MRPL32	P25348	YCR003W	1.38034812	0.00317850580	L	0.60806
MRPL28	P36527	YDR462W	1.37669517	0.00161419440	L	0.502779
MRP2	P10663	YPR166C	1.3065971	0.03292955044	S	0.032975
MRPS16	Q02608	YPL013C	1.239415	0.02104373111	S	0.733305

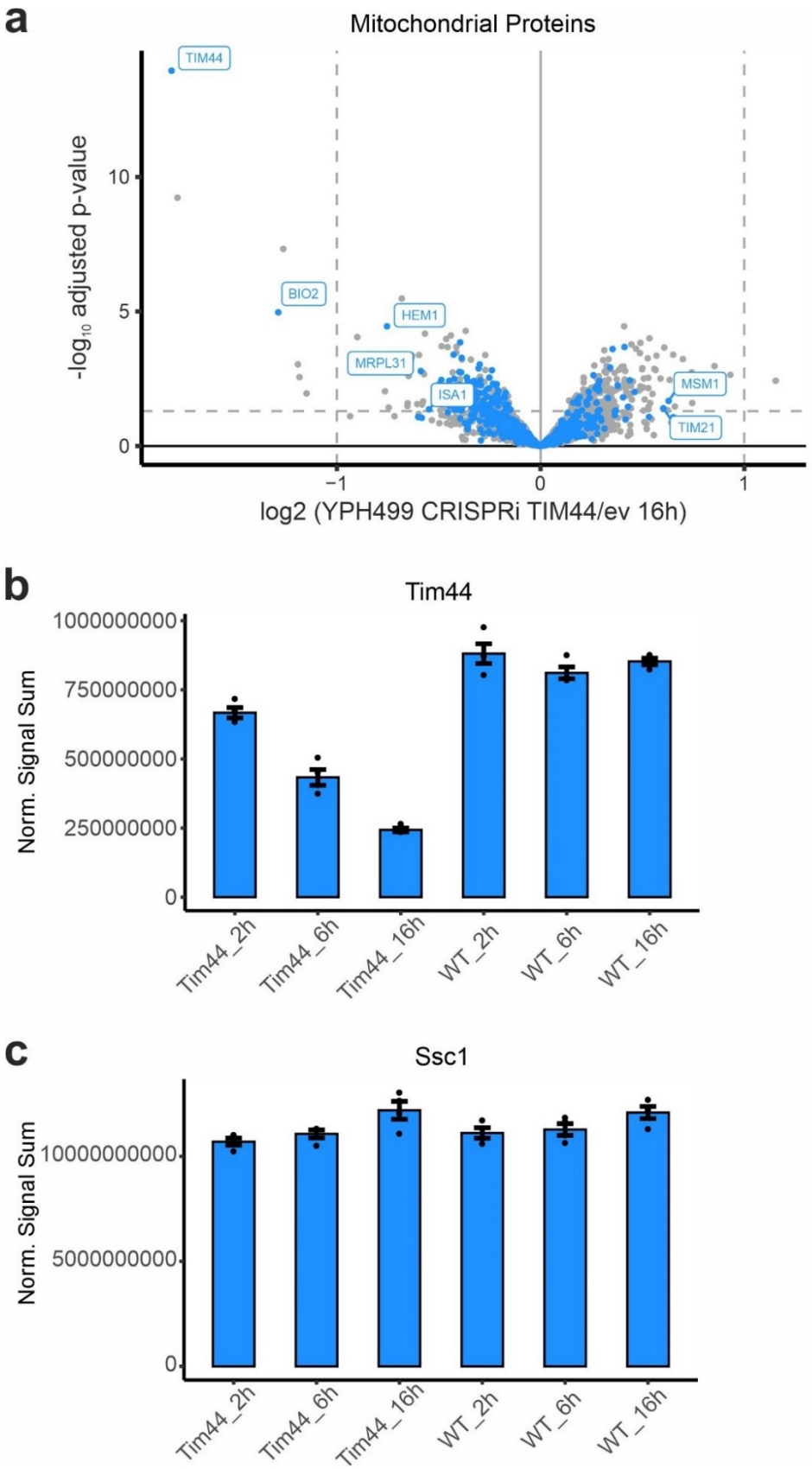

Appendix Fig. 1 | Depletion of Tim44 in whole cell lysates. (a) Comparison of the proteomes of wild type cells and Tim44-depleted cells. Mitochondrial proteins were indicated in blue. Whole cell lysates were harvested 16 hours after ATc addition and were analyzed by mass spectrometry. The log2 fold change (logFC) values were calculated from n=4 samples. **(b, c)** The bar plot represents the normalized signal sums of Tim44 and Ssc1. Whole cell lysates from WT cells or Tim44-depleted cells were harvested after 2, 6, or 16 hours of ATc induction.

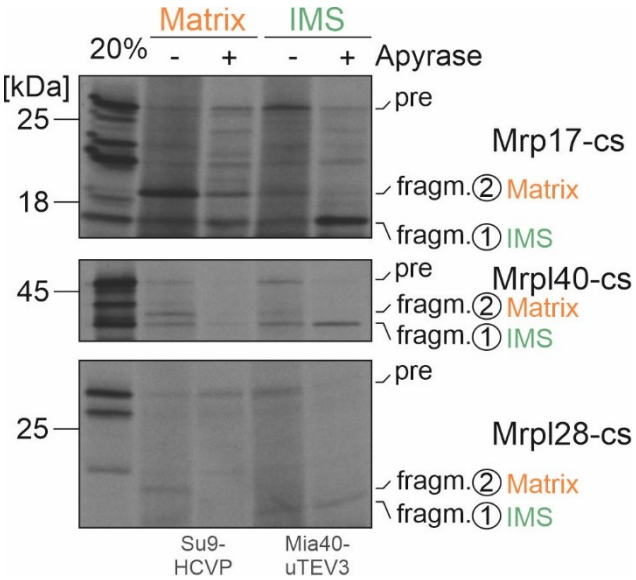

Appendix Fig. 2 | Mrpl40 and Mrpl28 are also mislocalized into the IMS. Radiolabeled Mrp17-cs, Mrpl40-cs, and Mrpl28-cs was incubated with isolated mitochondria from cells expressing Su9-HCVP or IMS-uTEV3. Apyrase was added to indicated samples and were incubated at 30°C for 5 minutes. Non-imported protein was removed by treatment with Proteinase K (PK). The 20% sample shows one fifth of the radiolabeled protein that was used per time point of the import reaction.

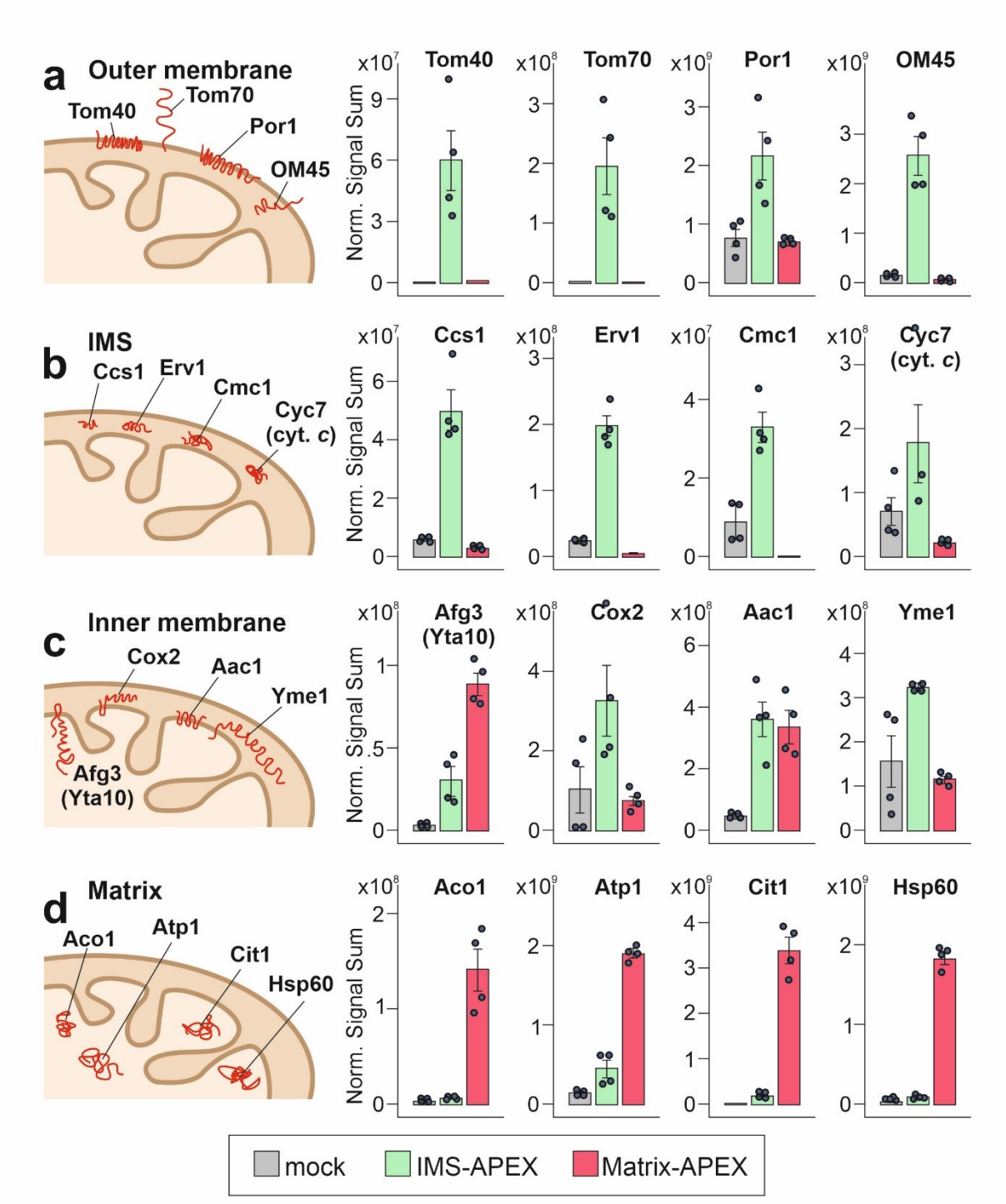

Appendix Fig. 3 | APEX-mediated biotinylation patterns reveal intramitochondrial distribution of proteins. (a-d) Protein levels were detected by mass spectrometry in the streptavidin pulldowns from lysed isolated mitochondria, derived from cells expressing no APEX (gray), or IMS-APEX (green) or matrix-APEX (red). Shown are the normalized signal sums of mitochondrial proteins of the four different mitochondrial subcompartments. Plotted were mean values and standard deviations from four replicates. The intramitochondrial localizations of the proteins are sketched on the left.

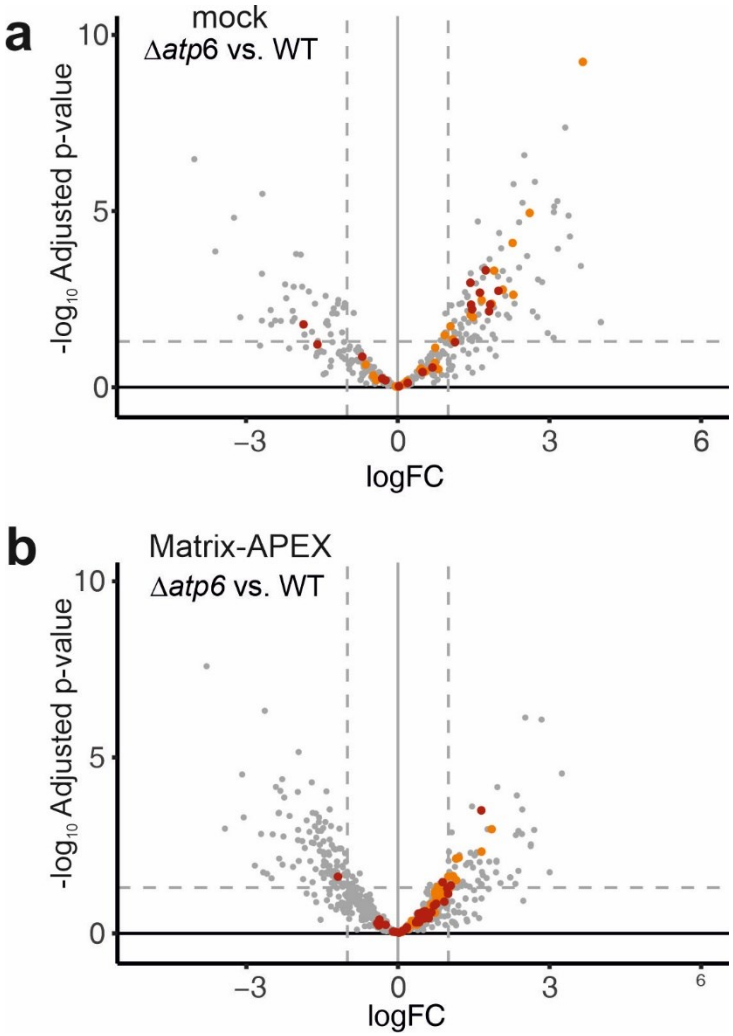

Appendix Fig. 4 | Volcano plots showing the proteins purified on streptavidin beads from mitochondrial extracts of the indicated samples. Proteins of the small and large subunit of the mitochondrial ribosome are shown in red or orange.

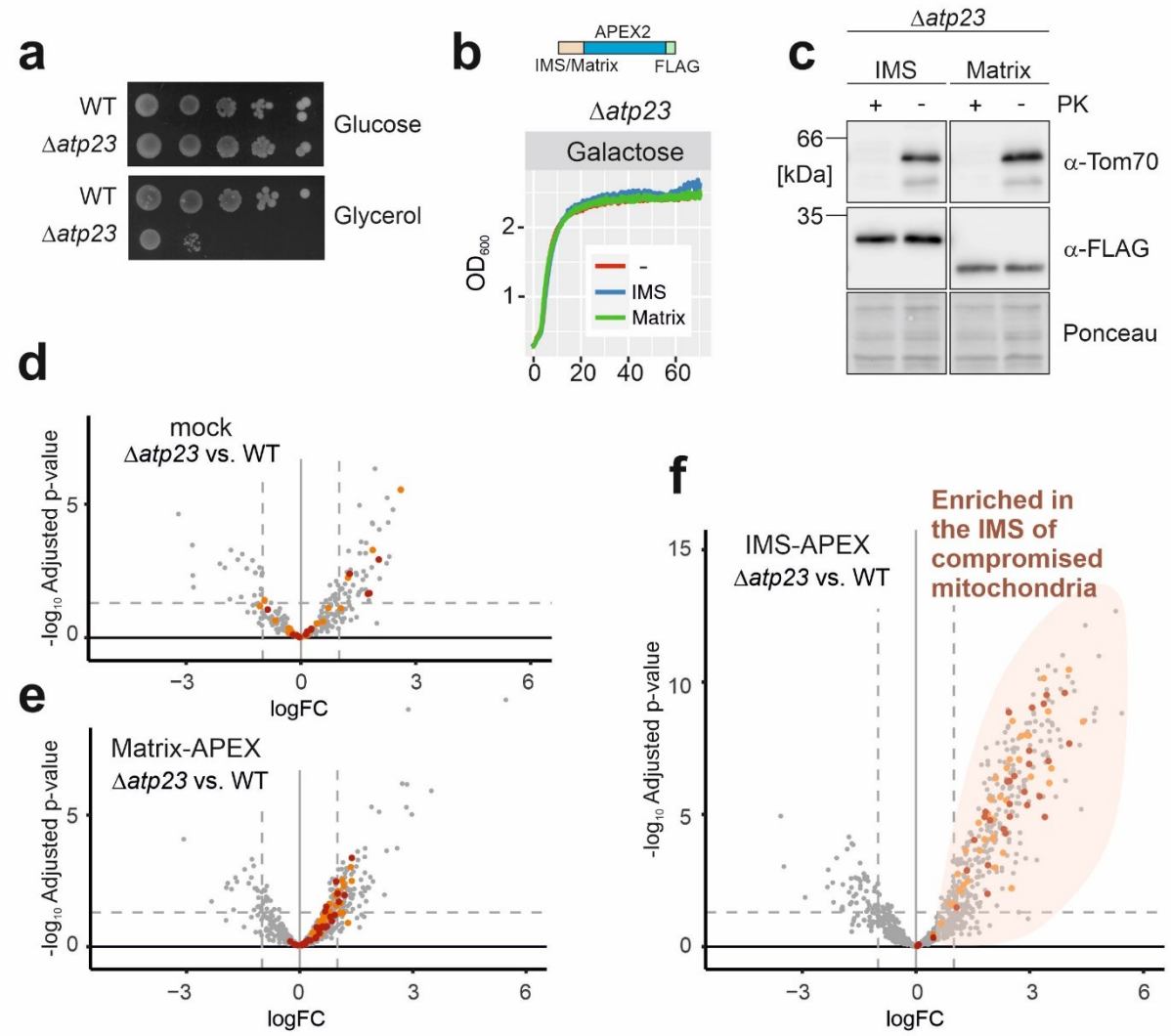

Appendix Fig. 5 | A nuclear model for mitochondrial dysfunction phenocopies the situation in *Δatp6* cells. (a) Wild type (WT) and *Δatp23* cells were grown to log phase in galactose-containing medium before tenfold serial dilutions were dropped onto medium containing glucose or glycerol as carbon sources. **(b)** The growth of *Δatp23* cells expressing the indicated APEX reporters was measured continuously. **(c)** Mitochondria were isolated from wild type and *Δatp23* cells and incubated with or without proteinase K (PK) to remove non-imported proteins. The presence of the surface protein Tom70 and of the FLAG-tagged APEX fusion proteins was verified by Western blotting. **(d-f)** Volcano plots showing the relative distribution of proteins purified with streptavidin beads in mitochondria from wild type and *Δatp23* cells. Please note the strong accumulation of MRPs (shown in color) in the IMS of *Δatp23* cells, that is reminiscent to the situation in *Δatp6* cells.

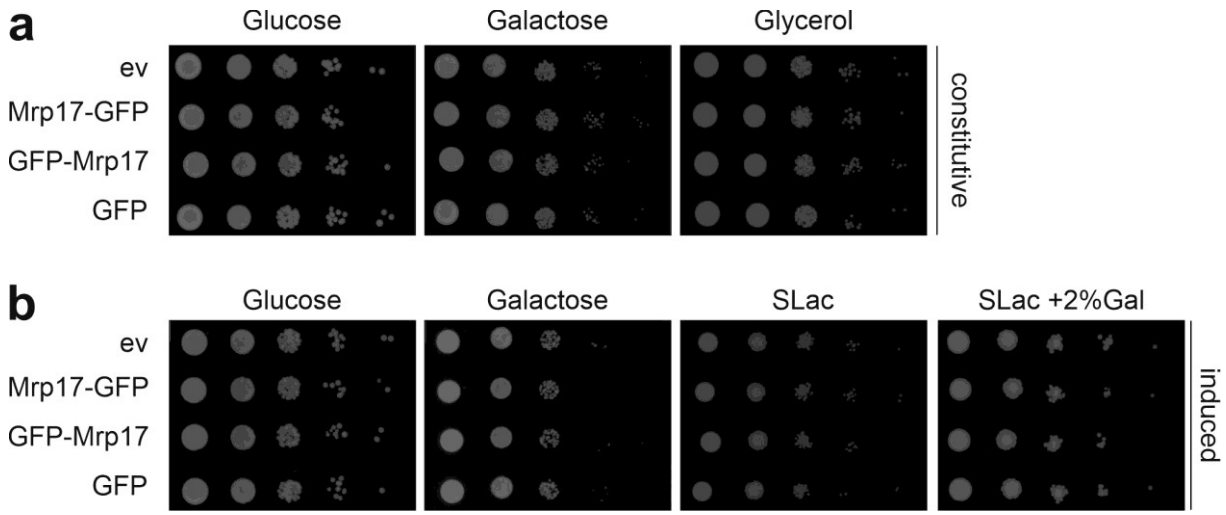

Appendix Fig. 6 | Growth is not impaired upon GFP-Mrp17 expression. (a) Wild type cells expressing the empty vector (ev), Mrp17-GFP, GFP-Mrp17, or GFP were grown to log phase in galactose-containing medium before tenfold serial dilutions were dropped onto medium containing glucose, galactose or glycerol as carbon sources. **(b)** Wild type cells expressing the empty vector (ev), Mrp17-GFP, GFP-Mrp17, or GFP were grown to log phase in **SLac** medium before tenfold serial dilutions were dropped onto plates containing the indicated medium. Expression was induced on plates containing galactose.

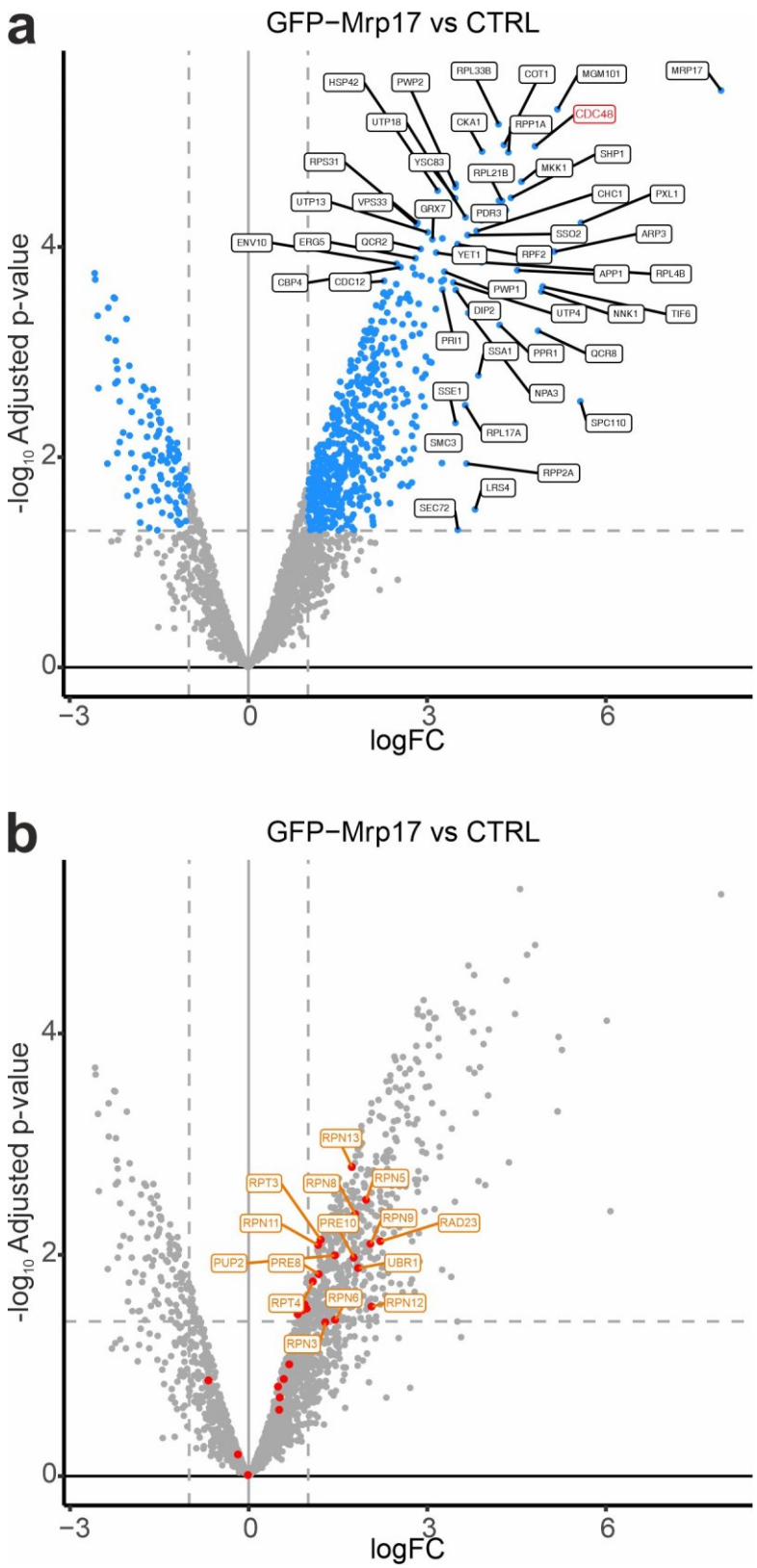

Appendix Fig. 7 | Cdc48 and proteasomal proteins are highly enriched. (a, b) GFP-Mrp17 was expressed for 5 h in wild type cells. GFP-Mrp17 was purified from cell extracts and co-isolated proteins were analyzed by mass spectrometry relative to proteins from a control sample (GFP). The log2 fold change (logFC) values were calculated from n=4 samples. **(a)** Significantly enriched proteins are labeld in blue. Cdc48 which is involved in mitoTAD is labeled in red. **(b)** Proteasomal proteins are indicated in red and significantly enriched proteasomal proteins are labeled.

REFERENCES

[1] L. Sagan, “On the origin of mitosing cells,” *Journal of theoretical biology*, vol. 14, no. 3, pp. 255–274, 1967.

[2] J. Martijn, J. Vosseberg, L. Guy et al., “Deep mitochondrial origin outside the sampled alphaproteobacteria,” *Nature*, vol. 557, no. 7703, pp. 101–105, 2018.

[3] H. Weidberg and A. Amon, “MitoCPR-A surveillance pathway that protects mitochondria in response to protein import stress,” *Science (New York, N.Y.)*, vol. 360, no. 6385, 2018.

[4] L. Wrobel, U. Topf, P. Bragoszewski et al., “Mistargeted mitochondrial proteins activate a proteostatic response in the cytosol,” *Nature*, vol. 524, no. 7566, pp. 485–488, 2015.

[5] F. Foury, “Human genetic diseases: a cross-talk between man and yeast,” *Gene*, vol. 195, no. 1, pp. 1–10, 1997.

[6] T. G. Frey and C. A. Mannella, “The internal structure of mitochondria,” *Trends in biochemical sciences*, vol. 25, no. 7, pp. 319–324, 2000.

[7] V. Shoshan-Barmatz, V. de Pinto, M. Zweckstetter et al., “VDAC, a multi-functional mitochondrial protein regulating cell life and death,” *Molecular Aspects of Medicine*, vol. 31, no. 3, pp. 227–285, 2010.

[8] D. M. Walther and D. Rapaport, “Biogenesis of mitochondrial outer membrane proteins,” *Biochimica et Biophysica Acta (BBA) - Molecular Cell Research*, vol. 1793, no. 1, pp. 42–51, 2009.

[9] C. Koch, S. Lenhard, M. Räschle et al., “The ER-SURF pathway uses ER-mitochondria contact sites for protein targeting to mitochondria,” *EMBO reports*, vol. 25, no. 4, pp. 2071–2096, 2024.

[10] J. J. Lemasters, “Modulation of mitochondrial membrane permeability in pathogenesis, autophagy and control of metabolism,” *Journal of gastroenterology and hepatology*, 22 Suppl 1, S31-7, 2007.

[11] W. Kühlbrandt, “Structure and function of mitochondrial membrane protein complexes,” *BMC biology*, vol. 13, p. 89, 2015.

[12] F.-N. Vögtle, J. M. Burkhart, S. Rao et al., “Intermembrane space proteome of yeast mitochondria,” *Molecular & cellular proteomics : MCP*, vol. 11, no. 12, pp. 1840–1852, 2012.

[13] V. Hung, P. Zou, H.-W. Rhee et al., “Proteomic mapping of the human mitochondrial intermembrane space in live cells via ratiometric APEX tagging,” *Molecular cell*, vol. 55, no. 2, pp. 332–341, 2014.

[14] F. J. Bock and S. W. G. Tait, “Mitochondria as multifaceted regulators of cell death,” *Nature reviews. Molecular cell biology*, vol. 21, no. 2, pp. 85–100, 2020.

[15] O. Khalimonchuk and D. R. Winge, “Function and redox state of mitochondrial localized cysteine-rich proteins important in the assembly of cytochrome c oxidase,” *Biochimica et biophysica acta*, vol. 1783, no. 4, pp. 618–628, 2008.

[16] F.-N. Vögtle, J. M. Burkhart, H. Gonczarowska-Jorge et al., “Landscape of submitochondrial protein distribution,” *Nature Communications*, vol. 8, no. 1, p. 290, 2017.

[17] A. Kohler, A. Barrientos, F. Fontanesi et al., “The functional significance of mitochondrial respiratory chain supercomplexes,” *EMBO reports*, vol. 24, no. 11, e57092, 2023.

[18] N. Desai, A. Brown, A. Amunts et al., “The structure of the yeast mitochondrial ribosome,” *Science (New York, N.Y.)*, vol. 355, no. 6324, pp. 528–531, 2017.

[19] F. Foury, T. Roganti, N. Lecrenier et al., “The complete sequence of the mitochondrial genome of Saccharomyces cerevisiae,” *0014-5793*, vol. 440, no. 3, pp. 325–331, 1998.

[20] L. Bertgen, J.-E. Bökenkamp, T. Schneckmann et al., “Distinct types of intramitochondrial protein aggregates protect mitochondria against proteotoxic stress,” *Cell reports*, vol. 43, no. 4, p. 114018, 2024.

[21] D. Roise, S. J. Horvath, J. M. Tomich et al., “A chemically synthesized pre-sequence of an imported mitochondrial protein can form an amphiphilic helix and perturb natural and artificial phospholipid bilayers,” *The EMBO journal*, vol. 5, no. 6, pp. 1327–1334, 1986.

[22] N. Wiedemann and N. Pfanner, “Mitochondrial Machineries for Protein Import and Assembly,” *Annual review of biochemistry*, vol. 86, pp. 685–714, 2017.

[23] O. Emanuelsson, S. Brunak, G. von Heijne et al., “Locating proteins in the cell using TargetP, SignalP and related tools,” *Nature protocols*, vol. 2, no. 4, pp. 953–971, 2007.

[24] M. W. Woellhaf, K. G. Hansen, C. Garth et al., “Import of ribosomal proteins into yeast mitochondria,” *Biochemistry and cell biology = Biochimie et biologie cellulaire*, vol. 92, no. 6, pp. 489–498, 2014.

[25] Y. S. Bykov, T. Flohr, F. Boos et al., “Widespread use of unconventional targeting signals in mitochondrial ribosome proteins,” *The EMBO journal*, vol. 41, no. 1, e109519, 2022.

[26] M. Kiebler, R. Pfaller, T. Söllner et al., “Identification of a mitochondrial receptor complex required for recognition and membrane insertion of precursor proteins,” *Nature*, vol. 348, no. 6302, pp. 610–616, 1990.

[27] T. Shiota, K. Imai, J. Qiu et al., “Molecular architecture of the active mitochondrial protein gate,” *Science (New York, N.Y.)*, vol. 349, no. 6255, pp. 1544–1548, 2015.

[28] Y. Abe, T. Shodai, T. Muto et al., “Structural basis of presequence recognition by the mitochondrial protein import receptor Tom20,” *Cell*, vol. 100, no. 5, pp. 551–560, 2000.

[29] K. Yamano, Y.-I. Yatsukawa, M. Esaki et al., “Tom20 and Tom22 share the common signal recognition pathway in mitochondrial protein import,” *The Journal of biological chemistry*, vol. 283, no. 7, pp. 3799–3807, 2008.

[30] S. Backes, S. Hess, F. Boos et al., “Tom70 enhances mitochondrial preprotein import efficiency by binding to internal targeting sequences,” *The Journal of cell biology*, vol. 217, no. 4, pp. 1369–1382, 2018.

[31] K. Dietmeier, A. Hönlinger, U. Bömer et al., “Tom5 functionally links mitochondrial preprotein receptors to the general import pore,” *Nature*, vol. 388, no. 6638, pp. 195–200, 1997.

[32] Y. Araiso, A. Tsutsumi, J. Qiu et al., “Structure of the mitochondrial import gate reveals distinct preprotein paths,” *Nature*, vol. 575, no. 7782, pp. 395–401, 2019.

[33] Y. Araiso and T. Endo, “Structural overview of the translocase of the mitochondrial outer membrane complex,” *Biophysics and physicobiology*, vol. 19, e190022, 2022.

[34] X. Zhou, Y. Yang, G. Wang et al., “Molecular pathway of mitochondrial preprotein import through the TOM-TIM23 supercomplex,” *Nature Structural & Molecular Biology*, vol. 30, no. 12, pp. 1996–2008, 2023.

[35] K. N. Truscott, P. Kovermann, A. Geissler et al., “A presequence- and voltage-sensitive channel of the mitochondrial preprotein translocase formed by Tim23,” *Nature structural biology*, vol. 8, no. 12, pp. 1074–1082, 2001.

[36] K. Malhotra, M. Sathappa, J. S. Landin et al., “Structural changes in the mitochondrial Tim23 channel are coupled to the proton-motive force,” *Nature Structural & Molecular Biology*, vol. 20, no. 8, pp. 965–972, 2013.

[37] L. F. Fielden, J. D. Busch, S. G. Merkt et al., “Central role of Tim17 in mitochondrial presequence protein translocation,” *Nature*, vol. 621, no. 7979, pp. 627–634, 2023.

[38] J. Martin, K. Mahlke, and N. Pfanner, “Role of an energized inner membrane in mitochondrial protein import. Delta psi drives the movement of presequences,” *The Journal of biological chemistry*, vol. 266, no. 27, pp. 18051–18057, 1991.

[39] P. J. Kang, J. Ostermann, J. Shilling et al., “Requirement for hsp70 in the mitochondrial matrix for translocation and folding of precursor proteins,” *Nature*, vol. 348, no. 6297, pp. 137–143, 1990.

[40] M. Horst, W. Oppliger, S. Rospert et al., “Sequential action of two hsp70 complexes during protein import into mitochondria,” *The EMBO journal*, vol. 16, no. 8, pp. 1842–1849, 1997.

[41] P. de Los Rios, A. Ben-Zvi, O. Slutsky et al., “Hsp70 chaperones accelerate protein translocation and the unfolding of stable protein aggregates by entropic pulling,” *Proceedings of the National Academy of Sciences of the United States of America*, vol. 103, no. 16, pp. 6166–6171, 2006.

[42] R. Banerjee, C. Gladkova, K. Mapa et al., “Protein translocation channel of mitochondrial inner membrane and matrix-exposed import motor communicate via two-domain coupling protein,” *eLife*, vol. 4, e11897, 2015.

[43] J. Ostermann, A. L. Horwich, W. Neupert et al., “Protein folding in mitochondria requires complex formation with hsp60 and ATP hydrolysis,” *Nature*, vol. 341, no. 6238, pp. 125–130, 1989.

[44] A. Chacinska, S. Pfannschmidt, N. Wiedemann et al., “Essential role of Mia40 in import and assembly of mitochondrial intermembrane space proteins,” *The EMBO journal*, vol. 23, no. 19, pp. 3735–3746, 2004.

[45] S. M. Gasser, A. Ohashi, G. Daum et al., “Imported mitochondrial proteins cytochrome b2 and cytochrome c1 are processed in two steps,” *Proceedings of the National Academy of Sciences of the United States of America*, vol. 79, no. 2, pp. 267–271, 1982.

[46] N. Mesecke, N. Terziyska, C. Kozany et al., “A disulfide relay system in the intermembrane space of mitochondria that mediates protein import,” *Cell*, vol. 121, no. 7, pp. 1059–1069, 2005.

[47] M. van der Laan, M. Meinecke, J. Dudek et al., “Motor-free mitochondrial presequence translocase drives membrane integration of preproteins,” *Nature cell biology*, vol. 9, no. 10, pp. 1152–1159, 2007.

[48] A. B. Schendzielorz, P. Bragoszewski, N. Naumenko et al., “Motor recruitment to the TIM23 channel's lateral gate restricts polypeptide release into the inner membrane,” *Nature Communications*, vol. 9, no. 1, p. 4028, 2018.

[49] J. L. Woolford and S. J. Baserga, “Ribosome biogenesis in the yeast Saccharomyces cerevisiae,” *Genetics*, vol. 195, no. 3, pp. 643–681, 2013.

[50] A. J. LaPeruta, S. Hedayati, J. Micic et al., “Yeast ribosome biogenesis factors Puf6 and Nog2 and ribosomal proteins uL2 and eL43 act in concert to facilitate the release of nascent large ribosomal subunits from the nucleolus,” *Nucleic acids research*, vol. 51, no. 20, pp. 11277–11290, 2023.

[51] Y. N. Osheim, S. L. French, K. M. Keck et al., “Pre-18S ribosomal RNA is structurally compacted into the SSU processome prior to being cleaved from nascent transcripts in Saccharomyces cerevisiae,” *Molecular cell*, vol. 16, no. 6, pp. 943–954, 2004.

[52] J. L. Baxter-Roshek, A. N. Petrov, and J. D. Dinman, “Optimization of ribosome structure and function by rRNA base modification,” *PloS one*, vol. 2, no. 1, e174, 2007.

[53] T. Schäfer, D. Strauss, E. Petfalski et al., “The path from nucleolar 90S to cytoplasmic 40S pre-ribosomes,” *The EMBO journal*, vol. 22, no. 6, pp. 1370–1380, 2003.

[54] F. Dragon, J. E. G. Gallagher, P. A. Compagnone-Post et al., “A large nucleolar U3 ribonucleoprotein required for 18S ribosomal RNA biogenesis,” *Nature*, vol. 417, no. 6892, pp. 967–970, 2002.

[55] J. R. Warner, “The economics of ribosome biosynthesis in yeast,” *Trends in biochemical sciences*, vol. 24, no. 11, pp. 437–440, 1999.

[56] B. J. Greber and N. Ban, “Structure and Function of the Mitochondrial Ribosome,” *Annual review of biochemistry*, vol. 85, pp. 103–132, 2016.

[57] S. Pfeffer, M. W. Woellhaf, J. M. Herrmann et al., “Organization of the mitochondrial translation machinery studied in situ by cryoelectron tomography,” *Nature Communications*, vol. 6, p. 6019, 2015.

[58] D. Kampjut and L. A. Sazanov, “The coupling mechanism of mammalian respiratory complex I,” *Science (New York, N.Y.)*, vol. 370, no. 6516, 2020.

[59] A. J. Y. Jones, J. N. Blaza, F. Varghese et al., “Respiratory Complex I in Bos taurus and Paracoccus denitrificans Pumps Four Protons across the Membrane for Every NADH Oxidized,” *The Journal of biological chemistry*, vol. 292, no. 12, pp. 4987–4995, 2017.

[60] T. Joseph-Horne, D. W. Hollomon, and P. M. Wood, “Fungal respiration: a fusion of standard and alternative components,” *Biochimica et biophysica acta*, vol. 1504, 2-3, pp. 179–195, 2001.

[61] K. Stephan and M. Ott, “Timing of dimerization of the bc1 complex during mitochondrial respiratory chain assembly,” *Biochimica et biophysica acta. Bioenergetics*, vol. 1861, 5-6, p. 148177, 2020.

[62] P. Mitchell, “Protonmotive redox mechanism of the cytochrome b-c1 complex in the respiratory chain: protonmotive ubiquinone cycle,” *0014-5793*, vol. 56, no. 1, pp. 1–6, 1975.

[63] M. K. Wikstrom, “Proton pump coupled to cytochrome c oxidase in mitochondria,” *Nature*, vol. 266, no. 5599, pp. 271–273, 1977.

[64] W. Kühlbrandt, “Structure and Mechanisms of F-Type ATP Synthases,” *Annual review of biochemistry*, vol. 88, pp. 515–549, 2019.

[65] A. Tzagoloff, A. Barrientos, W. Neupert et al., “Atp10p assists assembly of Atp6p into the F0 unit of the yeast mitochondrial ATPase,” *The Journal of biological chemistry*, vol. 279, no. 19, pp. 19775–19780, 2004.

[66] Y. Kagawa and E. Racker, “Partial resolution of the enzymes catalyzing oxidative phosphorylation. X. Correlation of morphology and function in submitochondrial particles,” *The Journal of biological chemistry*, vol. 241, no. 10, pp. 2475–2482, 1966.

[67] I. Arnold, M. F. Bauer, M. Brunner et al., “Yeast mitochondrial F1F0-ATPase: the novel subunit e is identical to Tim11,” *0014-5793*, vol. 411, 2-3, pp. 195–200, 1997.

[68] I. Arnold, K. Pfeiffer, W. Neupert et al., “Yeast mitochondrial F1F0-ATP synthase exists as a dimer: identification of three dimer-specific subunits,” *The EMBO journal*, vol. 17, no. 24, pp. 7170–7178, 1998.

[69] J. Velours and G. Arselin, “The Saccharomyces cerevisiae ATP synthase,” *Journal of Bioenergetics and Biomembranes*, vol. 32, no. 4, pp. 383–390, 2000.

[70] R. E. Gray, D. G. Grasso, R. J. Maxwell et al., “Identification of a 66 KDa protein associated with yeast mitochondrial ATP synthase as heat shock protein hsp60,” *0014-5793*, vol. 268, no. 1, pp. 265–268, 1990.

[71] J. M. Herrmann, R. A. Stuart, E. A. Craig et al., “Mitochondrial heat shock protein 70, a molecular chaperone for proteins encoded by mitochondrial DNA,” *The Journal of cell biology*, vol. 127, no. 4, pp. 893–902, 1994.

[72] C. Osman, C. Wilmes, T. Tatsuta et al., “Prohibitins interact genetically with Atp23, a novel processing peptidase and chaperone for the F1Fo-ATP synthase,” *Molecular biology of the cell*, vol. 18, no. 2, pp. 627–635, 2007.

[73] F. den Brave, A. Gupta, and T. Becker, “Protein Quality Control at the Mitochondrial Surface,” *Frontiers in cell and developmental biology*, vol. 9, p. 795685, 2021.

[74] T. Shiota, K. Imai, J. Qiu et al., “Molecular architecture of the active mitochondrial protein gate,” *Science (New York, N.Y.)*, vol. 349, no. 6255, pp. 1544–1548, 2015.

[75] F. Boos, L. Krämer, C. Groh et al., “Mitochondrial protein-induced stress triggers a global adaptive transcriptional programme,” *Nature Cell Biology*, vol. 21, no. 4, pp. 442–451, 2019.

[76] S. G. Rolland, S. Schneid, M. Schwarz et al., “Compromised Mitochondrial Protein Import Acts as a Signal for UPRmt,” *Cell reports*, vol. 28, no. 7, 1659-1669.e5, 2019.

[77] P. Bragoszewski, M. Turek, and A. Chacinska, “Control of mitochondrial biogenesis and function by the ubiquitin-proteasome system,” *Open biology*, vol. 7, no. 4, 2017.

[78] L. Kowalski, P. Bragoszewski, A. Khmelinskii et al., “Determinants of the cytosolic turnover of mitochondrial intermembrane space proteins,” *BMC biology*, vol. 16, no. 1, p. 66, 2018.

[79] M. Basch, M. Wagner, S. Rolland et al., “Msp1 cooperates with the proteasome for extraction of arrested mitochondrial import intermediates,” *Molecular biology of the cell*, vol. 31, no. 8, pp. 753–767, 2020.

[80] C. U. Mårtensson, C. Priesnitz, J. Song et al., “Mitochondrial protein translocation-associated degradation,” *Nature*, vol. 569, no. 7758, pp. 679–683, 2019.

[81] U. Schulte, F. den Brave, A. Haupt et al., “Mitochondrial complexome reveals quality-control pathways of protein import,” *Nature*, vol. 614, no. 7946, pp. 153–159, 2023.

[82] V. P. Shakya, W. A. Barbeau, T. Xiao et al., “A nuclear-based quality control pathway for non-imported mitochondrial proteins,” *eLife*, vol. 10, 2021.

[83] C. Enam, Y. Geffen, T. Ravid et al., “Protein Quality Control Degradation in the Nucleus,” *Annual review of biochemistry*, vol. 87, pp. 725–749, 2018.

[84] F. Frottin, F. Schueder, S. Tiwary et al., “The nucleolus functions as a phase-separated protein quality control compartment,” *Science (New York, N.Y.)*, vol. 365, no. 6451, pp. 342–347, 2019.

[85] T. Xiao, V. P. Shakya, and A. L. Hughes, “ER targeting of non-imported mitochondrial carrier proteins is dependent on the GET pathway,” *Life science alliance*, vol. 4, no. 3, 2021.

[86] S. A. Paschen, U. Rothbauer, K. Káldi et al., “The role of the TIM8-13 complex in the import of Tim23 into mitochondria,” *The EMBO journal*, vol. 19, no. 23, pp. 6392–6400, 2000.

[87] N. Petrakis, F. Alcock, and K. Tokatlidis, “Mitochondrial ATP-independent chaperones,” *IUBMB life*, vol. 61, no. 9, pp. 909–914, 2009.

[88] E. R. Weber, T. Hanekamp, and P. E. Thorsness, “Biochemical and functional analysis of the YME1 gene product, an ATP and zinc-dependent mitochondrial protease from S. cerevisiae,” *Molecular biology of the cell*, vol. 7, no. 2, pp. 307–317, 1996.

[89] L. van Dyck and T. Langer, “ATP-dependent proteases controlling mitochondrial function in the yeast Saccharomyces cerevisiae,” *Cellular and molecular life sciences : CMLS*, vol. 56, 9-10, pp. 825–842, 1999.

[90] M. J. Baker, V. P. Mooga, B. Guiard et al., “Impaired folding of the mitochondrial small TIM chaperones induces clearance by the i-AAA protease,” *Journal of molecular biology*, vol. 424, no. 5, pp. 227–239, 2012.

[91] X. Wu, L. Li, and H. Jiang, “Mitochondrial inner-membrane protease Yme1 degrades outer-membrane proteins Tom22 and Om45,” *The Journal of cell biology*, vol. 217, no. 1, pp. 139–149, 2018.

[92] K. T. Kan, M. G. Nelson, C. M. Grant et al., “Understanding the Role of Yeast Yme1 in Mitochondrial Function Using Biochemical and Proteomics Analyses,” *International journal of molecular sciences*, vol. 23, no. 22, 2022.

[93] K. Leonhard, J. M. Herrmann, R. A. Stuart et al., “AAA proteases with catalytic sites on opposite membrane surfaces comprise a proteolytic system for the ATP-dependent degradation of inner membrane proteins in mitochondria,” *The EMBO journal*, vol. 15, no. 16, pp. 4218–4229, 1996.

[94] H. L. Fiumera, M. J. Dunham, S. A. Saracco et al., “Translocation and assembly of mitochondrially coded Saccharomyces cerevisiae cytochrome c oxidase subunit Cox2 by Oxa1 and Yme1 in the absence of Cox18,” *Genetics*, vol. 182, no. 2, pp. 519–528, 2009.

[95] K. Leonhard, A. Stiegler, W. Neupert et al., “Chaperone-like activity of the AAA domain of the yeast Yme1 AAA protease,” *Nature*, vol. 398, no. 6725, pp. 348–351, 1999.

[96] R. N. Rainey, J. D. Glavin, H.-W. Chen et al., “A new function in translocation for the mitochondrial i-AAA protease Yme1: import of polynucleotide phosphorylase

into the intermembrane space," *Molecular and cellular biology*, vol. 26, no. 22, pp. 8488–8497, 2006.

[97] P. Bragoszewski, A. Gornicka, M. E. Sztolsztener et al., "The ubiquitin-proteasome system regulates mitochondrial intermembrane space proteins," *Molecular and cellular biology*, vol. 33, no. 11, pp. 2136–2148, 2013.

[98] P. Bragoszewski, M. Wasilewski, P. Sakowska et al., "Retro-translocation of mitochondrial intermembrane space proteins," *Proceedings of the National Academy of Sciences of the United States of America*, vol. 112, no. 25, pp. 7713–7718, 2015.

[99] R. Edwards, S. Gerlich, and K. Tokatlidis, "The biogenesis of mitochondrial intermembrane space proteins," *Biological chemistry*, vol. 401, 6-7, pp. 737–747, 2020.

[100] C. Prip-Buus, B. Westerman, M. Schmitt et al., "Role of the mitochondrial DnaJ homologue, Mdj1p, in the prevention of heat-induced protein aggregation," *0014-5793*, vol. 380, 1-2, pp. 142–146, 1996.

[101] Z. Xu, A. L. Horwich, and P. B. Sigler, "The crystal structure of the asymmetric GroEL-GroES-(ADP)7 chaperonin complex," *Nature*, vol. 388, no. 6644, pp. 741–750, 1997.

[102] E. Dibrov, S. Fu, and B. D. Lemire, "The Saccharomyces cerevisiae TCM62gene encodes a chaperone necessary for the assembly of the mitochondrial succinate dehydrogenase (complex II)," *The Journal of biological chemistry*, vol. 274, no. 13, p. 9128, 1999.

[103] H. Arlt, R. Tauer, H. Feldmann et al., "The YTA10-12 complex, an AAA protease with chaperone-like activity in the inner membrane of mitochondria," *Cell*, vol. 85, no. 6, pp. 875–885, 1996.

[104] J. Yang, A. S. Song, R. L. Wiseman et al., "Cryo-EM structure of hexameric yeast Lon protease (PIM1) highlights the importance of conserved structural elements," *The Journal of biological chemistry*, vol. 298, no. 3, p. 101694, 2022.

[105] S. A. Leonhardt, K. Fearson, P. N. Danese et al., “HSP78 encodes a yeast mitochondrial heat shock protein in the Clp family of ATP-dependent proteases,” *Molecular and cellular biology*, vol. 13, no. 10, pp. 6304–6313, 1993.

[106] C. Vazquez-Calvo, V. Kohler, J. L. Höög et al., “Newly imported proteins in mitochondria are particularly sensitive to aggregation,” *Acta physiologica (Oxford, England)*, vol. 238, no. 3, e13985, 2023.

[107] Tamara Flohr, *Mrp17 – Ein Protein ohne Zielsequenz und dessen Importweg in die mitochondriale Matrix,* Master thesis, Technische Universität Kaiserslautern, 25.05.2020.

[108] X. Zeng, W. Neupert, and A. Tzagoloff, “The metalloprotease encoded by ATP23 has a dual function in processing and assembly of subunit 6 of mitochondrial ATPase,” *Molecular biology of the cell*, vol. 18, no. 2, pp. 617–626, 2007.

[109] H.-W. Rhee, P. Zou, N. D. Udeshi et al., “Proteomic mapping of mitochondria in living cells via spatially restricted enzymatic tagging,” *Science (New York, N.Y.)*, vol. 339, no. 6125, pp. 1328–1331, 2013.

[110] S. S. Lam, J. D. Martell, K. J. Kamer et al., “Directed evolution of APEX2 for electron microscopy and proximity labeling,” *Nature methods*, vol. 12, no. 1, pp. 51–54, 2015.

[111] E. D. Wong, S. R. Miyasato, S. Aleksander et al., “Saccharomyces genome database update: server architecture, pan-genome nomenclature, and external resources,” *Genetics*, vol. 224, no. 1, 2023.

[112] N. Alikhani, A.-K. Berglund, T. Engmann et al., “Targeting capacity and conservation of PreP homologues localization in mitochondria of different species,” *Journal of molecular biology*, vol. 410, no. 3, pp. 400–410, 2011.

[113] L. Lefebvre-Legendre, J. Vaillier, H. Benabdelhak et al., “Identification of a nuclear gene (FMC1) required for the assembly/stability of yeast mitochondrial F(1)-ATPase in heat stress conditions,” *The Journal of biological chemistry*, vol. 276, no. 9, pp. 6789–6796, 2001.

[114] T. E. S. Kauppila, J. H. K. Kauppila, and N.-G. Larsson, “Mammalian Mitochondria and Aging: An Update,” *Cell metabolism*, vol. 25, no. 1, pp. 57–71, 2017.

[115] M. Rak and A. Tzagoloff, “F1-dependent translation of mitochondrially encoded Atp6p and Atp8p subunits of yeast ATP synthase,” *Proceedings of the National Academy of Sciences of the United States of America*, vol. 106, no. 44, pp. 18509–18514, 2009.

[116] E. Hurt, J. Cheng, J. Baβler et al., “SnapShot: Eukaryotic ribosome biogenesis I,” *Cell*, vol. 186, no. 10, 2282-2282.e1, 2023.

[117] M. Eilers, W. Oppliger, and G. Schatz, “Both ATP and an energized inner membrane are required to import a purified precursor protein into mitochondria,” *The EMBO journal*, vol. 6, no. 4, pp. 1073–1077, 1987.

[118] C. Voisine, E. A. Craig, N. Zufall et al., “The protein import motor of mitochondria: unfolding and trapping of preproteins are distinct and separable functions of matrix Hsp70,” *Cell*, vol. 97, no. 5, pp. 565–574, 1999.

[119] D. P. Hutu, B. Guiard, A. Chacinska et al., “Mitochondrial protein import motor: differential role of Tim44 in the recruitment of Pam17 and J-complex to the presequence translocase,” *Molecular biology of the cell*, vol. 19, no. 6, pp. 2642–2649, 2008.

[120] M. I. Sanchez and A. Y. Ting, “Directed evolution improves the catalytic efficiency of TEV protease,” *Nature methods*, vol. 17, no. 2, pp. 167–174, 2020.

[121] X. J. Gao, L. S. Chong, M. S. Kim et al., “Programmable protein circuits in living cells,” *Science (New York, N.Y.)*, vol. 361, no. 6408, pp. 1252–1258, 2018.

[122] M. Morgenstern, S. B. Stiller, P. Lübbert et al., “Definition of a High-Confidence Mitochondrial Proteome at Quantitative Scale,” *Cell reports*, vol. 19, no. 13, pp. 2836–2852, 2017.

[123] T. Vyshkina, A. Sylvester, S. Sadiq et al., “Association of common mitochondrial DNA variants with multiple sclerosis and systemic lupus

erythematosus," *Clinical immunology (Orlando, Fla.)*, vol. 129, no. 1, pp. 31–35, 2008.

[124] S. E. Ahari, M. Houshmand, M. S. S. Panahi et al., "Investigation on mitochondrial tRNA(Leu/Lys), NDI and ATPase 6/8 in Iranian multiple sclerosis patients," *Cellular and molecular neurobiology*, vol. 27, no. 6, pp. 695–700, 2007.

[125] M. Kumar, M. Tanwar, R. Saxena et al., "Identification of novel mitochondrial mutations in Leber's hereditary optic neuropathy," *Molecular vision*, vol. 16, pp. 782–792, 2010.

[126] C. A. Brambley, J. D. Marsee, N. Halper et al., "Characterization of Mitochondrial YME1L Protease Oxidative Stress-Induced Conformational State," *Journal of molecular biology*, vol. 431, no. 6, pp. 1250–1266, 2019.

[127] S. Longen, M. W. Woellhaf, C. Petrungaro et al., "The disulfide relay of the intermembrane space oxidizes the ribosomal subunit mrp10 on its transit into the mitochondrial matrix," *Developmental cell*, vol. 28, no. 1, pp. 30–42, 2014.

[128] D. Weckbecker, S. Longen, J. Riemer et al., "Atp23 biogenesis reveals a chaperone-like folding activity of Mia40 in the IMS of mitochondria," *The EMBO journal*, vol. 31, no. 22, pp. 4348–4358, 2012.

[129] A. Chacinska, M. Lind, A. E. Frazier et al., "Mitochondrial presequence translocase: switching between TOM tethering and motor recruitment involves Tim21 and Tim17," *Cell*, vol. 120, no. 6, pp. 817–829, 2005.

[130] A. Chacinska, M. van der Laan, C. S. Mehnert et al., "Distinct forms of mitochondrial TOM-TIM supercomplexes define signal-dependent states of preprotein sorting," *Molecular and cellular biology*, vol. 30, no. 1, pp. 307–318, 2010.

[131] L. Krämer, N. Dalheimer, M. Räschle et al., "MitoStores: chaperone-controlled protein granules store mitochondrial precursors in the cytosol," *The EMBO journal*, vol. 42, no. 7, e112309, 2023.

[132] N. J. Krogan, W.-T. Peng, G. Cagney et al., “High-definition macromolecular composition of yeast RNA-processing complexes,” *Molecular cell*, vol. 13, no. 2, pp. 225–239, 2004.

[133] J. Pérez-Fernández, A. Román, J. de Las Rivas et al., “The 90S preribosome is a multimodular structure that is assembled through a hierarchical mechanism,” *Molecular and cellular biology*, vol. 27, no. 15, pp. 5414–5429, 2007.

[134] J. E. G. Gallagher, D. A. Dunbar, S. Granneman et al., “RNA polymerase I transcription and pre-rRNA processing are linked by specific SSU processome components,” *Genes & development*, vol. 18, no. 20, pp. 2506–2517, 2004.

[135] M. Wery, S. Ruidant, S. Schillewaert et al., “The nuclear poly(A) polymerase and Exosome cofactor Trf5 is recruited cotranscriptionally to nucleolar surveillance,” *RNA (New York, N.Y.)*, vol. 15, no. 3, pp. 406–419, 2009.

[136] T. MacVicar, Y. Ohba, H. Nolte et al., “Lipid signalling drives proteolytic rewiring of mitochondria by YME1L,” *Nature*, vol. 575, no. 7782, pp. 361–365, 2019.

[137] R. Banerjee, V. Trauschke, N. Bertram et al., *mtHsp70 converts mitochondrial proteostasis distress into impaired protein import*, 2022.

[138] R. Gomkale, A. Linden, P. Neumann et al., “Mapping protein interactions in the active TOM-TIM23 supercomplex,” *Nature Communications*, vol. 12, no. 1, 2021.

[139] Y. Li, C. Tian, K. Liu et al., “A Clickable APEX Probe for Proximity-Dependent Proteomic Profiling in Yeast,” *Cell chemical biology*, vol. 27, no. 7, 858-865.e8, 2020.

[140] M. J. Casadaban and S. N. Cohen, “Analysis of gene control signals by DNA fusion and cloning in Escherichia coli,” *Journal of molecular biology*, vol. 138, no. 2, pp. 179–207, 1980.

[141] M. Meselson and R. Yuan, “DNA restriction enzyme from E. coli,” *Nature*, vol. 217, no. 5134, pp. 1110–1114, 1968.

[142] B. Güngör, T. Flohr, S. G. Garg et al., “The ER membrane complex (EMC) can functionally replace the Oxa1 insertase in mitochondria,” *PLoS biology*, vol. 20, no. 3, e3001380, 2022.

[143] R. S. Sikorski and P. Hieter, “A system of shuttle vectors and yeast host strains designed for efficient manipulation of DNA in Saccharomyces cerevisiae,” *Genetics*, vol. 122, no. 1, pp. 19–27, 1989.

[144] M. Ralser, H. Kuhl, M. Ralser et al., “The Saccharomyces cerevisiae W303-K6001 cross-platform genome sequence: insights into ancestry and physiology of a laboratory mutt,” *Open biology*, vol. 2, no. 8, p. 120093, 2012.

[145] Ł. Opaliński, J. Song, C. Priesnitz et al., “Recruitment of Cytosolic J-Proteins by TOM Receptors Promotes Mitochondrial Protein Biogenesis,” *Cell reports*, vol. 25, no. 8, 2036-2043.e5, 2018.

[146] T. Becker, L.-S. Wenz, V. Krüger et al., “The mitochondrial import protein Mim1 promotes biogenesis of multispanning outer membrane proteins,” *The Journal of cell biology*, vol. 194, no. 3, pp. 387–395, 2011.

[147] R. Gomkale, L. D. Cruz-Zaragoza, I. Suppanz et al., “Defining the Substrate Spectrum of the TIM22 Complex Identifies Pyruvate Carrier Subunits as Unconventional Cargos,” *Current biology : CB*, vol. 30, no. 6, 1119-1127.e5, 2020.

[148] B. D. Gambill, W. Voos, P. J. Kang et al., “A dual role for mitochondrial heat shock protein 70 in membrane translocation of preproteins,” *The Journal of cell biology*, vol. 123, no. 1, pp. 109–117, 1993.

[149] M. Rak, E. Tetaud, F. Godard et al., “Yeast cells lacking the mitochondrial gene encoding the ATP synthase subunit 6 exhibit a selective loss of complex IV and unusual mitochondrial morphology,” *The Journal of biological chemistry*, vol. 282, no. 15, pp. 10853–10864, 2007.

[150] S. Backes, Y. S. Bykov, T. Flohr et al., “The chaperone-binding activity of the mitochondrial surface receptor Tom70 protects the cytosol against mitoprotein-induced stress,” *Cell reports*, vol. 35, no. 1, p. 108936, 2021.

[151] J. D. Smith, S. Suresh, U. Schlecht et al., “Quantitative CRISPR interference screens in yeast identify chemical-genetic interactions and new rules for guide RNA design,” *Genome biology*, vol. 17, p. 45, 2016.

[152] K. J. Livak and T. D. Schmittgen, “Analysis of relative gene expression data using real-time quantitative PCR and the 2(-Delta Delta C(T)) Method,” *Methods (San Diego, Calif.)*, vol. 25, no. 4, pp. 402–408, 2001.

[153] U. K. Laemmli, “Cleavage of structural proteins during the assembly of the head of bacteriophage T4,” *Nature*, vol. 227, no. 5259, pp. 680–685, 1970.

[154] J. Kyhse-Andersen, “Electroblotting of multiple gels: a simple apparatus without buffer tank for rapid transfer of proteins from polyacrylamide to nitrocellulose,” *Journal of biochemical and biophysical methods*, vol. 10, 3-4, pp. 203–209, 1984.

[155] J. Rappsilber, M. Mann, and Y. Ishihama, “Protocol for micro-purification, enrichment, pre-fractionation and storage of peptides for proteomics using StageTips,” *Nature protocols*, vol. 2, no. 8, pp. 1896–1906, 2007.

ACKNOWLEDGMENTS

Hannes, früh im Bachelor war mir klar, dass ich in der Zellbiologie meine Bachelorarbeit schreiben will und vielleicht sogar meine Masterarbeit. Als ich mich dann in dem AP-Bewerbungsgespräch nicht so geschickt angestellt hatte, habe ich schon gedacht, dass mein ganzer Plan den Bach runter geht. Nervös habe ich ständig meine E-Mails aktualisiert und gehofft, dass von dir doch noch eine Zusage für das AP kommt. Und tatsächlich, nach ein paar Tagen kam die Zusage. Danke, dass ich meine Bachelor-, Master- und sogar meine Doktorarbeit bei dir schreiben durfte. Danke für die perfekte Menge an Förderung als auch Forderung. Deine motivierende Art hat immer geholfen aus der Komfort-Zone auszubrechen und an neuen Aufgaben zu wachsen.

Danke **Tanja** für die Übernahme meines Zweitgutachtens.

Danke **Michael** für die Übernahme des Vorsitzenden meiner Prüfungskommission

Markus, danke dass du dir immer so viel Mühe mit den ganzen Proteomics-Experimenten gegeben hast. Dank deiner kritischen Fragen, Überlegungen und deiner Expertise konnten wir immer das Beste aus den Experimenten rausholen.

Lea, wo soll ich nur anfangen. Als wir uns den sowieso schon knappen Laborplatz neben Steffen geteilt haben, dachte ich noch die ruhige Lea, aber schnell habe ich begriffen, dass man mit dir jeden Schabernack machen kann. Danke für die vielen Rotwein-Abende und die guten (reflektierenden) Gespräche. Eine bessere Konferenz-Begleitung hätte ich mir nicht wünschen können. Danke, dass ich im Labor mit jeder noch so dummen Frage zu dir kommen konnte. Ich hoffe wir verlieren uns nie aus den Augen und können uns noch in vielen Jahren an unsere Kurzurlaube, Unipartys und Sportsessions zurückerinnern. Und ich sage nur was auf Konferenzen passiert …

Lena, danke für deine immer hilfsbereite Art. Und wenn ich etwas Aufmunterung brauche, muss ich eigentlich nur unsere TikTok-Dance Videos anschauen. Egal ob der Weihnachtsmann-Dance oder unsere Minions Performance, ich sage nur 1, 2, 3, 4, 5, 6, siiiiiieeeeeben, 8.

Carina, mit dir konnte man einfach die besten kurz-vor-Feierabend Gespräche führen. Die sind manchmal zeitlich zwar ein bisschen außer Kontrolle geraten, aber das spricht natürlich nur für die Qualität unserer ausgewählten Themen. Mal schauen, ob wir uns in 20 Jahren immer noch über unsere Pflanzen austauschen. Und ich hätte gerne eine Revenge beim Limbo.

Carina, Lena, Lea wir waren einfach das beste Ecklabor.

Anna, das Physikpraktikum entscheidet, ob man seinen Labor Partner abgrundtief hasst oder denjenigen heiraten könnte. Bei uns war auf jeden Fall zweiteres der Fall. Ob das Meistern der Testate an physikalischem Verständnis oder an der Überdosis Schokomilch lag, bleibt ein Mysterium. Danke für die schöne Studienzeit und ich hoffe „die Einheit“ bleibt für immer bestehen.

Christian, wenn ich nicht weiter wusste im Labor bin ich mal kurz zu dir rüber getigert, um dich nach deinem Rat zu fragen. Mit dir konnte ich jede noch so verzwickte Klonierung oder Experiment durchdenken. Danke für die vielen R-Tipps, das hat mir sehr viel Frust und Zeit erspart. Danke für die schönen Abende am Vogelwoog und spontanen Wein Sessions im Labor.

Jana, eine bessere Begleitung für Israel hätte ich mir nicht wünschen können.

Anna-Lena, danke dass du mich in Welt der TV-Memes eingeführt hast. Und wenn irgendwo ABBA läuft, werde ich wohl immer an dich denken. Deine herzliche Art schätze ich sehr.

Lorenz, danke dass man mit dir über alles quatschen kann und du mich in die Kunst des Swingolf eingeweiht hast. Kümmere dich gut um die Entwicklermaschine.

Saskia, wer hätte gedacht, dass wir den ersten als auch die letzten Tage an der Uni gemeinsam meistern. Danke, dass du dich immer geopfert und die schärfste Peperoni rausgepickt hast.

Büsra, du warst meine erste Studentin, die ich betreuen durfte. Danke, dass du mir den PhD Einstieg so leicht und angenehm gemacht hast. Danke für deine positive und fröhliche Art. Deine Luftsprünge, wenn eine Klonierung funktioniert hat, haben einem

immer den Tag versüßt. Und wenn du lachst, sind wir im Ecklabor von deiner Lache angesteckt, ohne zu wissen, worum es geht.

Annika alias Anneliese, du warst meine letzte Studentin die ich als Doktorandin betreut habe. So Studenten kann man sich nur wünschen. Ich hoffe du bekommst selbst auch so angenehme und pflegeleichte Studenten. Aber ein letzter Tipp: rege dich nicht über die nicht so guten Studenten auf und sehe es gelassen :D

Yura, Thank you for making my stay in Israel in Maya's lab so pleasant. I really appreciate that it is always important for you to share your knowledge and enthusiasm for the project.

Katja, mein erster Gedanke als Bachelorstudentin im Zellbio Praktikum war, was ist das denn für eine verrückte Nudel. Ich bin mir ziemlich sicher, dass sich die jetzigen Studenten das auch bei mir denken. Danke für deine immer herzliche Art. Deine Erfahrungsberichte aus Israel haben mir sehr geholfen und mich bestärkt mich für das Praktikum bei Maya in Israel zu entscheiden.

Simone, meist die erste Person, die mich morgens im Labor herzlich begrüßt und anlächelt. Wichtige Infos und Updates habe ich direkt am Spint von dir erfahren. Danke dass du dich immer um alles so ordentlich kümmerst, ohne dich würde der Laden nicht laufen.

Sabine, mit dir kann man einfach über alles reden. Egal ob die Zusammensetzung eines Puffers oder über die Gesundheit der Wälder. Deine direkte und offene Art schätze ich sehr.

Vera, Danke für deine Hilfe bei vielen Experimenten und Mitopreps. Egal wie kurzfristig ich zur dir kam, du hast einen immer (auch spontan) unterstützt.

Andrea, Danke für deine Sorgfältigkeit und Fürsorge.

Connie, deine positive Art ist einfach ansteckend. Auch wenn ich morgens noch nicht so ganz auf der Höhe war, hat dein fröhliches Guten Morgen mir direkt ein Lächeln ins Gesicht gezaubert.

Svenja, Danke für deine immer hilfsbereite Art und dass du mich beim Pausenexpress nicht alleine hast da stehen lassen.

Nikita, Thank you for introducing me into Indian flavors. I really enjoyed going to sports and uniparties with you. It was always fun.

Pavel, you are an expert in MoClo and nonverbal communication. Thank you for teaching me to communicate only through facial expressions.

Aleks, thank you for staying up all night in Thallichtenberg.

Annika N., Danke für die Hilfe mit R und die schönen Abende auf Unipartys.

Janina und Steffen, Danke für die Unterstützung in meiner Bachelor- und Masterarbeit. Ihr habt immer alle meine Fragen beantwortet und hattet immer ein offenes Ohr für mich.

Magnus, Danke dass du dir all die Geschichten aus dem Labor angehört hast. Egal ob ich mich über Studenten oder nicht funktionierende Experimente aufgeregt habe. Du hast mich immer wieder auf den Boden der Tatsachen gebracht und mich immer aufgemuntert, wenn ich mal nicht so gut drauf war. Danke, dass du mich oft am Wochenende ins Labor begleitet hast und geduldig gewartet hast, bis ich mal „kurz“ die Kleinigkeiten erledigt hatte.

Ein riesiges Dankeschön geht an **Mama und Papa**! Ohne euch wäre das hier alles gar nicht möglich gewesen. Ihr habt mich immer in allem bestärkt und mir immer den Freiraum gelassen, um meinen eigenen Weg zu gehen. Ich weiß, dass ich immer mit allem, was mir auf dem Herzen liegt zu euch gehen kann und ihr für mich da seid. Meine (meist) positive, gelassene und offene Art habe ich ganz klar von euch und dafür bin ich euch sehr dankbar.

Haiko, mit dir kann man stundenlang über alles Mögliche reden, am besten nachts um drei. Danke dass du dir geduldig meine Geschichten und Probleme anhörst.

Danke an **ALLE**, jeder von euch hat mich auf irgendeine Weise geprägt, und somit den Menschen aus mir gemacht der ich heute bin. Ich bin für jede Begegnung und jedes Erlebnis dankbar. Vielleicht nicht diese Arbeit an sich, aber die vielen Jahre im Labor haben mich geprägt und ich denke, ich bin an den verschiedensten Aufgaben bzw. Herausforderungen gewachsen und will diese PhD Zeit keinen Falls missen.